JOURNAL OF APPLIED PHYSICS

Physics Lib
AUG 2 2 1945

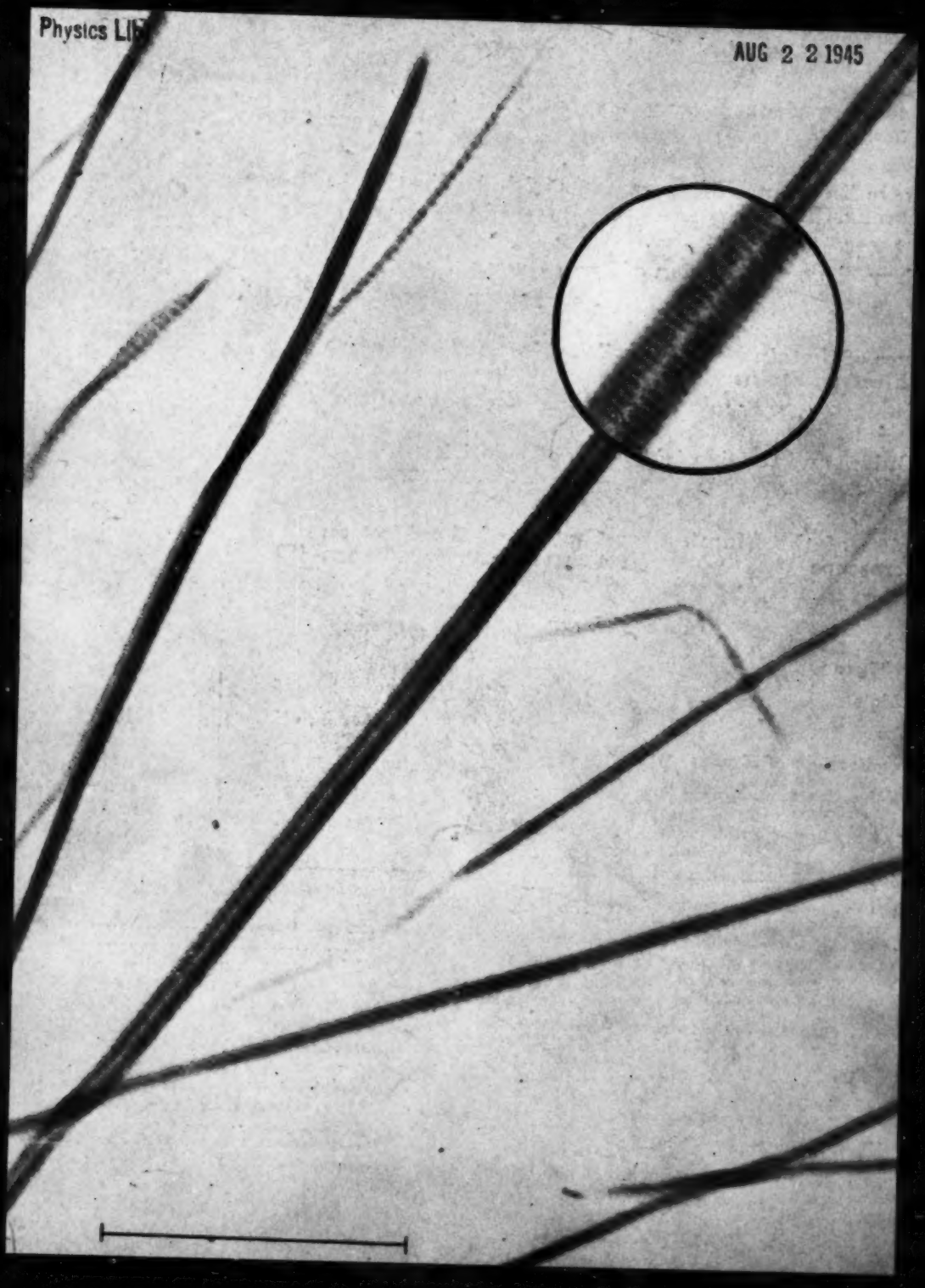

JOURNAL OF APPLIED PHYSICS

Vol. 16, No. 8 AUGUST, 1945

In This Issue

Page

Contributed Original Research

Microwave Impedance Measurements with Application to Antennas. I D. D. KING 435

Microwave Impedance Measurements with Application to Antennas. II RONOLD KING AND D. D. KING 445

Secondary Electron Emission of Pyrex Glass C. W. MUELLER 453

Structure of Certain Muscle Fibrils as Revealed by the Use of Electron Stains C. E. HALL, M. A. JAKUS, AND F. O. SCHMITT 459

Wave Guides and the Special Theory of Relativity W. D. HERSHBERGER 465

Discussion of the Illuminating System of the Electron Microscope JAMES HILLIER AND R. F. BAKER 469

In Every Issue

Here and There 484

New Booklets 485

New Books 485

Recent Applications of Physics 486

Index to Advertisers xxviii

BOARD OF EDITORS

ELMER HUTCHISSON, *Editor*

Associate Editors

R. B. BARNES
OTTO BEECK
W. F. BUSSE
S. H. CALDWELL
CLARK GOODMAN
SELIG HECHT
W. J. LYONS
MORRIS MUSKAT
THOMAS H. OSGOOD
PAUL E. SABINE
FREDERICK SEITZ
J. R. TOWNSEND

Publication of the
American Institute of Physics

ADMINISTRATIVE STAFF

HENRY A. BARTON, *Director*

MARGARET S. GRIFFIN, *Publications Manager*

THEODORE VORBURGER, *Business Manager*

JOHN T. TATE, *Adviser on Publications*

GOVERNING BOARD

PAUL E. KLOPSTEG, *Chairman*

WALLACE WATERFALL, *Secretary*

GEORGE B. PEGRAM, *Treasurer*

T. D. COPE
R. B. DOW
L. A. DUBRIDGE
FLOYD A. FIRESTONE
HARVEY FLETCHER
R. C. GIBBS
K. S. GIBSON
HERMANN MARK
A. G. WORTHING
JOHN T. TATE
L. W. TAYLOR
N. W. TAYLOR
WALLACE WATERFALL

The JOURNAL OF APPLIED PHYSICS, published monthly at Prince and Lemon Sts., Lancaster, Pa., is devoted to physics in its role as the science basic to other natural sciences and to the arts and industries. Previous to 1937 this publication was known as PHYSICS. The JOURNAL OF APPLIED PHYSICS publishes editorials, news of physicists, and reviews, as well as technical papers of applied physics.

Manuscripts should be submitted to Elmer Hutchisson, Editor, Case School of Applied Science, Cleveland 6, Ohio.

Subscriptions and orders for back numbers should be addressed to Prince and Lemon Streets, Lancaster, Pa. or to the American Institute of Physics, 57 East 55 Street, New York 22, N. Y.

Subscription Price

	U. S. AND CANADA	ELSEWHERE
To members of scientific societies	$5.00	$5.70
To all others	7.00	7.70

Back Number Prices

Complete set: Vol. 1, July, 1931–Vol. 15, 1944—$94.50
Yearly back number rate: $7.70
Single copies: $0.70 each.

Changes of address and proofs should be addressed to the Publications Manager.

Advertising rates supplied on request. Orders, advertising copy, and cuts should be sent to the American Institute of Physics.

Entered as second class matter January 22, 1937, at the Post Office at Lancaster, Pennsylvania, under the Act of March 3, 1879
Accepted for mailing at the special rate of postage provided for in the Act of February 28, 1925, authorized May 2, 1932.

Copyright 1945, by the American Institute of Physics.

Journal
of
Applied Physics

Volume 16, Number 8 August, 1945

Microwave Impedance Measurements with Application to Antennas. I

D. D. KING
Cruft Laboratory and the Research Laboratory of Physics, Harvard University, Cambridge, Massachusetts
(Received February 16, 1945)

The problem of impedance measurement at centimeter wave-lengths is discussed with special reference to the practical aspects. The description of the various transmission-line methods available is supplemented by a detailed account of the apparatus and procedure used to determine the input impedance of a symmetrical antenna.

INTRODUCTION

TRANSMISSION lines are commonly used for making impedance measurements at centimeter wave-lengths and are particularly well suited for determining antenna impedances. The purpose of this paper is to examine the general problem of transmission-line measurements at very high frequencies from the practical point of view. The physical limitations on the apparatus as well as the demands of the theory are considered. This approach is essential for the evaluation of experimental data in the light of the restrictions under which they are obtained. To illustrate the principles involved, application is made to a practical case: the measurement of antenna impedances at a forty-centimeter wave-length. The description of the apparatus and its probable accuracy should serve also to define more completely the significance of the curves displayed in Part II.

The problem of impedance measurement is best started with a definition of impedance. No more elaborate formulation than $Z=V/I$ is needed, but the definitions of the voltage and current involved in this ratio must be clearly understood. The situation is illustrated in Fig. 1. The impedance between the points z and z' is given by the ratio V/I, where V is the potential difference between the two conductors measured from z to z', and I is the current through the element dz. Taking the potential difference from z' to z and the current in the element dz' must give the same value of impedance as before. It follows that the currents in the two conductors must be equal and opposite at the point of impedance measurement, for if they are not, the impedance cannot be defined uniquely.

The symmetry of the line conductors relative to the surroundings is of primary importance, since it influences the current distribution along the line and at the junction of the line and its terminating impedance. It is at this junction that the measurements are made. Both transmission lines and terminal impedances may be divided into two general classes: symmetrical or balanced, and asymmetrical or unbalanced. A parallel line with conductors in the plane above the earth represents a balanced arrangement.

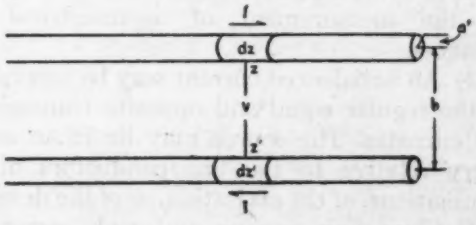

FIG. 1. Current and voltage on parallel line conductors.

The end of such a line furnishes two terminals at equal potential with respect to the surroundings. In a concentric line the terminals available at the end are not symmetrical, since the outside surface of the outer conductor forms part of one of the terminals. If a parallel line is attached to an asymmetrical terminal impedance, the currents at the ends of the line conductors become unbalanced. For measuring purposes this circuit is not satisfactory, since the unequal currents are not consistent with the definition of impedance given above. On the other hand, a concentric line attached to a balanced terminal impedance induces unbalanced currents in the termination. The current from the inside to the outside surface of the outer coaxial conductor causes this. A system which is completely symmetrical or completely asymmetrical preserves the original current distribution of both line and termination, and hence gives the correct ratio V/I.

The equal and opposite currents required for the definition of impedance, are also a basic postulate of transmission-line theory in general. Since transmission-line measurements depend on this theory, the currents on the two conductors must remain balanced at all times. This implies the use of symmetrical methods of excitation and detection, as well as proper terminations. A further assumption of transmission-line theory is that the radiation from the line is negligible. This requirement may be met by making the spacing b between the conductors small compared with the operating wave-length. In an open-wire line the length b should also be kept small relative to the distance from the conductors to the ground. Too close proximity to ground may cause image currents large enough to produce the current distribution of a four-wire line.

The above discussion imposes certain demands on the experimental measuring procedure. These may be summarized as follows:

(1) A parallel line is useful for the measurement of symmetrical impedances, a coaxial line for the measurement of asymmetrical impedances.

(2) An unbalanced current may be superposed on the regular equal and opposite transmission line currents. The source may lie in an asymmetry relative to the line conductors of the terminations, of the excitation, or of the detector.

(3) Close line spacing and wide separation from nearby metal surfaces and ground are important where currents are anywhere on open conductors.

A convenient subdivision of the problem as a whole may be made along the lines of the laboratory apparatus itself, namely (I) the transmission line to which the unknown impedance is connected; (II) the excitation including generator, feeder, and coupling unit; and (III) the detector, i.e., the current and voltage measuring devices with their calibration. Actually these topics are by no means independent of each other, as will become apparent.

THE TRANSMISSION LINE

Treatment of the transmission line ordinarily begins with the fundamental differential equations which are solved subject to boundary conditions yielding useful relations. The practical utility of these final forms is of primary importance to the experimental physicist and engineer. With this in mind, one may proceed from the opposite starting point; that is with those quantities which can be measured conveniently on two concentric or parallel conductors. They are few, consisting of the shape and position of (1) the resonance curve and (2) the current and voltage distribution curves. Specifically, the relative positions of the maxima for two measurements determine a phase shift, where the maxima may be either of current or voltage, or the peaks of the resonance curves. The breadth of the resonance curve is one measure of the damping in the circuit; another method for obtaining the damping depends on the "standing wave" ratio of maximum to minimum in the current or voltage distribution curves. The theoretical basis for these measurable quantities will now be considered, with special reference to the practical consequences.

Let the circuit be as in Fig. 2; the transmission-line parameters are r, l, c, and g, respectively in units of ohms, henrys, farads, and mhos, all per loop unit length of line. The following derived quantities are useful; their mathematical derivation may be found elsewhere.[1,2]

$$k=\alpha+j\beta=[(r+j\omega l)(g+j\omega c)]^{\frac{1}{2}}, \qquad (1a)$$

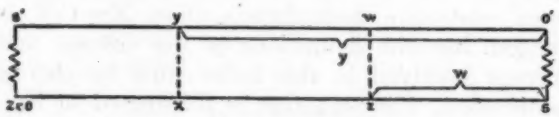

FIG. 2. Circuit of a two-wire line.

[1] R. King, Proc. I.R.E. 29, 640 (1941).
[2] R. King, J. App. Phys. 14, 577 (1943).

where k is the complex propagation constant, α the attenuation in nepers per unit length, and β the phase shift in radians per unit length.

$$Z_c = R_c(1-j\varphi) = [(r+j\omega l)/(g+j\omega c)]^{\frac{1}{2}}, \quad (1b)$$

where Z_c is the characteristic impedance of the line with real part R_c, and imaginary part, $-\varphi R_c$

$$\varphi = 1/2\omega(r/l - g/c), \quad (1c)$$

$$\Theta_n = \rho_n + j\Phi_n = \coth^{-1}(Z_n/Z_c); \quad n = o, s. \quad (1d)$$

The subscripts o and s refer to the two ends of the line respectively.

$$A = \alpha s + \rho_o + \rho_s; \quad (1e)$$

$$F = \beta s + \Phi_o + \Phi_s. \quad (1f)$$

In general, A represents the total damping of the entire circuit. It contains the term αs for the length of line s, ρ_o for the termination at $z=o$, and ρ_s for the termination at $z=s$. Similarly, F is a measure of what might be called the total phase shift, and contains three terms also; βs for the line of length s, Φ_o for the termination at $z=o$, and Φ_s for the termination at $z=s$. A movable bridge with tandem or a piston terminates the line at $z=0$, and various impedances may be attached at $z=s$. Initially, let the detector be located at z along the line, and the driving unit at x, with $x<z$. For the case of a voltage fed line with *loosely coupled* driving unit placed along the line, the current is given by

$$|I_z| = \frac{W_x'}{Z_c}\left[\frac{(\sinh^2(\alpha x+\rho_0)+\sin^2(\beta x+\Phi_0))(\sinh^2(\alpha w+\rho_s)+\sin^2(\beta w+\Phi_s))}{\sinh^2 A+\sin^2 F}\right]^{\frac{1}{2}}, \quad (2a)$$

where $w=s-z$ and W_x' is proportional to the generator voltage. If the line is current fed from a driving unit at x, $\sin^2(\beta x+\Phi_0)$ is replaced by $\cos^2(\beta x+\Phi_0)$ in the numerator. In either case, the voltage distribution is obtained from (2a) by substituting $\cos^2(\beta w+\Phi_s)$ for $\sin^2(\beta w+\Phi_s)$. Therefore only the form of the numerator is affected by changes in the type and location of driving unit and detector. The various forms of this equation are taken from Eqs. (75)–(77) of the second reference, where the derivation may be found. All the information necessary for the resonance-curve method of measuring phase shift and damping can be obtained from the simplified equation.

$$|I_s|^2 = \left(\frac{W_x'}{Z_c}\right)^2 \frac{f(x,w)}{\sinh^2 A+\sin^2 F}. \quad (2b)$$

This form tacitly assumes that tuning to resonance will be accomplished by changing the length of the line and not by varying the frequency. Experimentally this is convenient; mathematically it is essential.

The condition for a maximum value of $|I_s|$ may be derived from (2b) by solving the equation $(\partial|I_s|/\partial s)_{x,w}=0$. The result so obtained specifies the location of the resonance-curve peak in terms of the variable length of line s. It is

$$F = n\pi, \quad n = 0, 1, \cdots, \quad (3)$$

provided

$$(\alpha/\beta)^2 \sinh^2 2A \ll 1. \quad (4)$$

If the resonance curve is to be useful for measuring purposes, the conditions (4) must be satisfied. In a low loss line the quantity $(\alpha/\beta)^2$ is of the order of magnitude of 10^{-6}; the value for the actual case to be discussed was 0.905×10^{-6}. It follows that $\sinh^2 2A$ must take on very large values before the limitation imposed by Eq. (4) takes effect. Since αs will be small for all lengths of transmission line attainable indoors, the terminal impedance is the dominant term for large values of over-all damping A. Curves plotted elsewhere[2] show that the line must then be nearly non-resonant: for $\sinh^2 2\rho_s > 1000$, R_s is within 5 percent of R_c. Except for this narrow range of values near the characteristic resistance of the measuring line, the terminal impedances to be determined are unrestricted by (4).

For phase-shift determinations, Eq. (3) suffices. For arbitrary damping, let F_1 be the initial condition of resonance along the transmission line, and F_2 the final. The first resonant length s_1 involves the terminations ρ_{01}, Φ_{01} and ρ_{s1}, Φ_{s1}. Suppose the second resonance was obtained with a new termination at s, ρ_{s2}, Φ_{s2}, but with the same piston or bridge at $s=0$. Then

$$F_1 = \beta s_1 + \Phi_{01} + \Phi_{s1} = n\pi; \quad (5a)$$

$$F_2 = \beta s_2 + \Phi_{01} + \Phi_{s2} = n\pi. \quad (5b)$$

Subtraction gives

$$\beta(s_1 - s_2) + (\Phi_{s1} - \Phi_{s2}) = 0. \quad (6)$$

Since $\beta = 2\pi/\lambda$ here, Eq. (6) conveniently relates the phase shift of two different terminations. There is, however, a restriction on the measuring procedure implied in Eq. (2b),

namely the numerator of the expression for I_s must not be a function of the total length s. This can be satisfied in two ways.

(a) The driving unit at x is moved with the bridge or piston at 0, and the detector is located at a fixed distance w from the end at s. Thereby x and w are kept constant and independent of the total length s.

(b) By the simple transformation $o'=s$ and $s'=o$, the ends at o and s are interchanged. This amounts to an interchange of x and w. Therefore, the detector at w is now moved with the bridge or piston at the new o', and the driving unit at y is kept at a fixed distance x from s'.

Which of these two arrangements is adopted depends on whether it is more convenient to move the driving unit or the detector. However, *one or the other must be used*, for otherwise the condition for maximum (3) contains the damping terms in a complicated fashion. Unless all damping is negligible, this prevents a simple solution for the phase factors alone.

The width of the resonance curve between the points $I_s^2/2$ will yield the over-all damping provided this is not too large. The necessary formula is obtained from (2b), as before. Let the subscript m denote the values of A and F at the maximum $|I_s|$, and the subscript p those at the half-power point $I_s^2/2$. Then

$$|I_s|^2_{\max}=\frac{(W_x^e)^2f^2(x,w)}{Z_c^2}\left[\frac{1}{\sinh^2 A_m}\right]; \quad (7a)$$

$$\frac{|I_s|^2_{\max}}{2}=\frac{(W_x^e)^2f^2(x,w)}{Z_c^2}\left[\frac{1}{\sinh^2 A_p+\sin^2 F_p}\right]. \quad (7b)$$

Eliminating the common factors gives

$$\sinh^2 A_m=\tfrac{1}{2}[\sinh^2 A_p+\sin^2 F_p]. \quad (8)$$

Now put

$$A_p=A_m\pm\delta A, \quad F_p=F_m\pm\delta F. \quad (9)$$

Upon substituting for A_p and F_p and using addition formulas, one obtains:

$$\sinh^2 A_m=\sin^2 \delta F, \quad (10)$$

subject to the condition that

$$\tanh A_m\gg 2\tanh \delta A. \quad (11)$$

The fulfillment of this condition also assures a symmetrical resonance curve, which had been assumed in Eq. (9). In practice, both computations and measurements are more easily carried out if the over-all damping is kept low enough to permit substituting the arguments for the functions in Eq. (10). For a maximum error of 4 percent values of A_m up to 0.5 can still be handled in the simplified form

$$A_m=\delta F. \quad (12a)$$

Since only the length is varied, this reduces to

$$A_m=\beta\left(\frac{\delta s'+\delta s''}{2}\right) \quad (12b)$$

where $(\delta s'+\delta s'')$ is simply the width Δs of the resonance curve at the half-power point. With (12b) the condition (11) reduces to

$$\beta/2\alpha\gg 1, \quad (13)$$

which is the equivalent of requiring a high Q transmission line.

A companion formula to the phase shift Eq. (6) can be obtained directly from (12b). Only the damping factors of the two terminations and the half-power widths of the resonance curves are involved if $\alpha(s_1-s_2)$ is negligible:

$$\alpha(s_1-s_2)+\rho_{s1}-\rho_{s2}=\beta/2(\Delta s_1-\Delta s_2). \quad (14)$$

Equations (6) and (14) constitute the resonance-curve method of comparing the phase shift and damping due to two different terminations, one of which is presumably known. An alternative procedure using the current or voltage distribution curves is also possible. Since the resonance peak is always sharper than the distribution maxima, the method is less accurate for phase-shift measurements. A comprehensive discussion of the subject in general may be found elsewhere.[3] However, if the damping is large, the resonance-curve method is no longer applicable. In this case one can certainly write

$$(\rho_o+\alpha s)\ll\rho_s, \quad (15)$$

which gives, from (2a)

$$\rho_s=\coth^{-1} S, \quad (16)$$

where S is the standing wave ratio. The determination of the standing wave ratio usually requires a detector accurate over a wider range than does the half-power point procedure. On the other hand, Eq. (16) is very satisfactory for values of $\rho>0.4$, and therefore complements the other method. To summarize, for standing wave

[3] O. Schmidt, Zeits. f. Hochfrequenz. 41, (January, 1933).

ratios of less than three, Eq. (16) is convenient; for ratios greater than three, the resonance-curve procedure with Eq. (14) is usually more accurate.

Two further questions appropriate to the line itself remain. The first concerns the standards of comparison ρ_{s1}, Φ_{s1}. Open ends are generally unsatisfactory because they involve boundary conditions that cannot be analyzed simply, thus making the precise calculation of damping and phase factor impossible. A conducting piston in a concentric line gives almost exactly

$$\rho_s=0; \quad \Phi_s=\pi/2.$$

The wire bridge on a parallel line of spacing and radius $b/a>5$ has the same values, provided one measures to the center of the bridge in computing the total length of resonant line.[2] A short dipole antenna offers another possible standard, since the analysis of the Hertzian dipole is accurate for short antenna lengths. This method is considered in Part II of this paper.

TABLE I.

Length s in meters	R_{in} in ohms	X_{in}
0.4990	1×10^3	25×10^3
.4998	200×10^3	200×10^3
.5000	300×10^3	about 0
.5002	40×10^3	-100×10^3
.5010	$.8\times10^3$	-20×10^3

The second question is a structural one: how shall the conductors of the line be supported to give two terminals for connection to the known and unknown impedances in turn? The effect of the supports may alter seriously the values obtained. The situation at the end of the line is represented by the circuit in Fig. 3. A support of admittance Y_s is located at $x=s-w$ on a line terminated in Y_s. The input admittance of the circuit at z is obtained at once from (1c)

$$Y_{in}=1/Z_c[\tanh(kw+\theta_s)+Z_cY_s]. \quad (17)$$

Assuming a low loss line and expanding, one has

$$G_{in}-jB_{in}=(G-jB)+\frac{\cosh\rho_s\sinh\rho_s+j\cos(\beta w+\Phi_s)\sin(\beta w+\Phi_s)}{R_s[\cosh^2\rho_s\cos^2(\beta w+\Phi_s)+\sinh^2\rho_s\sin^2(\beta w+\Phi_s)]}. \quad (18)$$

In order to minimize the effect of the shunt admittance of the support, the second term in (18) must be made large compared with the first term. Maximizing the imaginary part yields the condition

$$\tan(\beta w+\Phi_s)=\coth\rho_s=S, \quad (19)$$

where S is the standing wave ratio. This is equivalent to locating the support at a voltage node along the line. The susceptance of the support is thereby made negligible for all but very low standing wave ratios. The conductance of insulating supports is usually small. In a low loss line, $\alpha s<\rho$, this may be lumped with ρ_0 and subtracted, if it isn't already negligible. If more than one support is used, all must be moved to the proper positions *for each measurement*. In a concentric line with several supports this may prove difficult; on the other hand, the whole problem does not exist for a homogeneous (filled) coaxial system. Insulating stubs must satisfy the same conditions. Ordinarily the tuning of such stub sections of line is far too critical for precise adjustment to the desired value, as may be seen from computed curves of input admittance.[2] Thus, for example, the approximate table (Table I) is for a closed-end coaxial stub with $a=1$ cm, $b=3.5$ cm. This gives $R_c=75.13$ ohms, $\alpha=3.577\times10^{-4}$ nepers/meter. The wave-length is two meters. The whole table extends over a change in stub length amounting to 0.1 percent of the wave-length. Evidently extraordinary accuracy in adjustment is required to keep even the input resistance above say $100R_c$. The corresponding parallel wire system is very similar, but with a larger R_c.

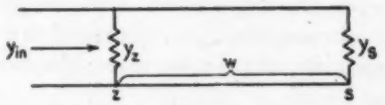

FIG. 3. End of a terminated line with a support.

DRIVING UNIT AND GENERATOR

According to Eq. (2a) the driving unit may be located anywhere along the line, including the ends. Coupling at either end has disadvantages for some applications. The end at $z=0$ is moved continually in the resonance-curve methods. This entails moving the feeder and coupling unit for every reading, if the line is driven from the end at $z=0$. Furthermore, locating the coupling unit along the line away from the ends facilitates detector calibration, as

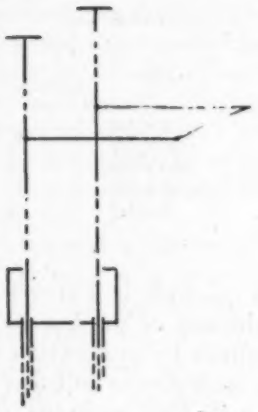

FIG. 4. Diagram of a balanced driving unit.

will be shown in the next section. Therefore, a driving unit placed along the measuring line between the ends is ordinarily preferable. A number of fairly stringent requirements should be fulfilled in a successful design for such a unit; they may be listed as follows:

(1) No significant external electric fields except near the point of coupling, are allowed in a parallel system, no surface currents on the outside of a concentric type. This is to avoid disturbance of the current distribution on measuring line and terminal impedance through stray fields and currents. A completely coaxial system automatically satisfies the requirement unless the slit area is made too large. If a parallel wire measuring line is used, a satisfactory result is achieved with a completely enclosed oscillator of the balanced type, feeding through a double coaxial line. The outside surfaces of the two coaxial cables are grounded, while the inner conductors are extended to form a parallel line near the point of coupling. Locating the change from double coaxial to open line at a voltage node leaves the outer surfaces unexcited, and thereby avoids possible strong fields along the outside of the feeder. Equal and opposite currents are also maintained on the short parallel section by this method. Such a driving arrangement is shown schematically in Fig. 4.

(2) There must be adequate provision for matching the oscillator to the feeder and the feeder to the coupling unit. This permits maximum power transfer to the coupling unit.

(3) Freedom of adjustment is required to allow change of spacing between coupling unit and measuring line, as well as motion along the length of the measuring line. In a parallel system it is of especial importance that the excitation of the line be balanced by keeping the coupling unit symmetrically beneath the wires. Thereby the necessary equal and opposite currents in the line conductors are maintained.

The generator itself is to furnish adequate power at constant amplitude and frequency. In order to secure a fixed amplitude a separate indicator is best attached to the oscillator tank circuit. The accuracy of this device should be at least equal to that of the current or voltage indicator used on the measuring line. The frequency must be kept within much closer limits since the phase constant β is multiplied by the total length of line used. Thus, in a line four wave-lengths long, an error of 1 mm in the wavelength is equivalent to an error of 4 mm in the location of the resonance-curve peak. This also requires a separate meter of the requisite accuracy loosely coupled to the oscillator.

A properly operated driving unit of this type should furnish ample excitation to the line without disturbing the relations used for making the measurements. Since action and reaction are inseparable here, the goal of adjustment must be to minimize or cancel out the effect of the coupling unit on the measuring line. In general, coupling units may be grouped in two classes, directly connected and electromagnetically coupled. In a direct connection loose coupling demands a very high input impedance as seen from the measuring line. This approximates the case of the insulating support, where tuning is extremely critical. Therefore, the other coupled types are easier to manipulate and are usually to be preferred. The degree of coupling is then a function of the spacing between coupling unit and driven line, as well as of the coupling unit's position along this line, and of the feeder tuning. Thus, a voltage antinode along the line gives the largest electric field about the conductors and permits close coupling to a sine-symmetrical or capacitive type of driving unit. A voltage node along the line conductors gives the largest magnetic field for close coupling to a cosine-symmetrical or inductive type of driving unit. A detailed discussion of the problem of electromagnetic coupling to a transmission line may be found elsewhere.[4]

Whatever the type used, a slight increase or decrease of coupling, as obtained by altering tuning, spacing, or position along the line, should

[4] R. King, Rev. Sci. Inst. 10, 325 (1939).

produce no detectable change in oscillator or line. By this is meant that oscillator amplitude and frequency should remain unaffected, as should the tuning of the resonant measuring line. Of course the amplitude on the measuring line will increase as one couples more closely. This precaution is made necessary by the nature of the secondary circuit. It can be shown that the degree of coupling between two circuits with distributed constants depends on their standing wave ratios as well as their separation and tuning. Hence, if the known and unknown measurements involve different damping, the effect of the driving unit will not remain constant. In addition, the location of the driving element along the measuring line should always be at the same electrical position. The point of maximum coupling is easily located for this purpose. The foregoing steps taken to minimize reaction back on the generator, and to maintain constant coupling, permit lumping the now constant loading of the driver with ρ_0, Φ_0, as was done with the support insulators.

DETECTORS

Simple high frequency detectors are often crystals or diodes in series with a microammeter. Both abstract energy from the line to cause the measured current. Therefore they must load the line, and again coupling must be reduced to make this effect negligible. Evidently, in the ideal case of very loosely coupled driver and detector the meter reading will be reduced to zero. Likewise, an over-sensitive meter and detector arrangement operating at low line amplitudes suffers inordinately from poor contacts and stray coupling. The amplitude required depends on the type of detector used. Acorn diodes work well at large signal amplitudes. However, when the rectified current falls to the point where a bridge is needed to balance out the emission current of 300 to 500 microamperes, they tend to drift. Furthermore, additional (heater) leads must be brought close to the high frequency circuits. By comparison, crystals require a minimum of space and wiring and are more stable when operated at low currents. Both types work best when properly loaded by the meter and series resistance if necessary.

Although a separate movable detector is useful for determining current and voltage distributions, the most elegant design incorporates the detector in the movable tandem bridge (or piston) used for tuning the measuring line. In this way the correct location along the line is automatically achieved for all bridge settings. The line itself carries the meter current, and the d.c. leads are thus completely detuned by the piston or tandem bridge. The over-all detector loading is now rigorously lumped with ρ_0, Φ_0 at all times, and subtracted in the analysis. If the detector is moved along the line independently this is no longer possible, and therefore constitutes a source of error in standing wave ratio measurements.

The last link in securing data is the calibration curve of the meter. There is no reason to suppose that the detector characteristic will remain invariant over the entire radiofrequency spectrum. Hence calibration is required *at the frequency and over the amplitude range to be used.* Inspection of Eq. (2a) shows that two convenient relations are available for this purpose. Suppose the line tuned to resonance; then

$$I_s \sim \sin \beta w, \tag{20a}$$

provided

$$\sinh^2 (\alpha x + \rho_0) \ll 1, \tag{20b}$$

and

$$I_s \sim \sin \beta x, \tag{21a}$$

provided

$$\sinh^2 (\alpha w + \rho_s) \ll 1. \tag{21b}$$

Equation (20a) is for motion of the detector along the line, (21a) for motion of the driving unit. One or the other of these relations permits repeated calibrations without any rearrangement of apparatus. A rapid test of the validity of the method is included in the procedure: if the current vanishes at the minima and the curve is symmetrical, the conditions for a sinusoidal current distribution have been met. Should the terminal impedance introduce excessive damping for (21b), the line usually can be short circuited without removing the termination at all.

A final test of the adjustment of driver and detector may be found in the shape of the resonance curves. A symmetrical curve is desired, and appreciable asymmetry is a good indication of undesirable close coupling. Often incipient double peaks can be found on such curves, and discontinuities (drag loops) are of course symptoms of extremely tight coupling. In this case the width and position of the curves bears no simple relation to the phase shift and damping introduced by the terminal impedances.

The results yielded by the method described are in terms of measured phase shifts. The transformations to X_s and R_s may be made

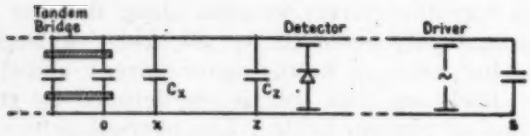

FIG. 5. Circuit for measuring a standard termination.

according to the relations

$$X_s = -R_c\left[\frac{\sin 2\Phi_s + \varphi \sinh 2\rho_s}{\cosh 2\rho_s - \cos 2\Phi_s}\right], \quad (22a)$$

$$R_s = R_c\left[\frac{\sinh 2\rho_s - \varphi \sin 2\Phi_s}{\cosh 2\rho_s - \cos 2\Phi_s}\right]. \quad (22b)$$

The term in φ usually may be neglected for low loss lines as the evaluation of φ from (1b) will show. In interpreting the results, it should be noted that although ρ_s and Φ_s are the products of independent measurements, their transformation gives R_s and X_s each a function of both independent variables. Hence an error in either measurement will cause both ohmic values to be incorrect in certain ranges of R_s and X_s. Specifically, ρ_s is the determing factor at resonance and anti-resonance, otherwise Φ_s has the greater effect on both R_s and X_s.

APPARATUS AND TECHNIQUE FOR MEASURING ANTENNA IMPEDANCES

The precise specifications of the apparatus used for determining the impedance of a symmetrical antenna are listed in the same sequence as in the preceding discussion.

The dimensions of the two-wire line made of brass wire are: $a = 8.95\times10^{-4}$ meter, $b = 1.0\times10^{-2}$ meter. This gives the following values for the parameters listed.

$r = 11.14\times10^{-2}$ ohm/meter.
$l = 1.242\times10^{-8}$ henry/meter.
$c = 9\times10^{-12}$ farad/meter.
g = negligible.
$R_c = 372.5$ ohms.
$\alpha = 1.50\times10^{-2}$ neper/meter.
$\phi = 9.48\times10^{-4}$.

The load end of the line was supported by a Bakelite disk 2 cm in diameter and 1.5 cm thick; small steel set screws held the line under tension. By measurement from the tandem bridge at resonance, the center of the disk was located at a voltage node ±0.5 mm. Although the maximum phase shift obtainable from the support alone was over 1 cm when moved to a current node, no change was discernible over an interval ±1 mm about the voltage node. All linear measurements were made on standard meter sticks at an estimated accuracy of ±0.5 mm. Since the resonance curves are the result of numerous points, their accuracy is much better than this.

The standard termination was a 30-mmf postage-stamp capacitor with leads some 5 mm long. ρ_{s1} was assumed to be zero for lack of a better standard. The evidence at short antenna lengths indicates that this introduced an appreciable error only for values of R_s less than 20 ohms. Φ_{s1} was measured with the arrangement[5] in Fig. 5.

The circuit was tuned to resonance with the capacitors at x and z removed. Next, by placing C_z exactly one-quarter wave-length ahead of the tandem bridge, the previous resonance was destroyed, and the detector output reduced from maximum to zero. Finally, C_z was moved along the line from x toward s. After passing through a resonant point near $z = x + (\lambda/4)$ the line was again completely detuned near the point $z = x + (\lambda/2)$. Then

$$2\Phi_{1s} + \beta(z - x) = \pi. \quad (23)$$

The average value so obtained was $\Phi_{1s} = \pi/2 + 0.55\beta \pm 0.05\beta$. The limit of error here, together with a similar error in the exact location of resonant peaks in all the measurements, gives a total error of ±0.03 radian for Φ_{1s}. The value of β at the wave-length used is 0.1576 rad./cm.

The design of the oscillator used may be found elsewhere.[6] The oscillator and a 9002-voltmeter diode were completely enclosed in an aluminum case fitted with long shielded power supply leads. Two flexible cables formed a double coaxial feeder which terminated in a 25-cm section of paralliel line mounted vertically on a movable base beneath the measuring line. In order to permit adjustment for maximum power transfer and minimum surface currents, each coaxial cable contained an adjustable length section at the oscillator end, and a movable stub was mounted on the open parallel line section. Two 5-cm rods formed a double "T" at the end of the feeder. The tops of the "T" sections were 3 cm from the measuring line. The driving unit is as in Fig. 4.

Oscillator output amplitude was kept constant to within less than one-half percent of peak, as measured on the auxiliary diode volt-

[5] R. King, Proc. I.R.E. **23**, 408 (1935).
[6] R. King, Rev. Sci. Inst. **11**, 270 (1940).

meter in the casing. A calibrated coaxial wavemeter coupled permanently to the oscillator indicated the standard wave-length: 39.86 ± 0.005 cm. Frequency was varied by means of the plate voltage, while amplitude compensation was achieved through filament current adjustment. Thermal drifts and poor regulation of input voltages could be equalized readily. Also, at very low oscillator power input, there was some reaction on its amplitude from line tuning, which had to be compensated. Frequency changes occurred only as slow drifts with the operating temperature rise and were fully compensated.

Tungsten-silicon crystals in 1-cm polystyrene cartridges were used in series with a 334-ohm Weston 0–30 microammeter. Equation (23) required a movable detector; otherwise a tandem-bridge current detector was used. The circuit arrangement of this device, as shown in Fig. 6,

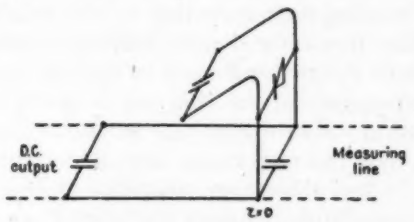

FIG. 6. Tandem bridge with crystal detector.

allows for motion of both crystal and capacitor along the stub sector above the tandem bridge. By adjusting these two variable elements, both high sensitivity and low line loading could be attained. Thus the phase shift for the bridge with detector tuned for high sensitivity was $\Phi_{10}=\pi/2+0.65\beta$ as compared with $\pi/2+0.55\beta$ without the crystal and stub assembly mounted. A calibration was made for each resonance curve by moving the driving unit. Only five points are needed for this: two minima, a maximum, and two at $0.707\,I_{max}$. Equal spacing between these points and minima less than 1 percent of peak reading assure the existence of a true sine distribution along the line as required. In the course of the measurements the half-power point drifted slowly within the interval 14.2 and 15.5 (30 was peak throughout).

One of the three sets of curves obtained is shown in Fig. 7. The group illustrates the consistency of the experimental data and the uniform symmetry of the peaks, but not the true shape of the resonance curve of the circuit. This is because the calibration has been incorporated in fixing the level of the half-power point rather than in reshaping the curves. Thereby the single point calibration suffices for each curve. The smoothness of the curves should check any sudden changes in calibration or intermittent contacts along the line wires. However, in spite of the independent calibrations used for each resonance peak, an error of 5 percent in ρ_{2s} seems quite possible.

Three individual peaks are drawn separately in Fig. 8. They comprise the broadest and the narrowest curves of the whole series of measurements, together with a curve of average width. As a concrete illustration of the methods described, the numerical values of the phase shift

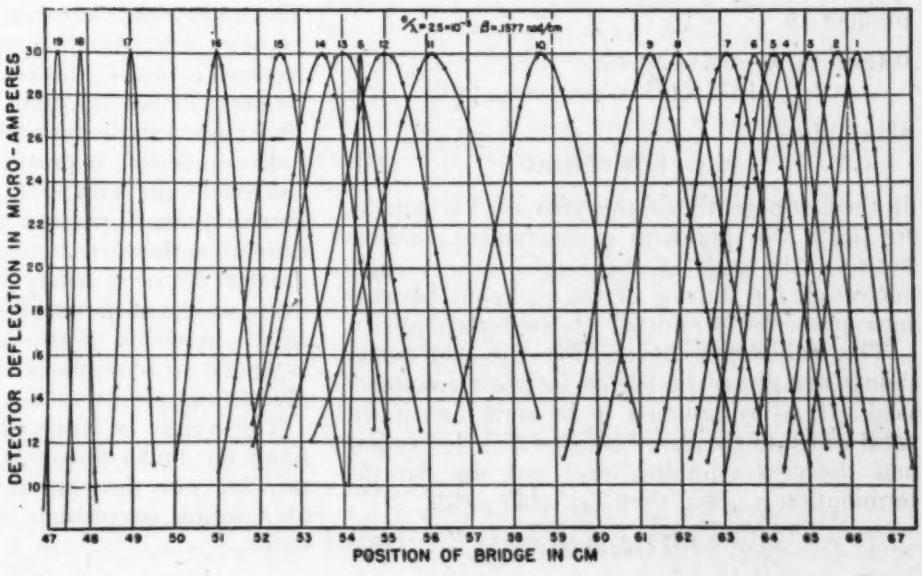

FIG. 7. A family of measured resonance curves. The termination is very close to 194 on the scale for all curves.

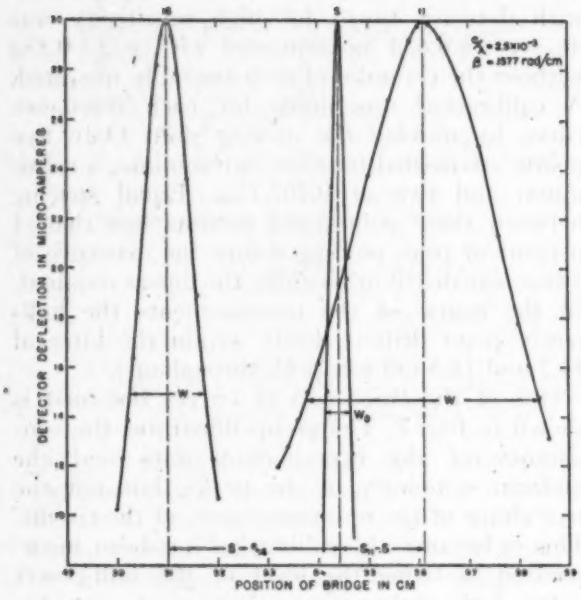

FIG. 8. Detail for sample calculation. The antenna half-lengths h are 11.9 cm for curve 11 and 8.75 cm for curve 16.

and damping function Φ_{s2} and ρ_{s2} for the curves 11 and 16 are calculated by means of Eqs. (6) and (14). Taking the value 0.55β for Φ_{s1} and the positions for s_1 and s_2 given by the graph, one has from Eq. (6)

$$0.1577[(56.1-0.5)-54.4]+[(0.1577\times0.55+\pi/2)-\Phi_{s2}]=0, \quad (24a)$$

which gives

$$\Phi_{s2}=1.75 \text{ radians} \quad (24b)$$

for curve number 11. Similarly, for curve number 16

$$0.1577[(51.0-0.5)-54.4]+[(0.1577\times0.55+\pi/2)-\Phi_{s2}]=0, \quad (25a)$$

which gives

$$\Phi_{s2}=1.04 \text{ radians}. \quad (25b)$$

In the first parenthesis, the term -0.5 is included to place the point of measurement midway between the ends of the conductors. A slight correction for shifting of the endpoint between measurements is omitted above for simplicity.

The calibration levels for the half-power points are drawn in Fig. 8 for each resonance peak. If ρ_{s1} is assumed to be zero, i.e., if the total width of the curve labelled S is due to line and detector damping, and not due to the termination ρ_{s1}, Φ_{s1}, then Eq. (14) yields

$$\rho_{s2}=(0.1577/2)(4.63-0.5), \quad (26a)$$

or

$$\rho_{s2}=0.326 \quad (26b)$$

for curve 11, and for curve 16.

$$\rho_{s2}=(0.1577/2)(1.495-0.5), \quad (27a)$$

or

$$\rho_{s2}=0.0785. \quad (27b)$$

In connection with the last results, it is interesting to compare the procedure used with the standing wave-ratio method given by Eq. (16). The standing wave ratio S, as calculated from this relation, turns out to be 2.9 for curve 11 and 12.7 for curve 16. The smaller value of S agrees approximately with an experimental value taken merely as a check. On the other hand, no experimental check was attempted for large values of the standing wave ratio S. Thus, for the larger standing wave ratio above, the minimum is so low that it lies in the curved portion of the parabolic calibration curve. The meter reading corresponding to this minimum is according to a crystal calibration extending over the whole range from zero to the maximum of 30 microamperes. In this particular case, the calibration curve was so flat in the extreme low ranges that the meter was virtually without sensitivity, and therefore useless. Operation at larger amplitudes makes the curvature of the crystal response less unfavorable for standing wave-ratio determinations, but the resonance-curve method always involves a straighter and shorter segment of the calibration graph. This fact, together with the complete elimination of detector loading in the resonance-curve procedure, prompted the adoption of this method for the measurements of antenna impedances. The range near non-resonance, excluded because of very low standing wave ratio and broad resonance peaks, turned out to be of no consequence, since it could be shifted by altering the characteristic impedance of the line.

In conclusion, it must be noted that although the maximum error in R_a and X_a should not be greater than 10 percent according to the above estimates, there are two regions where it may be greater. Namely, when either the numerator or denominator of the expressions (22) becomes very small. In effect, a two-place accuracy is then extended to four places since the first two significant figures are zeros.

The writer is indebted to Professor Ronold King for much encouragement and advice in carrying out the experimental work, and also for valuable suggestions in preparing the manuscript.

Microwave Impedance Measurements with Application to Antennas. II

RONOLD KING AND D. D. KING
Cruft Laboratory and the Research Laboratory of Physics, Harvard University, Cambridge, Massachusetts
(Received February 16, 1945)

Following a critical discussion of the problems of theory and experiment and their coordination, experimentally determined curves for the impedance of a symmetrical, cylindrical antenna terminating a two-wire line are given and interpreted. The conclusion is reached that the impedance of an antenna, especially near anti-resonance, depends in a large measure on the proximity and the nature of the input terminals.

INTRODUCTION

THE solution of problems in applied electromagnetism, such as the general determination of the impedance of an antenna, may be resolved into three parts. They are, first, a theoretical analysis consisting of a more or less exact solution of Maxwell's equations based on suitably chosen boundary conditions; second, a sequence of experimental measurements involving an appropriately designed apparatus and tables of pointer readings; and third, a critical coordination of the conditions existing in the experiment and its observations with the postulates and qualitative as well as quantitative predictions of the theory. In a systematic study, a preliminary examination of the difficulties of coordination may advantageously precede both the theoretical and experimental investigations, since the boundary conditions in the theory and the construction of the apparatus, as well as the technique of measurement in the experiment, may depend in a large measure upon the ability to resolve the problem of establishing a direct and simple correspondence between predicted and observed pointer readings. A not uncommon and dangerously misleading practice is to display theoretical and experimental results in juxtaposition and assume as a matter of course that a one-to-one correspondence necessarily exists between them. In some cases this may be true approximately; in others it is certainly not true. In no case should experimental data be plotted with theoretical curves without a careful examination into the foundations of the analysis and the experiment actually involved. In many instances disagreement between experimental and theoretical results may be a better check on the theory than close agreement.

The determination of the self-impedance of an antenna of non-vanishing cross section is one of the more difficult problems in electromagnetic engineering from the points of view alike of theory, experiment, and the coordination of theory with experiment. The complete investigation of an antenna must concern itself with three things: the antenna proper, the driving device with its terminals, and the surrounding universe. All three of these individually and together interpose serious difficulties in the way of a completely accurate and simple solution of the theoretical and experimental problems. It is not the purpose of this discussion to consider in detail either the mathematical difficulties encountered in the solution of the theoretical boundary-value problem, nor the experimental questions involved in accurate measurement using a particular apparatus. These are considered in companion papers[1,2] and elsewhere in the literature.[3–8] The purpose of this paper is to study in some detail the problem of interpreting and coordinating theoretical and experimental results on the impedance of simple antennas by examining the hypotheses and approximations contained in the theory and the apparatus used in typical experiments. Since on the whole theory is somewhat more severely restricted by the mathematical difficulties involved in obtaining a dependable solution than is experiment by the available apparatus, it seems well to begin the discussion by considering how a theoretical antenna can be approximated experimentally by an actual one.

THEORETICAL ANTENNA

The theoretical problem originally analyzed by Hallén[3] and re-examined by others[3–6, 8–10]

[1] D. D. King, J. App. Phys. 16, 435 (1945).
[2] R. King and D. Middleton (submitted to J. App. Phys.).
[3] E. Hallén, Nova Acta, Upsala (1938).
[4] R. King and F. G. Blake, Jr., Proc. I.R.E. 30, 335–349 (1942).
[5] R. King and C. W. Harrison, Jr., Proc. I.R.E. 31, 548–567 (1943).
[6] R. King and C. W. Harrison, Jr., J. App. Phys. 15, 170–185 (1944).
[7] S. A. Shelkunoff, J. App. Phys. 15, 54–60 (1944).
[8] L. Brillouin, Quart. App. Math. I, 201–214 (1943); Elec. Commun. 22, 11–39 (1944).

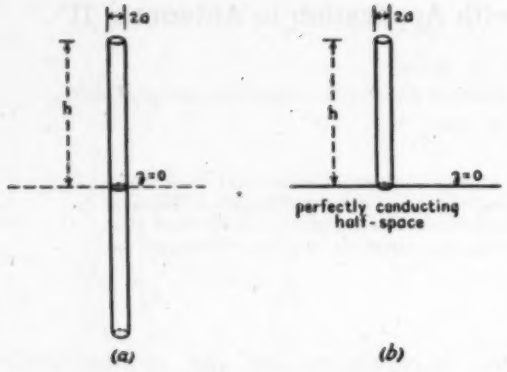

FIG. 1. (a) Center driven symmetrical antenna with flat ends; (b) base driven antenna over an infinite perfectly conducting plane. An idealized "slice" generator is shown shaded.

investigates the theoretical model of an antenna consisting of a symmetrical conductor of radius a and half-length h, shown in Fig. 1a. It is driven at its center $z=0$ by a periodically varying discontinuity in the scalar potential,

$$\Phi_{+0}-\Phi_{-0}=V_0^e.$$

An alternative, and theoretically equivalent problem is that of an antenna of length h and radius a erected vertically on a perfectly conducting half-space defined by $z=0$ in Fig. 1b, and driven at its base, $z=0$, by a discontinuity in scalar potential $\Phi_{+0}-0=\frac{1}{2}V_0^e$.

Subject to the conditions

$$\beta a=(2\pi a/\lambda)\ll 1;\quad a\ll h, \tag{1}$$

it is an excellent approximation to assume that the cross-sectional distribution of current in the conductor is independent of the axial distribution and, therefore, the same as in a conductor of the same radius but infinite in length. In this manner a difficult, three-dimensional problem is reduced to the simpler, one-dimensional problem of determining the total axial current I_z as a function of the driving potential difference V_0^e (or $\frac{1}{2}V_0^e$). The cross-sectional distribution is that given by conventional skin-effect theory which, in fact, always assumes it to be independent of the axial distribution. The conditions (1) limit the solution depending upon them to conductors of quite small cross section so that no legitimate application to antennas of large radius can be made. These involve an essentially three-dimensional problem.

[9] M. C. Gray, J. App. Phys. 15, 61–65 (1942).
[10] J. Bouwkamp, Physica 9, 609 (1942).

END SURFACES

As a consequence of the one-dimensional nature of the problem actually solved, no account is taken of the end surfaces of the antenna at $z=\pm h$. Although the area πa^2 of each of these is very small compared with the cylindrical half-surface $2\pi ah$, they are necessarily at points of maximum concentration of charge on the antenna, so that the error involved in nelgecting them is much greater than the ratio $a/2h$ of the areas of the end and cylindrical surfaces. This is true especially because very great concentrations of surface charge must exist at the sharp edges of the cylindrical ends. Thus the boundary condition

$$I_h=0, \tag{2}$$

which is imposed in the solution is applied correctly to an antenna which has *only* a cylindrical surface and *no* end surfaces or edges. It might be supposed that a metal tube is a physical counterpart of such an antenna. But this is not true. A tube has not only sharp edges but also an inner surface which is just as significant near the open end as the flat ends of the solid metal cylinder. The theoretically assumed condition (2) is not correct for either a solid or a hollow cylinder. In both cases, small currents exist at the ends, on the one hand to charge the flat end surfaces, on the other hand to charge a part of the inner surfaces near the ends. Although this current is small if (1) is true, its existence is roughly equivalent to making the antenna longer than h by an amount *at least* of the order of magnitude of the radius a. If h is near values producing anti-resonance, the curves of both resistance and reactance as functions of βh are so steep that a small error in h may lead to very large errors in R_0 and X_0. This difficulty is overcome quite simply and to a satisfactory degree of approximation whenever (1) is satisfied, if the theoretical and fictitious antenna of half-length h and radius a which satisfies (2) is assumed to be the approximate equivalent of an actual antenna (of the same radius and half-length measured along the axis) which has hemispherical ends. It is to be noted that the fictitious antenna has a superficial area equal to $4\pi ah$ not including the end surfaces since they are assumed to remain uncharged in the one-dimensional analysis. The actual antenna has an external surface given by $2[(h-a)2\pi a+2\pi a^2]=4\pi ah$. Thus the surfaces which are assumed to be chargeable in the two cases are equal in area and have essentially the same radii of curvature. Moreover, neither the

analysis of the fictitious antenna nor the approximate physical equivalent includes sharp edges where especially large concentrations of charge must exist. Accordingly, the one-dimensional analysis of the fictitious antennas of Figs. 1a, b subject to (1) and (2) and completely disregarding the end surfaces, should be a good approximation of Figs. 2a, b also subject to (1) and (2) at least insofar as the ends of the antenna are concerned.

DRIVING CONDITIONS

Just as the condition (2) makes the theoretically analyzed antenna fictitious at its ends, so the driving condition

$$\Phi_{+0}-\Phi_{-0}=V_0^e \qquad (3)$$

makes it fictitious at its center. Clearly, a driving potential difference consisting merely of a discontinuity in scalar potential at $z=0$ in a conductor extending from $z=-h$ to $z=h$ is physically unrealizable. Since the conductor is continuous and unbroken at $z=0$, and since concentrations of charge and of high frequency current can be maintained only on or near the surface of a good conductor, it follows that the discontinuity which acts to maintain a scalar potential difference on the two sides of the plane $z=0$ through the antenna, must be localized primarily in a thin ring around the surface at $z=0$. Thus the driving generator actually assumed in the theory is *not a point-generator* but is a disk or *ring generator* of zero thickness. Although physically neither ring generators nor point generators are available, such generators are the only ones that are theoretically sufficiently simple to permit a straightforward analysis of the distribution of current, and hence of the impedance which is defined as the ratio of the discontinuity of the scalar potential at $z=0$ to the total axial current at $z=0$.

A ring generator such as is assumed in the theoretical analysis involves no adjacent, parallel, chargeable surfaces. Therefore, two wires placed end to end with a gap between them differ significantly from the theoretical antenna in that they have two adjacent surfaces each of area πa^2. Since these surfaces are necessarily very close together compared with the wave-length, conventional or near-zone circuit theory is a good approximation in determining their effect. Accordingly, the two adjacent, chargeable surfaces may be treated as the approximate equivalent of a parallel-plate condenser connected across

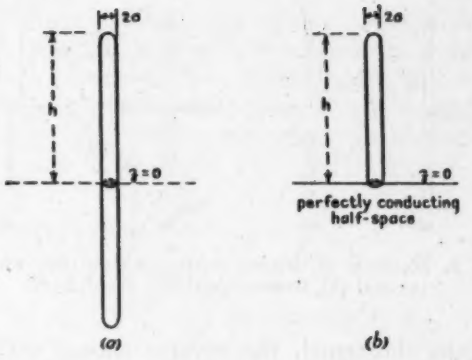

FIG. 2. Like Fig. 1 with antennas with hemispherical ends

the driving terminals of the antenna. The magnitude of this capacitance depends upon the separation of the ends. If the gap is less than the radius of the wire the capacitance is relatively large and significant. Its effect on the impedance of the antenna has been discussed elsewhere.[6] In broad outline, its effect is to lower anti-resonant resistances, to decrease the inductive lobes as compared with the capacitive lobes of the reactance curves, and to shift all resistance and reactance curves toward smaller values of $\beta h=\omega h/v_0$; $v_0=3\times10^8$ m/sec. The impedance of an antenna with a lumped capacitance across its terminals is in some respects similar to the impedance of an antenna of larger radius.[6]

Two wires placed end to end with a gap between them differ from the fictitious, continuous conductor with a disk or ring generator not only in having parallel end surfaces which may be approximated by a condenser, but also in having a gap. The additional, chargeable surfaces due to the adjacent circular ends are more or less offset by a reduction in the likewise adjacent, chargeable, *cylindrical* surfaces *cut out by the gap*. Thus, whereas the parallel, circular, end surfaces are approximately equivalent to an added capacitance in parallel across the terminals, the absence of adjacent cylindrical surfaces is roughly equivalent to a decrease in capacitance across the driving terminals. If the gap is small compared with the radius, the added capacitance due to the parallel end surfaces may exceed that effectively subtracted as a result of the non-existent cylindrical surfaces in the gap. If the gap is large compared with the radius, the subtracted capacitance very much exceeds that added. Whereas in the former case anti-resonant resistances were reduced, reactances made more capacitive, and anti-resonant

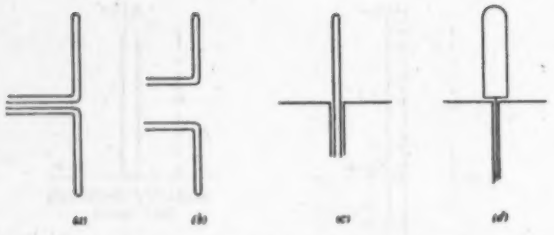

FIG. 3. Methods of driving antennas from two-wire line (*a*) and (*b*), from coaxial line (*c*) and (*d*).

lengths shortened, the reverse should occur in the latter case. Several practical methods of driving antennas from transmission lines are shown in Fig. 3. None of these is equivalent to the axially dimensionless disk or ring generator assumed in the theory. In Fig. 3a the adjacent end surfaces of the antenna halves, across which a potential difference is maintained by the line, may be expected to be at least roughly equivalent to the theoretical antenna with an *added* capacitance in parallel. The wide gap in Fig. 3b should be equivalent to an antenna with less capacitance across the generator than in the theoretical case. The coaxial drive of Fig. 3c probably approximates the theoretical antenna most nearly insofar as the driving potential difference is concerned. The ring generator at the base of the theoretical antenna is replaced by a gap in the conducting plane across which a potential difference is maintained by the line. The arrangement in Fig. 3d undoubtedly involves an added capacitance across the driving terminals as compared with the theoretical antenna. Convincing experimental verification is given in a recent paper.[11]

THE SURROUNDING UNIVERSE

The theoretical analysis of the impedance of a cylindrical antenna assumes the antenna to be so far from all conductors and dielectrics that the forces due to currents and charges in them are negligible at all points in and on the antenna compared with the forces due to currents and charges in other parts of the antenna. This does not mean that the antenna is isolated in the sense of being completely shielded from the effects of the universe at large. Quite on the contrary, it means that all *parts* of the universe are kept sufficiently far away so that *only the composite effect* of the completely and roughly symmetrically surrounding universe is experienced by the accelerated charges in the antenna. All parts of the universe are said to be in the *far* or *radiation zone* of a driven antenna, if moving or removing any one part produces no detectable effect on the distribution of current and hence on the impedance of the antenna. This usually means that an antenna must be many wave-lengths from all conductors. If the antenna is many meters long, as at broadcast frequencies, it is usually physically impossible to remove the antenna sufficiently from the surface of the earth to satisfy the condition for the far zone. Therefore, long wave measurements must be in terms of antennas consisting of arrangements of conductors of which the earth is an inevitable and highly significant part. Because of the irregularity of surface and the variety of electrical properties, an antenna which includes the earth as an important part is most undesirable from the theoretical point of view of calculating impedance. The earth is neither perfectly conducting nor infinite so that the theoretical boundary-value problem of a cylindrical conductor over the earth is hopelessly intricate insofar as an accurate solution for the impedance is concerned.

On the other hand, long wave measurements have the great advantage over those at very short wave-lengths that they can be made with instruments that in themselves are of such negligible dimensions compared with the wave-length that ordinary electric circuit theory is an excellent approximation and experimental techniques are relatively simple and exact.

An antenna that is to be many wave-lengths away from all parts of the universe, and hence from all surrounding objects, must be comparatively small and, therefore, operated at frequencies in the hundreds of megahertz. If measurements are to be made indoors, the wave-length must be short compared with the minimum dimensions of the laboratory. Furthermore, the walls of the building may not contain sheets of metal comparable in size with or larger than the wave-length. In practice, this means that using specially constructed outdoor facilities a vertical, center-driven antenna may be assumed to be symmetrical and isolated for purposes of impedance measurement, if its nearest point is a wave-length or two from the earth's surface, and five to ten wave-lengths from *parallel* conductors including the feeder. If the antenna is horizontal, the distance from the earth must be five or more wave-lengths. Clearly, broadcast frequencies are

[11] G. H. Brown and O. M. Woodward, Proc. I. R. E. **33**, 257–262 (1945).

completely out of the question and only pretentious facilities would permit the use of frequencies much below 50 megahertz. For indoor measurements using a center-driven antenna in the middle of a large room, frequencies in excess of 600 megahertz are required if the antenna is to be at least five wave-lengths from walls, floor, and ceiling. An antenna erected vertically over a conducting ground plate as in Fig. 3c is desirable because its driving conditions approximate the theoretical ring generator moderately well. On the other hand, the infinite, perfectly conducting half-space is completely unavailable, and any ground plate of finite size differs from the infinite conducting surface in that radial *standing waves* of current exist on it, rather than traveling waves as in an infinite plane. As a result, the field due to the finite metal plate differs considerably from that due to an infinite conducting surface. In particular, the field in the lower half-space in the case of a finite plate is not zero as it is with the unbounded surface. If the field due to the current is different in the two cases, the current and, hence, the impedance also must be different. Therefore, experimental measurements of impedance made on a vertical antenna over a metal plate of finite radius may be compared correctly only with the theoretical analysis of an antenna over such a *finite plate*, and not with those of an antenna over an infinite plane. Unfortunately, the former is a vastly more difficult boundary value problem than the latter. Probably the best that can be done experimentally is to increase the radius of a circular metal plate in steps not larger than $\lambda/4$ (and certainly not $\lambda/2$) until a further increase produces no detectable difference in the measured impedance of the antenna, and then to *assume* that the impedance of the antenna consisting of a vertical conductor over a plate of finite radius is equal to that of the same vertical wire over a plate of infinite radius.

THE DEFINITION OF IMPEDANCE

As discussed in the introduction of Part I, the impedance connected between two terminals A and B is defined conventionally in terms of the potential difference V_{AB} across these terminals and the currents I_A and I_B, respectively, entering and leaving the terminals. Specifically,

$$Z_{AB}=V_{AB}/I_A=V_{AB}/I_B, \qquad (4)$$

where it is assumed that I_A and I_B are equal and in the same direction around the contour of the circuit. This definition implies that the terminals A and B are so close together that in integrating the electric field *across the air gap* from A to B, the contribution to the integral by the time-rate of change of the vector potential $\mathbf{A}$ is negligible compared with the contribution by the scalar potential Φ. That is,

$$\int_A^B (\boldsymbol{E}, d\boldsymbol{s})=-\int_A^B \left\{\frac{d\Phi}{ds}+j\omega A_s\right\}ds$$

$$\doteq -\int_A^B d\Phi=\Phi_A-\Phi_B=V_{AB}. \qquad (5)$$

It is to be noted that the line integral of the vector potential from A to B is not independent of the path of integration as is the integral of the scalar potential. (For example, if a coil is connected between the terminals, the line integral of $j\omega A_s$ around the contour of the wire forming the coil from one terminal to the other gives the total inductive reactance of the coil multiplied by the current entering and leaving the coil.[11] Since the distance between the terminals is not involved in the definition of impedance so long as it is sufficiently small to make (2) a good approximation, and so long as V_{AB} is maintained, the conventional definition of impedance is mathematically expressible in terms of a discontinuity in scalar potential between two adjacent points exactly as implied in (1). Since the right side of (5) is strictly correct only at zero frequency or at zero distance between the terminals, the identification of the scalar potential difference with the line integral of the electric field along the surface of the conductor is rigorously true only for a fictitious "ring or disk impedance" of zero thickness and of the same radius as the connecting wire. Such an impedance is entirely comparable with the "ring or disk generator" discussed above. Such a mathematically ideal impedance is as unavailable physically as a similarly idealized generator; furthermore, the same difficulties are encountered if attempts are made to approximate it by actual circuit elements connected between terminals formed by gaps in a conductor.

The conventional analysis of the two-wire transmission line in which radiation is neglected is rigorously accurate only for a line of zero spacing. An impedance connected across one end of such a line is strictly of zero thickness. In a practical line with a separation of wires b that is small compared with the wave-length, it is cus-

[11] R. W. P. King, *Electromagnetic Engineering* (McGraw-Hill Book Company, Inc., New York, 1945), Vol. I, Ch. VI.

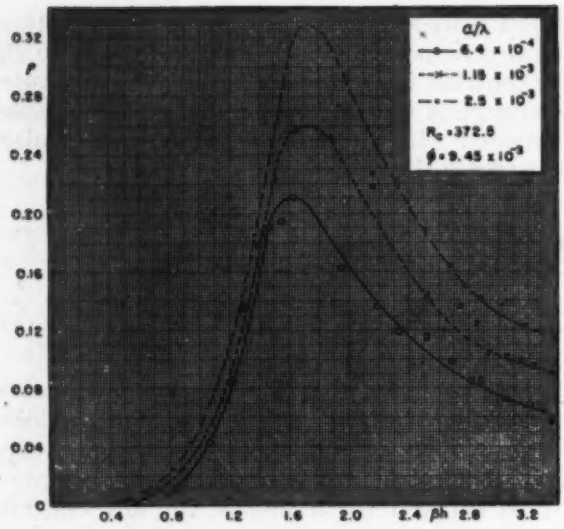

FIG. 4. Experimentally determined terminal attenuation function ρ for three symmetrical antennas center driven as in Fig. 3a as the half-length h is varied at constant frequency. (h is the corrected or effective half-length.)

tomary to neglect the distance b in the determination of an impedance connected across the end of the line. An analytically more accurate method is to treat the terminating impedance as though concentrated at the center of a straight wire across the end of the line. It is then possible to take account of the length b of this wire. If the radius a of the terminating wire and of the line wires is small compared with b, a good approximation is to treat the two-wire line of actual length s, distance between wires b, and termination Z_t as equivalent to a fictitious line of length $s+b/2$ with zero distance between wires, and with a concentrated termination Z_t.

EXPERIMENTAL DATA AND ITS THEORETICAL INTERPRETATION

If a symmetrical antenna is center-driven at the end of a closely spaced two-wire line as in Fig. 3a, the antenna is a terminating impedance for the line, and the potential difference maintained at the end of the line is equivalent to a generator for the antenna. Since the conventional theoretical analyses of both impedance and generator assume them to be concentrated at the center of a terminating wire, a comparison of experimental results obtained using an antenna in the arrangement of Fig. 3a with theoretical predictions can be only approximate. The actual antenna is not a continuous conductor of length $2h$ with a discontinuity in scalar potential at its center in a ring of zero thickness. The actual line does not have zero spacing of the wires with a concentrated impedance at its end. In order to have actual measurements of lengths *approximate* the idealized conditions of the theory, the length of the antenna may be called $2h$ from end to end, including the gap of length b at the center. Similarly the length of each wire of the line may be taken to be $s+b/2$, thus also including the gap.

In order to provide a standard termination adjusted to these approximations, the capacitance between two cylinders each of length h and radius a may be calculated when placed end to end and separated a negligible distance. The formula is[6]

$$C=[2\pi\epsilon_0 h/(1-2.485/\Omega)], \qquad (6)$$

with $\Omega=2\ln(2h/a)$. Since the reactance of short antennas with half-length h very small compared with λ is given theoretically by $1/\omega C$ with C obtained from (6), it is possible to fit the measured reactances to the theoretical reactances and so determine an equivalent half-length h for the antenna. Since the total length of each line wire and half of the antenna attached to it was increased by b in filling the gap with a conductor for both line and antenna, it is to be expected that the effective half-length of the antenna should be about $h-b$ if antenna and line were of the same size wire. The actual corrections given with Fig. 7, differ only slightly from b. The net effect of these several corrections for

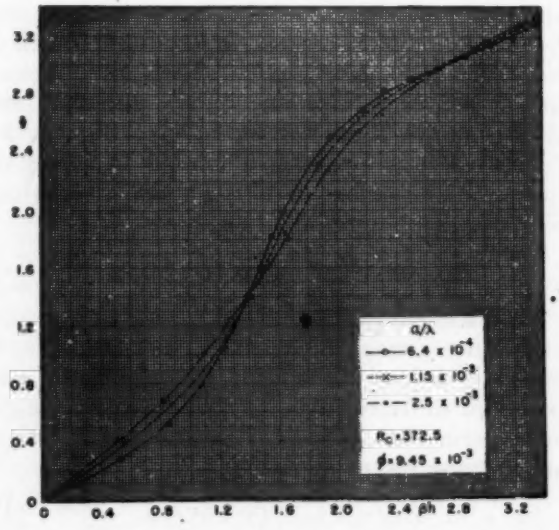

FIG. 5. Experimentally determined terminal phase function Φ for three symmetrical antennas center driven as in Fig. 3a as the half-length h is varied at constant frequency. (h is the corrected or effective half-length.)

measurements of length of line and antenna is very nearly the same as obtained by simply ignoring the distance b between wires and neasuring the actual length of *wire only* in both line and antenna.

However, the impedance computed from the measured phase shift and attenuation is actually that of an antenna with a *gap at the center*. If this impedance is to be interpreted in terms of the idealized impedance at the terminals of a concentrated ring generator at the center of an antenna of half-length near $h-b$ with *no gap* at the center, the best simple approximation that can be made is to include a lumped capacitance C_0 in parallel with the measured impedance. The magnitude of this capacitance cannot be determined precisely. However, its order of magnitude must be that of two cylinders each of length $b/2$ placed end to end as calculated from (6) with b written for h. For example, if the radius of the antenna is $a=0.46$ mm and the gap is $b=1$ cm, $C_0=0.066$ mmf. Thus the order of magnitude may be taken to be 0.1 mmf. Such a capacitance in parallel must be combined with the measured impedances in order to make these even roughly comparable with the values calculated theoretically in terms of a generator equivalent to a discontinuity in scalar potential.

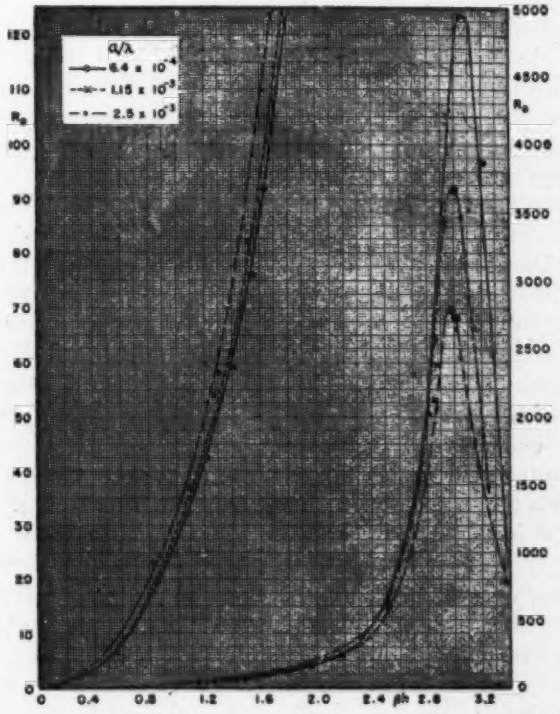

FIG. 6. Input resistance calculated from the terminal functions of the three antennas of Figs. 4 and 5.

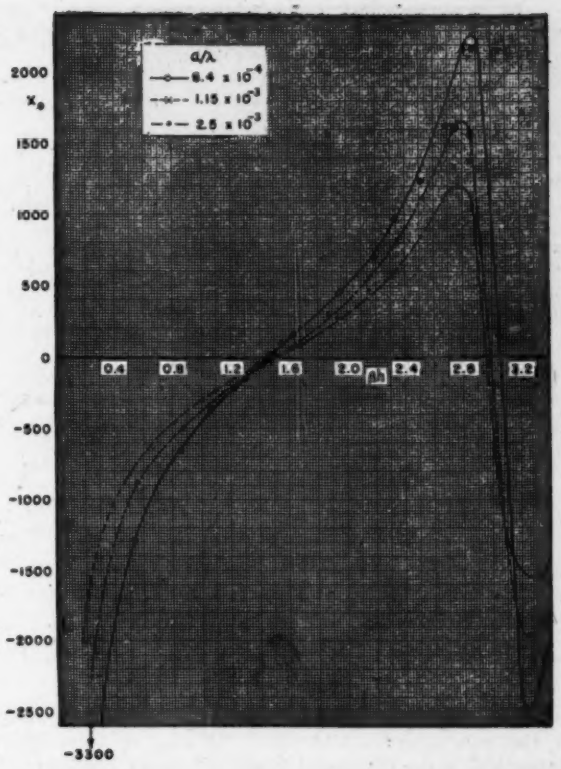

FIG. 7. Input reactance calculated from the terminal functions of the three antennas of Figs. 4 and 5. The effective values of h contained in βh were obtained by fitting the parts of the curves for which $\beta h \leqq 0.5$ to theoretical curves calculated from the formula for the static capacitance of cylinder placed end to end. The amounts subtracted from the distances measured from the center of the gap to one end of the antenna are $\Delta h=1.15$, 0.96, 1.37 cm, respectively, for the antennas with $a/\lambda=6.4\times10^{-4}$, 1.15×10^{-3}, 2.5×10^{-3}. They are seen to be very nearly equal to $b=1$ cm. (The antenna for which $a/\lambda=6.4\times10^{-4}$ was actually made of such extremely fine wire that it was not possible to have it perfectly straight and self-supporting. The length was measured from end to end, not along the wavy contour of the wire. Error introduced in this way may account in part for the fact that the curve for this antenna indicates resonance at a shorter length than the curves for the thicker antennas.)

EXPERIMENTAL RESULTS

The experimentally determined values of the terminal functions ρ and Φ for symmetrical antennas terminating a two-wire line in the arrangement of Fig. 3a are shown plotted in Figs. 4 and 5. They were calculated from measured lengths of the line (as described in Part I) to which were added $b/2$. The half-length h in the abscissa βh in the figures is the *effective half-length*. It is obtained from the distance measured from one end of the antenna to the center of the gap by subtracting that constant amount (near b) for each ratio a/λ necessary to make the measured reactance curves agree with the reactance cal-

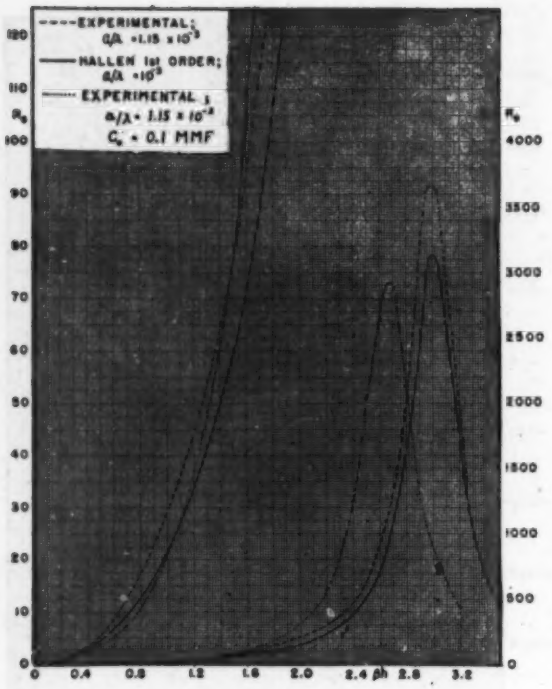

FIG. 8. Input resistance curves; broken line: same as one of the curves ($a/\lambda = 1.15 \times 10^{-3}$) in Fig. 6; solid line: theoretical value computed from first order solution by Hallen; dotted line: resistance computed from experimentally determined impedance in parallel with a lumped capacitance $C_0 = 0.1$ mmf.

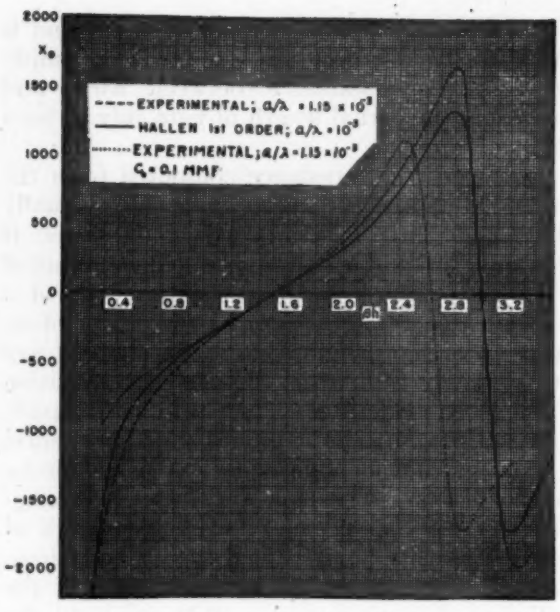

FIG. 9. Input reactance curves corresponding to the resistance curves of Fig. 8.

culated using (6) over the short range defined by $\beta h \leqq 0.5$.

The resistances and reactances calculated from the measured values of the terminal functions ρ and Φ plotted in Figs. 4 and 5 are shown in Figs. 6 and 7. The formulas involved are given in Part I (22a, b). All points shown in Figs. 6 and 7 are calculated directly from the experimental values of ρ and Φ except four in Fig. 6 and two in Fig. 7 which are distinguished by a larger circle drawn around the cross or dot. These points were calculated from values of ρ and Φ taken from the curves in Figs. 4 and 5 rather than from the individual measured values because these latter happen to be among the small number of points not on the curves, and the values of R and X are critical. It is clear that values taken from the smooth curves in Figs. 4 and 5 are more accurate than scattered individual points that are not on the curves. The resistance and reactance curves for the antenna with $a/\lambda = 1.15 \times 10^{-3}$ are replotted in Figs. 8 and 9 together with two additional curves in each case. Of these one set of curves is calculated from the same experimental data but with a lumped capacitance $C_0 = 0.1$ mmf in parallel with Z. The other set of curves shows the theoretical impedance of a cylindrical antenna for which $a/\lambda = 10^{-3}$ using only the first-order terms in Hallén's theory[3] as calculated by King and Blake.[4]

It is clear from Figs. 8 and 9 that a mere plotting together of theoretical and experimental results may be extremely misleading. In this case the unmodified experimental results might be interpreted to be an excellent verification of Hallén's first-order solution with the qualifying observation that these first-order theoretical values are throughout somewhat *too low*. If the theoretical curves are compared with the curves of the experimental results modified by a lumped parallel capacitance of $C = 0.1$ mmf as must be done to compensate for the gap, the first-order theoretical results are in much poorer agreement with experiment primarily as a result of the large shift of the modified experimental curves toward shorter lengths. This has the effect of increasing the impedance for lengths below anti-resonance.

A much more accurate theoretical analysis of the cylindrical antenna than is given by the theory of Hallén[3, 5, 10] or its modification by Gray[9] is presented in a companion paper[2] where a more complete discussion of the theoretical problem is included. The conclusion to be reached from the experimental results here presented is that the

impedance of an antenna depends in such a large measure upon the nature of its driving terminals that a conclusive and meaningful comparison with theory is not possible without exhaustive experimental measurements to determine not only the effect on the impedance of changes in length and radius of wire, but also the effect of the shape of the ends, and especially of the nature of the input terminals, and the method of driving. This evidently involves a systematic study using both open wire lines and coaxial lines in a large variety of possible arrangements of which that described in Part I is one.

The experimental measurements in this investigation were supported by a Grant from the Milton Fund of Harvard University. They were made by the second-named author in a single sequence, after which the work was interrupted before repeat runs could be taken to eliminate or verify irregularities. Further and more extensive measurements are planned. They will be carried out and reported as soon as circumstances permit.

The Secondary Electron Emission of Pyrex Glass*

C. W. MUELLER**
George Eastman Laboratories of Physics, Massachusetts Institute of Technology, Cambridge, Massachusetts

(Received February 16, 1945)

The total secondary emission of Pyrex glass is measured by a method utilizing the conductivity of the heated glass to carry the current. Necessary precautions for this type of measurement are pointed out. The secondary emission is measured over the bombarding voltage range of 50 to 10,000 volts. No temperature variation of secondary emission is observed.

THE measurement of secondary emission of poorly conducting substances has been neglected until within the past few years mainly because of the difficulties of measurement involved. The problem, however, acquired considerable practical importance early in the electronic art. As glass was commonly used to enclose electronic structures, it was inevitably struck by some stray electrons. These stray electrons would charge up the glass surface to an unknown voltage that might influence the motion of electrons in the tube in an undetermined and erratic way. The charging of a glass surface was usually guarded against by carefully confining the electrons to the desired space or by spraying the inside of the bulb with a conducting graphite coating. This study was undertaken to measure secondary emission and to obtain more knowledge of the action of Pyrex glass when bombarded with electrons.

In the measurement of the secondary emission of glass the following methods of measurement may be used: (1) the two-gun method; (2) the dynamic method; and (3) the heat-conduction method.

The two-gun method was first suggested by Nottingham[1] and has been applied by Salow.[2] This method consists essentially of bombarding the screen with two electron beams, one of which is used to fix the surface potential of the insulator, and the other used for the measurement of secondary emission. In order to distinguish the two currents one is modulated at a convenient frequency. Salow measured several samples of glass and his measurements of the secondary emission ratio of hard glass agree closely with those obtained in this work.

The dynamic method consists of using the front and rear surface of the insulator sample as a condenser and then using pulses in order to obtain a displacement current which can be interpreted to give a measure of the secondary emission yield. This method has been successfully employed by Heiman and Guyer.[3]

The heating method consists essentially of heating the substance until it becomes sufficiently conducting to permit current measurements through it. This method has limited application and is suitable only for certain materials such as glass. The heating of glass was first used by Nelson[4] for measuring the screen potential of conventional cathode-ray tubes. This method of measurement is simple in concept, but presents difficult measuring techniques.

* Extract from Doctor's thesis, 1942.
** Now at RCA Laboratories, Princeton, New Jersey.
[1] W. B. Nottingham, J. App. Phys. **8**, 762 (1937).
[2] H. Salow, Zeits. f. tech. Physik **21**, 8 (1940).
[3] W. Heiman and K. Guyer, E. N. T. **17**, 1 (1940).
[4] H. Nelson, J. App. Phys. **9**, 592 (1938).

CONDUCTIVITY IN GLASS

In secondary emission measurements when the secondary emission yield is appreciably different from unity, a current must flow through the glass. In order that the secondary emission measurements be properly interpreted the mechanism of the conductivity of glass must be appreciated.

Two phenomena contributing to the current take place: polarization and ionic current. Polarization phenomena are also referred to by various authors under the names of dielectric absorption and anomalous charging currents. These charging currents[5] which exist when voltages are applied or removed from glass vary with time. At high temperature, equilibrium may be reached in a few minutes, while at room temperatures several hours may be required. These currents may be minimized by allowing a sufficient time to elapse after applying a voltage before reading the current and then testing current variation as a function of time. Any voltages that need not be changed should be left on continuously.

Table I gives the composition of the Pyrex chemical resistant glass as given by the Corning Glass Company.

TABLE I.

SiO_2	80.7	CaO	0.3
B_2O_3	12.0	$Al_2O_3+Fe_2O_3$	2.3
K_2O	0.1	As_2O_5	0.4
Na_2O	4.1		

The mechanical structure of glass has been worked out by B. E. Warren.[6] The principal structure is composed of a silicon atom tetrahedrally bonded to four oxygen atoms. The sodium is in the form of positive ions which are distributed at random in the holes of the oxygen-silicon network, each sodium being surrounded by six oxygen atoms.

All workers in the field agree that the charge carrier in glass, at least during the initial stages of conduction, is the sodium ion. This fact is tested by the application of Faraday's law and is usually found to hold to within less than one percent. Since the sodium ion is the charge carrier, the resistance of the glass will vary with time as current is drawn unless precautions are taken to replenish the sodium transported from the vicinity of the positive electrode by the use of special materials, as sodium amalgams or compounds.

Most of the literature on the resistivity of glass gives the initial resistance or the resistance when the sodium ion is replaced. Normally in the use of glass as a conductor, intentionally or unintentionally, the sodium is not replaced, and one is interested in the flow of current as a function of time. The current flow follows that of most ionic conductors and can be expressed by the formula $I=At^{-n}$ where A and n are constants.[7] After passing current a short time, the voltage drop across the glass is concentrated at the anode.[7] About 20 percent of the Na^+ is tightly bound in the anode layer and is not removed by drawing current a long time. Thus some sodium remains in the glass even after a long period of conduction in one direction.

APPARATUS

As a source of primary electrons an electrostatic electron gun was used. This choice was made in preference to the simpler electromagnetic gun in order to permit sudden voltage changes for an impulse method of measurement. Due to insufficient time this method was never used. The geometrical design of the gun with the exception of the thermionic cathode is that of the RCA-912 cathode-ray tube. Instead of the oxide cathode, a filament was constructed of 0.0012 inch tungsten ribbon 0.080 inch wide. The tungsten filament eliminated the possibility of contaminating the glass surface as might be the case with an oxide cathode and also eliminated the necessity of replacing the cathode each time the tube was opened. The focusing electrodes of the gun and collector system were all constructed of well outgassed tantalum.

Details of the collector system are shown in Fig. 1 with parts labeled and discussed below. Since Pyrex was to be measured, the end of the tube was used as the target (1). A plate of Pyrex glass ground to a thickness of 0.095 cm was sealed to the end of the tube. The use of the end of the tube as the target required fewer leads through the glass and permitted longer leakage paths. An oven (2) was used to heat the entire end of the tube to get a uniform temperature in the glass sample. The collector (3) consisted of a tantalum cylinder supported from two stems (4) located outside the oven. All

[5] E. M. Guyer, J. Am. Cer. Soc. **16**, 607 (1933).
[6] B. E. Warren, J. App. Phys. **8**, 645 (1937).
[7] M. LeBlanc and F. Kerschbaum, Zeits. f. physik Chemie **72**, 468 (1910).
[8] C. A. Kraus and E. H. Darby, J. Am. Chem. Soc. **44**, 2783 (1922).

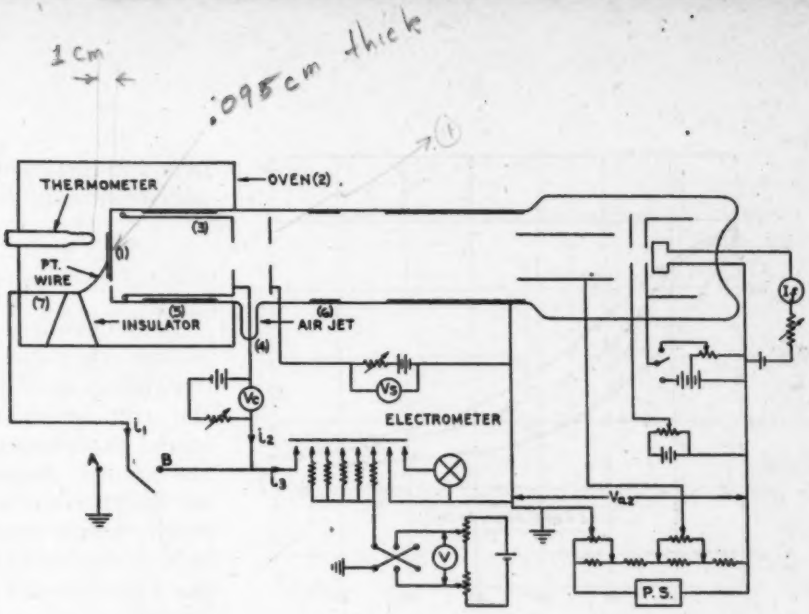

FIG. 1. Measuring circuit and oven assembly.

welded parts were placed in 30 percent nitric acid for several minutes to remove all traces of copper deposits left by the welding electrodes. A small stream of air was blown on the stems supporting the collector to cool them and to make the glass resistance as high as possible. The two guard rings (5) and (6) of platinum paint on the glass were also included to reduce leakage but were found unnecessary.

The insulation of the lead (7) to the rear collector was a troublesome problem. In order to make readings with the electrometer at very small currents, a resistance to ground of greater than 10^{10} ohms was desired at a temperature of 400°C. Since the rear collector was at ground potential no trouble from polarization caused by applied voltages occurred. However, trouble was encountered from a current which existed when the insulator was heated to 375°C, without any voltage having been previously applied. After merely connecting the ends of the hot insulator to an electrometer a current flowed that declined rapidly at first and then very slowly with time. These currents may have been caused by strains in the material, thermal electromotive force, or a voltaic action.

One insulating support tried consisted of a Pyrex-solid-glass-insulator tube 5 mm in diameter and coiled to give a length of 11 cm with tungsten electrodes at both ends which was annealed at 560°C for 30 minutes. After baking 26 hours at 500°C the current between the ends was 2.7×10^{-10} ampere at 390°C with no previous voltages applied. Further heat treatment would probably have reduced the current but this method of insulation was abandoned. A porcelain insulator which had been baked for several weeks at 350°C was found to be very good. The current of the porcelain insulator at 385°C with no voltage applied was 2×10^{-12} amp., an improvement of 100-fold over the glass described above.

The vacuum technique employed was similar to that previously described by Nottingham.[1] All measurements were made on sealed-off tubes that were gettered with barium located in a side tube extension. The target, as well as all other glass in the tube, was cleaned by washing in benzene, acetone, and 30 percent nitric acid. Each wash was followed by several distilled water rinses.

MEASUREMENTS

The temperature was measured with a 500°C thermometer placed about one centimeter from the glass target as shown in the sketch. A thermocouple on the glass surface would have introduced additional leakage paths. The guard disk voltage V_s was maintained at +15 volts with respect to ground to prevent most secondaries produced on it from leaving. Varying the voltage of this collector ±40 volts produced a maximum change of ±2½ percent in the yield curve. These changes were probably caused by some slow electrons in the beam. The oven current produced a symmetrical magnetic field that had a slight focusing action and also probably filtered out some low velocity electrons from the primary beam. The maximum change the oven current produced was to increase the yield by two percent. In view of this slight change extended runs were made with the oven current on to keep a more uniform temperature.

The beam size usually used was 3 to 4 mm in diameter. With the guard disk opening of 7 mm it was necessary to control the beam properly so

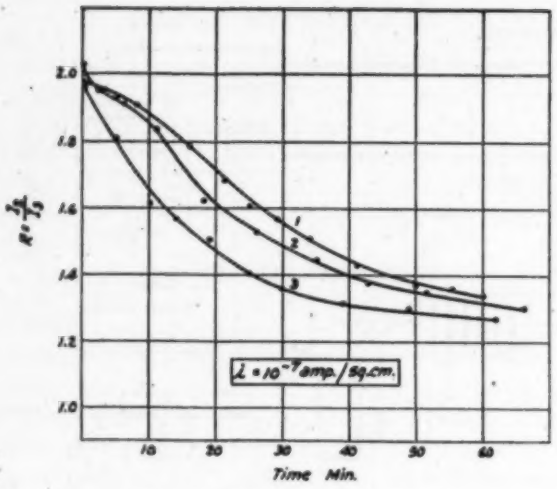

FIG. 2. Time variation of I_2/I_3.

that the same portion of the glass could be bombarded when desired. The position of the beam was determined by using crossed magnetic-deflection coils. By reading the current in the coils an accurate means of placing the beam was secured. The front face of the guard disk was lightly sprayed with willemite and by deflecting the beam onto it, the shape of the beam could be easily seen.

The yield δ, the number of secondary electrons per primary electron, was obtained from reading the current I_2 with the switch of Fig. 1 at A and i_1+i_2 with the switch at B. Since i_2 is the secondary emission current and i_1+i_2 the total beam current, $\delta=i_2/(i_1+i_2)=i_2/i_3$. All the leads, the switch, batteries, and voltmeter in the electrometer circuit were carefully insulated and shielded.

Careful checks were made to eliminate polarization currents caused by the application of voltage across any portion of the glass. In all readings in which the collector voltage was not a parameter, the voltage was left on at all times. In cases where V_c was varied, time tests were made which indicated when the polarization changes became negligible and this time interval was allowed to elapse each time before the beam was turned on and a reading was taken. The time necessary was usually of the order of ten minutes.

Considering the previous discussion plus the important factor of the previous history of the glass, which will be discussed in more detail later, we may place an over-all uncertainty in the measurements of approximately ± 5 percent. A larger variation than this is, of course, possible over the surface of the glass due to the effect of previous treatment.

RESULTS

1. Time Variations

In discussing current variations as a function of time, the ratio I_2/I_3 an apparent yield will be designated as R in order to distinguish it from the true secondary emission ratio δ. In the actual experiment the ratio I_2/I_3 is, of course, the quantity measured and then this result must be interpreted in the proper manner. Those results which were not altered by other factors were designated by δ while R is used to indicate the experimental ratio observed under a particular set of conditions. Figure 2 shows the apparent yield as a function of time. For these readings the potential of the guard disk was set at -20 volts, the collector at $+20$ volts. A concentrated beam carrying 10^{-7} amp./sq.cm, 1.5 millimeters in diameter was used.

A rapid decline of R as a function of time is evident from the initial curve 1 of Fig. 2. After the low value of 1.35 was reached the collector voltage was increased from 20 to 80 volts. The value of R increased directly with the voltage to a value of 1.5 at 80 volts showing no tendency to saturate. Moving the beam to a different position on the glass resulted in curve 2. After running the second curve both positions of the beam on the glass were checked and both gave the low end values of 1.3 indicating no change with time in the absence of current flow.

The entire area of the glass target was now bombarded with 3500-volt electrons which gave a value of R equal to 0.8. With a ratio less than unity the current through the glass is reversed. After 20 minutes of bombardment the original beam position and current were restored and curve 3 obtained. This shows the original conductivity of the glass was restored but the decay was now more rapid.

These measurements indicate a change in the conductivity of the glass due to the transport of the sodium ion through the glass and the desirability of using smaller values of current.

If we take from data of Bruining,[9] that the depth of penetration of the primary electrons of 500-volt velocity is 10^{-6} cm and calculated the time required to remove 80 percent* of the

[9] H. Bruining, Physica **3**, 1046 (1936).

* The reason for using 80 percent of the sodium present is that experiments have shown (see reference 8) that 20 percent of the sodium present is tightly bound and contributes only slightly to the current carrying capacity.

sodium from a cylinder of this depth and area equal to that of the beam we find the time required is about 1 minute for a beam of 0.017 sq. cm area and a current of 10^{-7} ampere. For a beam of 10^{-11} ampere and 0.1 sq. cm area the time is about 700 hours and the time variation should be small. To minimize time variations a beam current of the order of 5×10^{-11} amp./sq. cm was generally used.

2. Collecting Voltage

In the case of the secondary emission from a metal, the collector current saturates at a low value of collector voltage usually at values of 10 to 20 volts depending upon the collecting efficiency of the electrode. In the case of semiconductors several cases[10,11] have been reported for which there is a considerable increase of yield as the collector voltage is changed.

Figure 3 shows a curve of R *vs.* V_c (collector voltage). Since the current began to saturate at 60 volts, a somewhat larger voltage, namely 80 volts was used unless otherwise stated. This is not unreasonably high because the geometry is such that the field strength at the center of the target is not nearly as high as it is in cases where

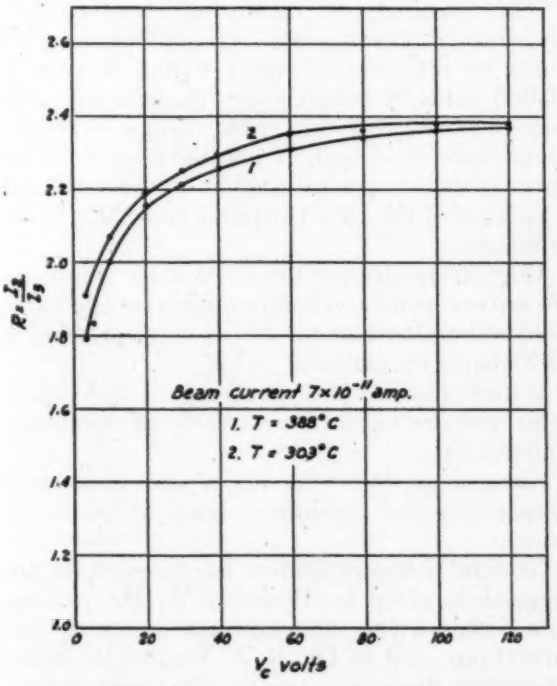

FIG. 3. Yield as a function of collector voltage.

[10] L. Malter, Phys. Rev. **50**, 48 (1936).
[11] H. Bruining and J. H. DeBoer, Physica **6**, 823 (1939).

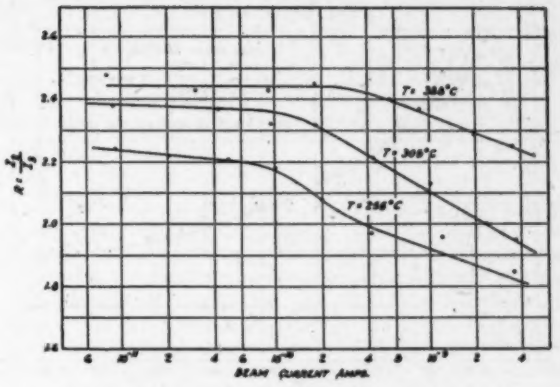

FIG. 4. Yield *vs.* beam current, $E_{g2}=400$ volts.

spherical symmetry exists. The field strength is also decreased by the RI drop through the glass.

3. *R vs.* Beam Current

As the beam current is increased the value of R decreases as shown in Fig. 4. The values plotted are actual currents in the beam of about 4-mm diameter; thus, to transfer the curve to current densities per sq. cm the values need only be multiplied by 10. These curves were taken at the peak of the yield curve where the maximum current had to flow through the glass. The point at which a definite bend in the curve occurs shifts to lower values of current as the temperature is decreased. At 255°C the curve is still rising at the lowest current values.

After taking the data for the curves from low to high currents and then returning to the original low currents a drop in R of about 4 percent was observed for both 388°C and 305°C curves but was not attempted for the 255°C case. The values of 4 percent lower were steady and no tendency to increase was observed. At currents of 5×10^{-11} ampere and at 388°C the beam could be left striking the glass for a period of one hour without changing the yield.

The following experiment was carried out to test more directly if an actual change in secondary emission occurred when the target was bombarded at relatively high currents for a considerable time. The glass was bombarded with a beam current of 10^{-8} ampere for 40 minutes at 350°C; during this time R decreased 28 percent. The current was then reduced to 10^{-11} ampere, the same portion of the glass bombarded, and readings taken as quickly as possible which was about one minute later. The yield at 10^{-11} ampere was the same as the

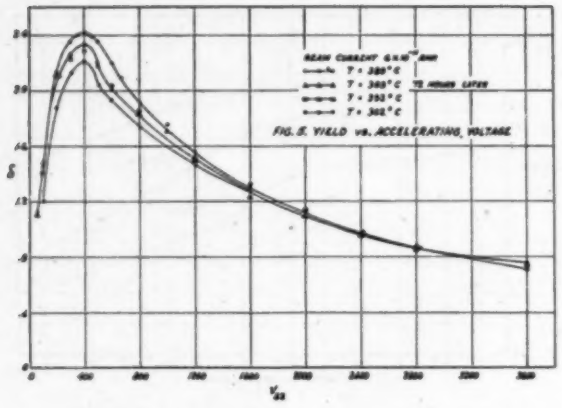

FIG. 5. Yield *vs.* accelerating voltage.

original yield before the high current bombardment to within one percent.

Since we cannot directly make independent measurements of the resistance of the glass we cannot determine definitely if the time yield varies with current density. The preceding data indicate that changes of measured yield with current are due to the voltage drop through the resistance of the glass and that the actual yield is unaffected by current density.

4. Yield *vs.* Accelerating Voltage

Figure 5 shows the relationship between yield and accelerating voltage at several temperatures. (A discussion of the temperature variation is given in a following paragraph.) A notable feature of the curve is the sharp maximum as contrasted with the broad maximum usually observed in metals. The second curve agrees very well with a hard glass sample prepared by blowing it out of molten glass as published by Salow.[2] Beyond the scale shown on the curve the secondary emission decreases monotonously as shown in Table II of values taken at 385°C with a current density of 10^{-11} amp./sq. cm.

Figure 5 showing secondary emission as a function of accelerating voltage shows three curves for different temperatures. These curves were not taken immediately following each other but between each a current of 10^{-8} ampere fell on the glass as a result of the measurements for the curves of Fig. 5. This probably resulted in a change in the actual resistance in the glass which could have been sufficient to account for the variation which is just within the accuracy of the experiments.

TABLE II.

Accelerating voltage	3600	4900	6400	8100	10,000
Yield	0.82	0.63	0.53	0.46	0.41

In order to check the yield more directly as a function of temperature values of δ *vs.* T were measured at an accelerating voltage of 400 volts over the temperature range 240°C to 420°C with a beam current of 5×10^{-11} ampere. For each reading the beam was only left on from one to two minutes. The yield was 2.3 ± 1 percent over the entire range of temperature.

Cross-Over Point Studies

At the cross-over points where the yield is unity no current need flow through the glass and the results are influenced the least by the resistance of the glass. These measurements can be made very accurately. The values of the cross-over points were checked over a temperature range from 100°C to 385°C and no change observed. Exploration of different portions of the glass surface gave an upper cross-over point variation from 2300 to 2650 volts. That portion of the glass that was bombarded the longest gave the lower value of 2300 volts.

CONCLUSIONS

The feasibility of measuring the secondary emission of Pyrex glass over the entire yield curve for accelerating voltages from 50 volts to 10,000 volts by conductivity through the glass was demonstrated and yield values over this range were measured. A notable feature of the curve is the sharp maximum at 400 volts as contrasted with the broad maximum usually found in metals.

Current densities of the order of 10^{-9} amp./sq. cm are necessary to eliminate serious time variations at bombardment voltages corresponding to high secondary emission yields.

Within the limits of accuracy of the experiment no temperature variations of secondary emission exist.

Changes in the behavior of the glass as a consequence of previous bombardment are evident.

Grateful acknowledgment is expressed for the suggestions given by Professor W. B. Nottingham under whose direction this research was carried out, and to Dr. R. J. Maurer for many interesting discussions on the electrical properties of glass. The author is also indebted to Mr. L. W. Ryan for performing the necessary glass-working operations.

The Structure of Certain Muscle Fibrils as Revealed by the Use of Electron Stains*

C. E. Hall, M. A. Jakus, and F. O. Schmitt
Department of Biology and Biological Engineering, Massachusetts Institute of Technology, Cambridge, Massachusetts

(Received April 4, 1945)

Fibrils from certain molluscan muscles, in particular the adductor muscles of the clam *Venus mercenaria*, were examined with the electron microscope and found to possess periodic variations in structure. In order to make these structural variations visible, it was necessary to treat the fibrils with reagents of high electron scattering power (electron stains). Phosphotungstic acid was found to be particularly suitable. This stain combines with specific regions in the fibrils, forming a remarkably regular geometrical pattern of which the most prominent feature is a regular cross striation, representing a fiber-axis spacing of about 145A. Within each stained band, the stain is more highly concentrated in spots spaced about 193A from center to center across the band. A line drawn through any such spot parallel to the fiber axis passes through other similar spots, spaced five cross bands apart, making the length of the fiber-axis period precisely five times the fiber-axis spacing. X-ray diffraction data obtained by Bear from the intact muscles are compared with the electron microscope observations. The small angle diffractions are in close agreement with those which would be expected from the observed structure except for the magnitude of the lateral spacing. Electron microscope values for this spacing are significantly smaller than the 325A indicated by the x-ray data, probably as a result of lateral shrinkage in the vacuum-dried electron microscope specimens. No significant difference in axis spacing has been observed in fibrils isolated from muscles fixed with alcohol in contracted and extended states.

IT has been shown by the use of small angle x-ray diffraction techniques that in certain protein fibers there exist large periodic structures with dimensions up to several hundred Angstrom units.[1–4] In two recent publications, Bear[5, 6] has presented such data for collagen fibers, two types of keratin (feather and porcupine quill), and clam muscles similar to those used in this investigation. The possibility of obtaining visual evidence of the structures responsible for the small angle x-ray diffractions has been demonstrated by the authors in the case of collagen,[7, 8] where the fiber-axis spacing appears in electron micrographs as a series of alternately dark and light cross bands. The average distance between consecutive like bands was found to be 640A, which value coincides with the x-ray spacing as first determined correctly by Bear.[3]

In collagen fibrils, the fiber-axis repeating pattern is characterized by a relatively large differential in electron scattering power. Consequently it can be observed in the electron microscope without any special preparative technique other than separation of fiber bundles. Such a fortunate circumstance cannot be expected in all structures of similar type. Structural variations of resolvable dimensions might exist without containing sufficient variation in electron scattering power to be distinguishable in the electron image. In these cases it will be necessary to enhance the contrast by the application of electron stains which combine preferentially with certain structural components. Electron stains will be efficient according to their scattering power for the electron beam and their selective deposition on significant structures. The muscle fibrils described here are an example of material in which no significant structure was observed until suitable electron stains were applied to accentuate the structural pattern.

PREPARATION OF SPECIMENS

The fibrils studied in this investigation were obtained from various molluscan muscles.* The adductor muscle of the clam, *Venus mercenaria*, was found to be most suitable for the preparation of electron microscope specimens. Descriptions of the light microscopic structure of the muscles may be found in the papers of Marceau[9] and Plenck.[10]

No specific method need be prescribed for the preparation of suitable electron microscope

* The substance of this paper was presented at the meetings of The Electron Microscope Society of America on November 17, 1944.

[1] G. L. Clark and J. A. Schaad, Radiology **27**, 339 (1936).
[2] R. B. Corey and R. W. G. Wyckoff, J. Biol. Chem. **114**, 407 (1936).
[3] R. S. Bear, J. Am. Chem. Soc. **64**, 727 (1942).
[4] I. MacArthur, Nature **152**, 38 (1943).
[5] R. S. Bear, J. Am. Chem. Soc. **66**, 1297 (1944).
[6] R. S. Bear, J. Am. Chem. Soc. **66**, 2043 (1944).
[7] C. E. Hall, M. A. Jakus, and F. O. Schmitt, J. Am. Chem. Soc. **64**, 1234 (1942).
[8] F. O. Schmitt, C. E. Hall, and M. A. Jakus, J. Cell. and Comp. Physiol. **20**, 11 (1942).

* Included were foot and adductor muscles of *Venus mercenaria*, neck and adductors of *Mya arenaria*, adductors of *Mytilus edulis*, *Ostrea virginica*, and *Pecten magellenica*, and the foot of *Viviparis* Sp.

[9] F. Marceau, Archiv. de Zool. Expérimentale et Générale [5] **2**, 295 (1909).
[10] H. Plenck, Zeits. f. wiss. Zoologie **122**, 68 (1924).

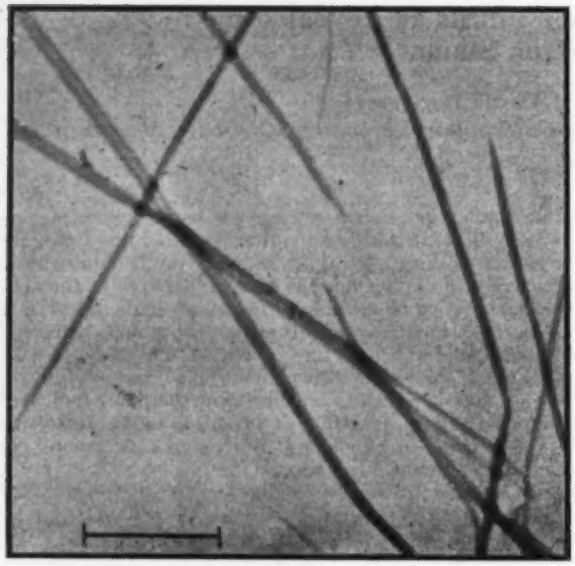

FIG. 1. Unstained fibrils from adductor muscle of *Venus mercenaria* (×17,700).

specimens. A typical procedure, however, is as follows: The *Venus* adductor muscle (preferably the white part) is macerated in a mortar with 0.3*M* KCl to form a highly viscous mass which is then diluted with more of the same salt solution and centrifuged in a clinical centrifuge. Centrifugation separates the suspension into three layers, the bottom containing large undispersed pieces of muscle, the top containing mostly fine granular material and the middle containing a dispersion of relatively clean, needle-shaped fibrils which can be readily seen in the dark field microscope. A drop from the middle layer is placed on a conventional electron-microscope specimen screen with supporting film. If the specimen is to be stained, a 0.1 percent solution of phosphotungstic acid in potassium acid phthalate-NaOH buffer (*p*H 5.1–5.5) is added. After about 1 minute the excess solution is drawn off with filter paper and the specimen is thoroughly washed in distilled water. The original dispersion can be carried out in distilled water or in KCl up to nearly 0.6*M* at which concentration the fibrils begin to go into solution. Also, a brief treatment with trypsin may be included before the staining in order to remove undesired protein contaminants. The fibrils are quite stable in salt solutions below about 0.3*M* and can be kept in the cold for several days.

The fibrils are soluble in salt solutions and the fibrillar protein may, therefore, be classified as a globulin. Since it appears to be the principal protein in these muscles it might be considered a type of myosin. However, there is not yet sufficient evidence on the amino acid composition of these fibrils or of the structure of the myosin components of other muscles to permit an adequate comparison. Hence to term these fibrils myosin would imply an identity which remains to be demonstrated.

ELECTRON MICROSCOPE OBSERVATIONS

Electron microscope observations were made with an RCA Type B electron microscope in which the original pole pieces had been replaced by a set designed in this laboratory to improve the imaging properties, particularly the flatness of field. Magnifications are judged to be accurate within ±2 percent.

A typical electron micrograph of unstained fibrils from adductor muscle of *Venus* is shown in Fig. 1. Fibrils range in width from 200 to 1000A and in length from 1 to 40 microns. The ends are tapered or rounded and show no obvious tendency for longitudinal cleavage. If the preparation is not well dispersed, fibrils appear in bundles. Occasionally they have a faintly mottled or granular appearance but the con-

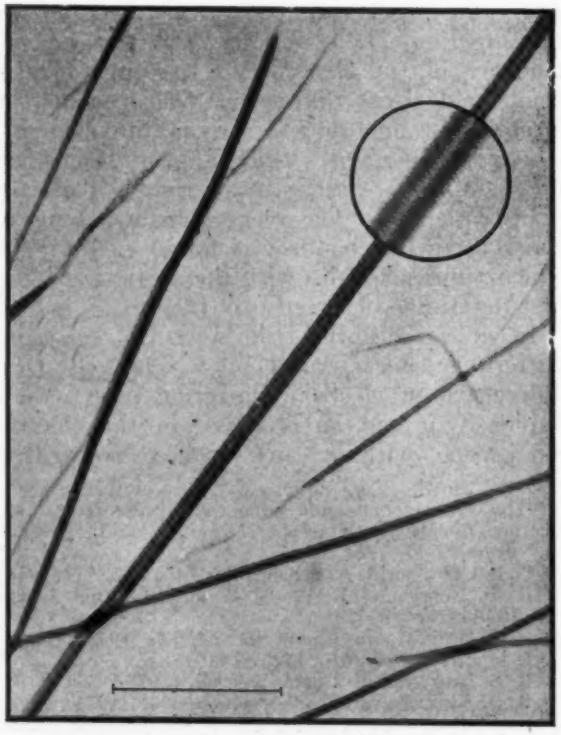

FIG. 2. *Venus* adductor muscle fibrils stained with phosphotungstic acid (×22,000, Inset ×52,000).

trast is so low that it is not possible to discern any definite structural pattern.

Fibrils stained with phosphotungstic acid present a complex but remarkably regular fine structure, of which the most obvious feature is a regular cross striation, as shown in Fig. 2. The inset in the figure is magnified by an additional factor of 2.36 to show the cross striation more clearly. There is a periodic structure in the fibrils consisting of alternate bands differing in their affinity for the stain. The distance between centers of consecutive like bands (spacing) in any fibril is constant over a considerable part of its length. It is, therefore, possible to measure the spacing in a given fibril with a high order of accuracy by measuring the distance covered by 20 to 100 spacings and dividing by the total number. Although the spacings are very nearly constant in any single fibril, they vary slightly from one fibril to another. The distribution of measured spacings in a group of some 200 fibrils from the white muscle of *Venus* is shown in Fig. 3. Spacings have values from 130 to 160A, the average for this set being 145A.

If stain is deposited in excess, the stained bands are quite opaque and are more or less uniform in density across the fibrils, but if the stain is deposited in appropriate amount, the bands consist of a series of equidistant spots separated by regions of lower density, as shown in Fig. 4. Lines passing through series of spots in consecutive cross bands can be drawn at two different angles to the fiber axis. The smaller of the two angles is designated α and the larger β. Frequently, stain tends to run along the diagonal directions. The location of spots and their relation to one another can be represented by a perfect geometrical lattice, as shown in Fig. 5, indicating a degree of structural order comparable to that existing in crystals. The diagram is designed to show only the spatial and geometrical relations between components of the lattice. Hence, the spots represent only the location of stained areas in the fibrils and bear no relation to their actual size or shape.

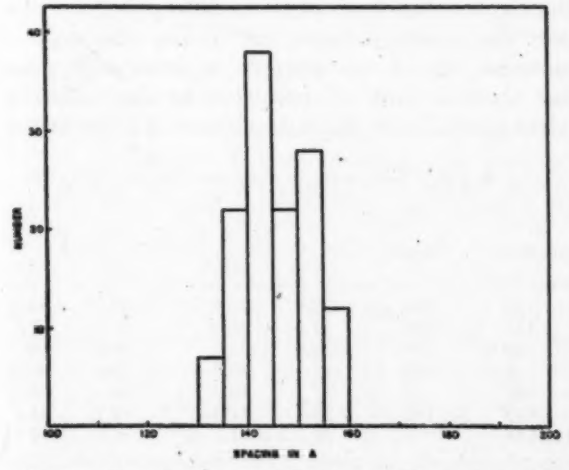

FIG. 3. Plot showing distribution of fiber-axis spacings in stained fibrils. Average spacing for this set of measurements is 145A.

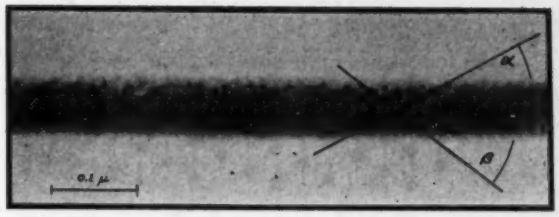

FIG. 4. Portion of muscle fibril showing geometrical disposition of stained regions (×113,000).

On the diagram are marked the average values for the various lattice constants obtained from a number of different fibrils. For this particular group of measurements the average fiber-axis spacing, d, is 144A (compare with 145A from the data in Fig. 3), while the lateral distance, s, is about 193A. The angles α and β are 28.2° and 38.8°, respectively, for these particular values of s and d. As a consequence of the lattice geometry, a line drawn through any spot parallel to the fiber axis passes through other spots spaced five bands apart. The length of the repeating period in the direction of the fiber axis is, therefore, 5×144 or 720A.

The lattice geometry can be conveniently described in terms of d, the spacing between adjacent like cross bands, s, the lateral distance between centers of adjacent spots, and the angles α and β. Thus

$$5d \tan \alpha = 2s, \quad 5d \tan \beta = 3s, \tag{1}$$

and

$$\tan \alpha / \tan \beta = \tfrac{2}{3}. \tag{2}$$

Numerical values for all quantities in (1) and (2) can be obtained with good accuracy from enlarged micrographs. Some representative data from six different fibrils are tabulated in Table I. Average measured values for d and s are shown in the first two columns. For each of the angles α and β there are two columns, the first showing angles calculated from d and s by means of Eq. (1) and the second showing corresponding measured angles to demonstrate the relative consistency of the results. At the bottom of each column is shown the resultant average for the

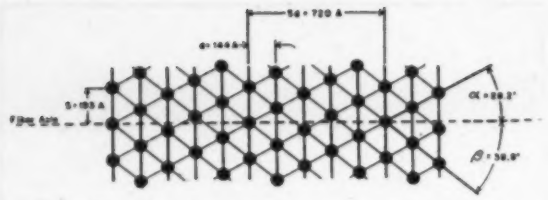

FIG. 5. Diagrammatic lattice showing geometrical relations and dimensions between stained regions in muscle fibrils.

six fibrils. The numerical values in Fig. 5 are the averages for s, d, and the calculated angles.

The consistency with which the two dimensional lattice appears in electron micrographs is evidence that the fibrils are like flat ribbons adhering to the supporting film with their faces parallel to that of the film. If they possessed cylindrical symmetry, the lateral spacing should appear foreshortened toward the edges and the diagonals should show curvatures corresponding to a helix wound on a cylinder. No significant anomalies of this sort have been observed, although the lattice has been measured in fibrils with widths over 1000A where such aspects would be apparent. The x-ray data to be discussed below are not inconsistent with the conclusion that the lattice points lie in a plane.

The first evidence of a large structural periodicity in this type of muscle fibril was obtained by the authors, using osmic acid as the electron stain.[11] This particular stain was deposited in regions spaced on the average every 360A along the fiber axis but it was not possible thus to discern the true lattice structure. Shortly after the periodicity was observed with the electron microscope, Bear demonstrated by the use of x-ray diffraction that the length of the axis period was, in fact, about 720A, from which it could be concluded that the osmic acid stained some structural aspect which recurs at the half period. The only feature in the lattice which recurs at this fraction of the axis period is the set of diagonals characterized by the angle α, and it seems probable that osmic acid deposits so as to accent regions associated in some way with these diagonals. The 360A repeat is most easily demonstrated in fibrils from adductors of *Mya arenaria* and is either absent or very weak in those from *Venus mercenaria*.

ROLE OF ELECTRON STAINS

The possibility of accentuating structures in electron microscope specimens of biological material by the application of reagents containing atoms of high mass has been generally recognized. To date, however, osmic acid is one of the few reagents which have been tried fairly generally for this purpose. As noted above, we have found in staining these particular muscle fibrils that this reagent does not bring out the structure which is well stained by phosphotungstic acid. Phosphomolybdic and silicotungstic acids also reveal the same fine structure but are not as effective as phosphotungstic. In most of the experiments the phosphotungstic acid used was a standard commercial preparation consisting of a mixture of phosphotungstic acids. A preparation consisting exclusively of phospho-12-tungstic acid* used as an analytical reagent for potassium determination by Rieben and Van Slyke gave the same results as the mixture.

At present, electron staining as applied to protein structure is largely of an empirical character and the specific chemical reactions involved are not well understood. When more data are available it may be possible to determine chemical properties of specific regions through their reaction with various stains. For the present analysis it suffices to note that certain reagents of high electron scattering power may combine with specific regions in protein fibrils.

COMPARISON WITH X-RAY RESULTS

In a concurrent investigation, R. S. Bear[6] reported the small angle x-ray diffractions from the same muscles but did not derive the space lattice. Since this is the first example in which the structure responsible for an x-ray pattern of this degree of complexity has been seen with the electron microscope, it is interesting to compare the results in some detail. For this type of material, the x-ray pattern is unusually good but there is lack of definition in some details, particularly in the pinhole pattern. A comparison

TABLE I. Fibril lattice measurements. (*Venus adductor*).

d (meas.) A	s (meas.) A	α calc.	α meas.	β calc.	β meas.
149	206	28.9°	28.5°	39.7°	39.9°
146	188	27.3	26.5	37.8	38.4
149	198	28.0	28.2	38.6	39.7
136	189	29.1	29.3	39.8	40.6
140	183	27.7	26.4	38.2	38.9
145	196	28.4	27.3	39.1	41.7
Av. 144	193	28.2	27.7	38.9	39.9

[11] M. A. Jakus, C. E. Hall, and F. O. Schmitt, J. Am. Chem. Soc. 66, 313 (1944).

* Obtained from the Anachemia Chemical Company, New York.

can best be made by first examining the small angle diffraction pattern which would be expected from the lattice as determined with the electron microscope, and comparing it with those details which can be resolved in the x-ray pattern.

The possible small angle diffractions resulting from radiation incident normal to the plane of the fibril pattern are given by the equations

$$x = N_1 D\lambda/s, \quad y = (N_2 + \tfrac{2}{5}N_1) D\lambda/d, \qquad (3)$$

where y is measured along the meridian (fiber axis) and x along the equator; λ is the wavelength, D is the distance from specimen to film, s and d are the distances as indicated in Fig. 5, and N_1, N_2 are 0, ± 1, ± 2, etc. Positions of diffractions given by (3) are shown diagrammatically in Fig. 6. There is a series of diffractions on the y axis, all of which are orders of the 145A spacing, d. Off-meridional diffractions occur in row lines separated by the distance $D\lambda/s$. Diffractions in the row lines occur at y distances which are all integral fifths of the distance between consecutive meridional spots, and only certain specific diffractions are possible in any particular row line, as indicated.

If the fibril is turned through 180° about its axis, the diffraction pattern is the mirror image of that in Fig. 6, and if the specimen consists of numerous fibrils randomly oriented about their axes, as is the case in x-ray specimens, diffractions should appear at the positions in Fig. 6, with the mirror image superimposed.

The diffractions which can be resolved in the experimental x-ray patterns reported by Bear fit those obtained from the electron microscope pattern very well, except for the magnitude of the lateral distance. In the experimental pinhole pattern, diffractions appear on the meridian and in two row lines, one on either side of the meridian. The meridional spots are all orders of 145A, in perfect agreement with the electron microscope results. Although the spots in the row lines are not well resolved, they are located in the meridional direction intermediate between the 145A diffractions and some can be discerned to be double. Their positions and double nature are consistent with what would be expected from Fig. 6 plus its mirror image, which in these row lines would result in pairs of diffractions at (2/5, 3/5), (7/5, 8/5), etc., of the meridional interval.

In order to determine accurately the meridional positions of the unresolved off-meridional diffractions, Bear limited the incident beam with a narrow slit in place of a pinhole. Thus the layer lines could be resolved, but at a sacrifice of resolution parallel to the equatorial direction. By this method he was able to determine that all layer lines occur at meridional distances which are integral fifths of the 145A distance and was able, therefore, to conclude that the fiber-axis period is $5 \times 145 = 725$A, which is in excellent agreement with the electron microscope data. The precise agreement between the two methods as to fiber-axis spacing and fiber-axis period leaves no doubt as to the identity of the structures studied in both cases.

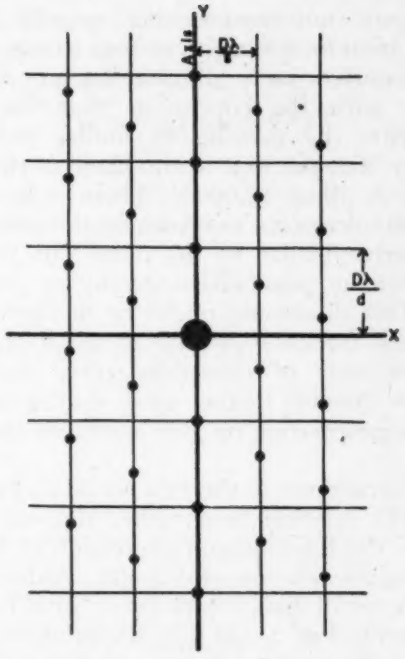

FIG. 6. Calculated small angle diffraction pattern for radiation incident normal to fibril lattice.

Bear has reported a lateral spacing of 325A which is considerably larger than the electron microscope value of about 200A. Since the x-ray specimens were strips of intact, air-dried muscle while those prepared for the electron microscope consisted of isolated vacuum-dried fibrils, it is possible that either the state of dispersion or the dehydration resulted in a lateral shrinkage in the electron microscope specimens. If this is so, the distance s in Fig. 5 would represent a minimum value associated with thorough dehydration.

DISCUSSION OF THE LATTICE GEOMETRY

The stained spots, as represented in the diagram (Fig. 5), locate similar points in units

which are equivalent in their reaction to stain and in their location with respect to one another. The reported x-ray diffractions are also consistent with the conclusion that the lattice represents the packing of similar units. The average area per unit in the plane of the lattice is $s \cdot d$, or about 29,000A^2. There is no reliable electron microscope evidence on the unit dimension perpendicular to the plane but there are two extreme possibilities worthy of consideration. This dimension might be of the order of the fibril thickness or else so small that each fibril consists of numerous grids stacked in register. Possibly further x-ray studies may contribute information on this aspect of the structure.

The occurrence of the axis period at five times the 145A spacing is a rather unusual lattice feature, the fundamental expression of which is the tangent relation of Eq. (2). Although the coincidence of like points every fifth band, as indicated in Fig. 5, can only be determined from micrographs to the order of experimental error, the tangent relation can be demonstrated to be consistent to a high order of accuracy, independent of any measurement of angles or distances. Thus, if the diagonals characterized by the angles α and β, respectively, are counted between similarly situated spots in long fibrils, it is found that there are two α-diagonals for every three β. This means that the tangents are in the ratio of two to three on the average between such points and since this holds true over distances of several microns, the precise ratio is judged to be significant. It seems probable that this integral relationship in the packing of the units results from some geometrical regularity within the units.

Description of the lattice by means of Eqs. (1) and (2) was found to be advantageous for the electron microscope analysis because they include the characteristic integral values and contain only readily measurable quantities. Other lattices of this general type could be described equally well by similar equations. The general equations, of which (1) and (2) are a special case, are

$$\tan \alpha = (m/n) \cdot s/d, \qquad (4)$$
$$\tan \beta = [(n-m)/n] \cdot s/d,$$

and

$$\tan \alpha / \tan \beta = m/(n-m), \qquad (5)$$

where α, β, s, and d have the significance indicated in Fig. 5; n is an integer and is equal to the number of spacings d between units coincident with the axis. Also, m is an integer equal to or less than n since α is taken to be equal to or less than β. Although this method of description was adopted as the most convenient for electron microscope analysis, the quantities s, d, m, and n, which completely determine this type of lattice, are just as conveniently measurable on diffraction diagrams from this type of structure, even though they be rotation diagrams.

RELATION OF FIBRIL STRUCTURE TO MUSCLE CONTRACTION

The present work is concerned exclusively with certain molluscan muscles and particularly with the adductor muscles, which have the function of closing the shells of bivalves. The physiological properties of the adductor muscles have been studied in some detail by Marceau.[9] Histologically, all those examined are classified as smooth muscles. They may be somewhat specialized and conclusions drawn as to their operation need not apply to muscles of other forms. However, information obtained about the mechanism of their contraction would contribute to the general problem.

Despite the fact that the fibrils, as prepared for electron microscope observation, are in a very abnormal environment, their structure is consistent with x-ray data from intact dried muscles. Similar invariance of structure was found in electron micrographs of fibrils obtained from muscles which had been fixed *in situ* with alcohol both in the extended and contracted states. Although the extended muscle was about four times the length of the contracted one, all measured values of the axis spacing from both samples fell within the range shown in Fig. 3.

Since the fibrils form a relatively large fraction of the muscle substance and possess certain physical and chemical properties similar to those of vertebrate myosin, it might be supposed that they represent the contractile substance. In this case, however, it is difficult to reconcile the invariance of the structure of fibrils from contracted and extended muscles with the concept of intramolecular supercontracture as proposed in current theories of muscle contraction.[12,13]

It is possible, though unlikely, that fibrils of the type here described, which had manifested

[12] W. T. Astbury and Sylvia Dickinson, Proc. Roy. Soc., **B129**, 307 (1940).

[13] K. Bailey, *Advances in Protein Chemistry* (1944), Vol. 1, p. 289.

an alteration of structure as a result of contraction were for some reason, excluded from observation. It is also possible that the inherent contractility of these muscles depends on other components, the fibrils here described playing a role associated, perhaps, with the rather specialized function of the adductor muscles. In any case, contractility depends on the structure and function of the muscle system as a whole and the particular role of these highly structured fibrils remains to be determined.

ACKNOWLEDGMENT

This investigation was supported by grants from Godfrey L. Cabot, Inc., and from the Rockefeller Foundation.

Wave Guides and the Special Theory of Relativity

W. D. HERSHBERGER

RCA Laboratories, Princeton, New Jersey

(Received March 15, 1945)

The Lorentz transformation is applied to the H_{01} solution of Maxwell's equations used to describe wave propagation in conducting pipes of rectangular cross section. When group velocity for the wave is employed in the transformation, the solution obtained is that one characterizing wave-guide operation at cut-off frequency, thus demonstrating that the speed associated with power or signal transmission is group velocity. When phase velocity for the wave is employed in the transformation, and we treat all quantities appearing in the new solution as real, we find that the problem has been reduced to one in magnetostatics and the significance of this solution is pointed out. The use of the inverse Lorentz transformation to find wave guide solutions from known solutions of problems in statics is indicated.

SEVERAL years ago a group of physicists and engineers at the RCA Laboratories conducted a seminar on the propagation of electromagnetic waves in hollow conducting pipes. In the course of the discussion several members of the group became interested in trying to form an intuitive picture of the electromagnetic field an observer moving with the wave would see in the wave guide. The intuitive picture, in particular insofar as it concerned the flow of currents in the side and top walls of the guide, was completely at variance with our common notions of electric current flow and the conditions necessary for the maintenance of current flow. The reason for this difficulty is that the intuitive transformation one is most likely to make—usually without resort to any algebraic manipulation—is one of the Galilean type. Such a transformation permits us to retain intact our notions, based on experience, on Newtonian mechanics but leads to an incorrect picture of electromagnetic phenomena. The difficulty was not removed until the use of the Lorentz transformation—the core of the special theory of relativity—revealed just what field a moving observer may reasonably expect to find. The whole matter is instructive enough in the light it throws on wave-guide operation to warrant a little study. In this paper no attempt is made to present the material in its most logical form but the approach is heuristic or pedagogical.

It is of course well known that one may calculate the current flowing in the walls of a wave guide from a knowledge of the tangential magnetic field at the interface between the wall and the interior of the guide. The configuration of the magnetic field, as well as of the electric field, is known from the appropriate solution of Maxwell's equations for the particular problem considered. Thus Figs. 1a, 1b, 2, and 3 depict fields for the wave variously known as the H_{01} or TE_{10} wave.

Figure 4 shows the orientation of the rectangular wave guide in a set of Cartesian coordinates. The width of the guide is b and its depth a. One characteristic of a wave of this type is that all components of electric field vanish, save E_x. The wave itself is traveling in the positive Z direction. Figure 1a shows the electric field viewed from the end of the guide while in Fig. 1b we view the electric field from a

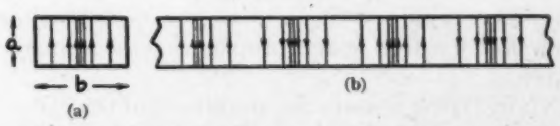

FIG. 1. (a) Electric intensity in wave guide, end view. (b) Electric intensity in wave guide, side view.

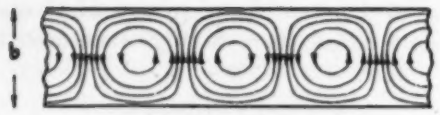

FIG. 2. Magnetic intensity in wave guide, top view.

direction parallel with the Y axis. In Fig. 2 we view the guide from the top, that is, from a direction parallel with the X axis. Figure 2 depicts the magnetic field for this particular type of wave. From a knowledge of this magnetic field at the guide boundary, we infer the magnitude and direction of current flow in the wall of the guide, and this direction of current flow is given by the lines shown in Fig. 3. This figure shows the current in the top of the guide, while the two side walls are shown bent up to display the direction of current flow in this part of the guide.

The H_{01} solution of Maxwell's equations which satisfies the boundary conditions imposed by the conductors lying the planes $X=0$ and $X=a$, and in the planes $Y=0$ and $Y=b$ is the following:

$$E_y \equiv 0, \quad E_z \equiv 0, \quad H_z \equiv 0,$$

$$E_x = (f/f_0)[\mu_0/\epsilon_0]^{\frac{1}{2}} H_0 \sin(\pi y/b) \times \sin(\omega t - \beta z); \quad (1a)$$

$$H_y = [(f/f_0)^2 - 1]^{\frac{1}{2}} H_0 \sin(\pi y/b) \times \sin(\omega t - \beta z); \quad (1b)$$

$$H_x = -H_0 \cos(\pi y/b) \cos(\omega t - \beta z). \quad (1c)$$

In this paper the m.k.s. system of units is employed and the values of μ_0 and ϵ_0 for vacuum will be used.

Then in Eq. (1) above

$$\mu_0 = 4\pi \times 10^{-7} \text{ henry/meter},$$
$$\epsilon_0 = 8.85 \times 10^{-12} \text{ farad/meter};$$

while

$$c = 1/(\mu_0 \epsilon_0)^{\frac{1}{2}} = 3 \times 10^8 \text{ meters/second}.$$

Also

$$f_0 = c/2b, \quad (2)$$

and represents the cut-off frequency for the guide; while

$$\beta = (\omega/c)[1 - (f_0/f)^2]^{\frac{1}{2}} \quad (3)$$

where $f = \omega/2\pi$. f is the frequency at which we operate the guide.

β is, of course, the propagation function for the wave guide while ω/c is the propagation function for free space propagation of a plane wave.

H_0 in (1) represents the amplitude of the wave.

It may readily be shown that the set of quantities in (1) satisfies not only the boundary conditions imposed by the walls of the guide, but also Maxwell's equations.

$$\nabla \times H = \epsilon_0 \dot{E}, \quad \nabla \times E = -\mu_0 \dot{H},$$
$$\nabla \cdot H = 0, \quad \nabla \cdot E = 0,$$

with f_0 and β defined in Eqs. (2) and (3).

Phase velocity for the guided wave is of course given by

$$v_P = \omega/\beta = c/[1 - (f_0/f)^2]^{\frac{1}{2}}, \quad (4)$$

while group velocity is given by

$$v_G = d\omega/d\beta = c[1 - (f_0/f)^2]^{\frac{1}{2}}. \quad (5)$$

Also, if λ_g represents wave-length in the guide, λ_s the free space wave-length, and $\lambda_0 = 2b$ the cut-off wave-length, it is readily shown that

$$(\lambda_s/\lambda_0)^2 + (\lambda_s/\lambda_g)^2 = 1. \quad (6)$$

It should be mentioned that the form of Eqs. (3)–(6) remains unchanged if we speak of propagation through pipes of circular or elliptical cross section rather than of rectangular pipes, and also holds for waves of a variety of types other than the H_{01}. In these other cases, the cut-off frequency will depend on other parameters associated with some dimension of the pipe and on modal indices identifying the type of wave propagated in the pipe. Up to this point the presentation is conventional and we are now ready to introduce a moving frame of reference.

The frame of reference shown in Fig. 4 was used in obtaining the solution given in (1). We now introduce a frame of reference moving with speed v in the Z direction by means of the Lorentz transformation.

$$x' = x, \quad (7a)$$

$$y' = y, \quad (7b)$$

$$z' = \{1/[1 - (v/c)^2]^{\frac{1}{2}}\}(z - vt), \quad (7c)$$

$$t' = \{1/[1 - (v/c)^2]^{\frac{1}{2}}\}(t - (v/c^2)z). \quad (7d)$$

At this point we digress for a moment to emphasize the invariance of Maxwell's laws under the Lorentz transformation. According to

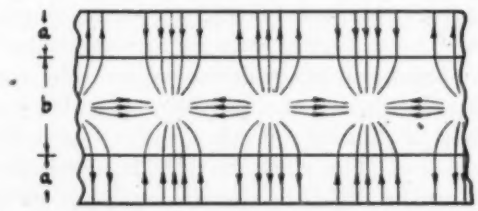

FIG. 3. Conduction current configuration in wave-guide walls.

Swann[1] "The fundamental outstanding dogma (of the restricted theory of relativity) which remains is that the laws of nature—the differential equations—shall be invariant under the Lorentz transformation." We are able to be even more specific in the present case. We have before us a particular solution of Maxwell's equations; namely,

$$E=E(x, y, z, t), \quad H=H(x, y, z, t),$$

for the rectangular wave guide. This solution at the same time satisfies the boundary conditions met in this particular problem. We now restrict the relative velocity v of the moving frame of reference with respect to the original frame to a direction parallel to the boundaries which gave our solution its specialized character. If we now introduce our moving reference frame in accordance with the transformation (7) with the restriction on v noted above, we will find a new set of quantities E' and H' which are functions of X', Y', Z' and t' thus:

$$E'=E'(x', y', z', t'),$$
$$H'=H'(x', y', z', t').$$

So far the procedure is strictly formal. But it follows, primarily because the Lorentz transformation is set up specifically for this very purpose, that our quantities E' and H' will

(1) satisfy Maxwell's equations, and
(2) satisfy the boundary conditions originally set up in the $OXYZ$ frame.

In short, in this paper the starting point is the invariance of Maxwell's equations under the Lorentz transformation.

First, let us see what form E' and H' take when we employ the group velocity v_G given in Eq. (5) in the Lorentz transformation as the relative velocity between our two frames of reference. We immediately find that

$$\omega t-\beta z=\omega_0 t',$$

and our solution in the primed coordinates becomes

$$E_y'\equiv 0, \quad E_z'\equiv 0, \quad H_x'\equiv 0, \quad H_y'\equiv 0;$$

while

$$E_x'=[\mu_0/\epsilon_0]^{\frac{1}{2}}H_0 \sin(\pi y'/b) \sin \omega_0 t', \quad (8a)$$

$$H_z'=-H_0 \cos(\pi y'/b) \cos \omega_0 t'. \quad (8b)$$

It will be noted that (8) satisfies Maxwell's equations and also the boundary conditions in the problem. In fact, it is precisely the solution we obtain from (1) by taking $f=f_0$, that is, by considering the operation of the wave guide at its cut-off frequency f_0. This is not a surprising result, particularly if we remember that on employing the Poynting vector to determine power flow in a guide operated at frequencies above f_0, we obtain power flow and have wave propagation in the usual sense. However, as we approach f_0, power flow diminishes and becomes zero when $f=f_0$, and at the same time the solution becomes independent of Z, and wave propagation ceases. The fact that no power flows down the guide when we employ a velocity approaching v_G in the Lorentz transformation may be considered as a demonstration that the speed associated with signal or power transmission in a wave guide is actually the group velocity.

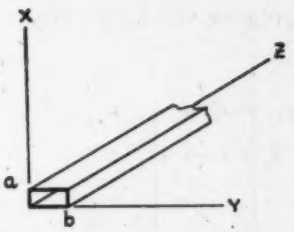

FIG. 4. Coordinate frame used in obtaining wave-guide solution.

In view of the interesting physical character of the result obtained on employing v_G in the Lorentz transformation, let us see what form E' and H' take when phase velocity v_P is used in the transformation.

$$v_P=c/[1-(f_0/f)^2]^{\frac{1}{2}}.$$

Someone may object that since phase velocity is greater than the speed of light c, we are not permitted to make this transformation. This might be a valid objection in case an experiment were proposed in which one would contemplate moving a wave guide at this speed, but we are confining ourselves to questions concerning the form a solution of Maxwell's equations will take under a transformation designed particularly for the examination of this type of problem.

We perform the indicated operation to find that under this transformation

$$(\omega t-\beta z)=i\pi z'/b.$$

So $\sin(\omega t-\beta z)$ becomes $-i \sinh(\pi z'/b)$, and $\cos(\omega t-\beta z)$ becomes $\cosh(\pi z'/b)$.

The solution of Maxwell's equations found on employing the transformation is then

$$E_z'\equiv 0, \quad E_y'\equiv 0, \quad E_x'\equiv 0, \quad H_z'\equiv 0;$$

[1] W. F. G. Swann, *Relativity and Electrodynamics* Rev. Mod. Phys. 2, 243 (1930).

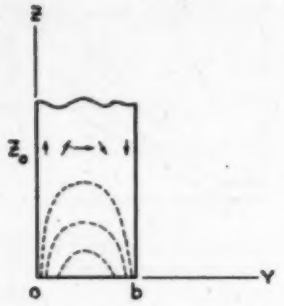

FIG. 5. Magnetostatic field obtained from wave-guide solution employing phase velocity in transformation.

while

$$H_y' = H_0 \sin(\pi y'/b) \sinh(\pi z'/b), \quad (9a)$$

$$H_z' = -H_0 \cos(\pi y'/b) \cosh(\pi z'/b). \quad (9b)$$

This solution is independent of t' and all components of E vanish, so the problem is reduced to one in magnetostatics. The Maxwell equations are, of course, satisfied and the boundary conditions initially imposed in obtaining our solution (1) are also met. Owing to the fact that $[1-(v/c)^2]^{\frac{1}{2}}$ is itself imaginary for values of v greater than c, both Z' and t' are imaginary. It is instructive to note the significance of our solution (9) treating E', H', and Z' as real quantities. In fact, this is the solution one obtains in setting $f=0$ in our original solution (1). This solution is finite at the origin but increases without limit as $Z' \to \infty$. This difficulty is eliminated if in the exponential form for $\sinh(\pi z'/b)$ and $\cosh(\pi z'/b)$ we employ only the term in $\exp(-\pi z'/b)$ since the term in $\exp(\pi z'/b)$ is responsible for the behavior of the function at $Z' \to \infty$.

We then obtain

$$H_y' = H_1 \exp(-\pi z'/b) \sin(\pi y'/b), \quad (10a)$$

$$H_z' = H_1 \exp(-\pi z'/b) \cos(\pi y'/b), \quad (10b)$$

where $H_1 = -H_0/2$.

The difficulty with the solution for $f=0$ at $Z' \to \infty$ was not introduced by the use of the Lorentz transformation but was already present in (1) which had not been properly restricted for this special case. This is most clearly shown by simply studying the zero frequency case in the original solution. Thus the use of the Lorentz transformation using phase velocity for guided waves as the relative velocity between our original coordinate frame and the moving coordinate frame gives us the zero frequency or so called d-c solution for the wave guide.

The physical significance of the solution will next be examined. It is the magnetic field that would arise from steady electric currents flowing in the walls and top and bottom of the guide which are introduced from an external current supply. The points of introduction of such currents are

$$x=0, \quad y=b/2, \quad z=0,$$

and

$$x=a, \quad y=b/2, \quad z=0.$$

In the side walls we have vertical currents. These side wall currents diminish as we go into the Z direction, falling to $1/e$ of their value for $Z=0$ at $Z=b/\pi$ and have their maximum value where $Z=0$. In the top and bottom of the guide we find that

$$(H_y')^2+(H_z')^2 = H_1^2 \exp(-2\pi z'/b)$$

which is a constant for given Z. At the same time

$$H_y'/H_z' = \tan(\pi y'/b)$$

so the resulting magnetic field changes in direction as y varies, as is shown in Fig. 5 in the plane $Z=Z_0$. Viewed from the top of the guide, the lines of magnetic force are shown dotted in this figure.

A quite interesting application of the foregoing theory is that the use of the inverse transformation, namely,

$$x = x', \quad (11a)$$

$$y = y', \quad (11b)$$

$$z = \{1/[1-(v/c)^2]^{\frac{1}{2}}\}(z'+vt'), \quad (11c)$$

$$t = \{1/[1-(v/c)^2]^{\frac{1}{2}}\}(t'+(v/c^2)z'), \quad (11d)$$

may be employed to convert the solution of a problem in statics such as given in (9) or (10) into the wave-guide solution (1). The velocity to use is again the phase velocity

$$v_P = c/[1-(f_0/f)^2]^{\frac{1}{2}}.$$

The fact that the expression for phase velocity has wide application permits us in similar fashion to start with a known steady current configuration in say a cylinder[2] to obtain solutions of wave-guide problems using only the Lorentz transformation and the known invariance of Maxwell's equations under this transformation.

I wish in particular to thank Dr. V. Bargmann of the Institute for Advanced Study for helpful discussions during the preparation of this paper.

[2] Weber, *Particllen Differential-Gleichungen der Mathematischen Physik* (Friederich Vieveg and Sohn, Braunschweig, 1900), Vol. 1, p. 438.

A Discussion of the Illuminating System of the Electron Microscope

JAMES HILLIER AND R. F. BAKER
RCA Laboratories, Princeton, New Jersey

(Received March 10, 1945)

A practical means for estimating the average performance of an electron microscope is proposed. Some first-order theory of the operation of an electron-microscope objective is given to demonstrate the extreme sensitivity of the instrument to the adjustment of the illuminating system. It is shown that by considering the illumination as being produced by a two-lens system it is possible to explain qualitatively all the effects observed in practice in connection with the illumination of the specimen. Practical information regarding the exact adjustment of the illuminating system is also given. The cause and elimination of multiple images is discussed. Changes in the design of the electron source and the use of an interchangeable aperture in the condenser lens are shown to improve the average performance of the instrument considerably.

I. INTRODUCTION

IN the various scientific journals and at scientific meetings during the past few years, an increasing number of the papers have been illustrated with electron micrographs. It has been apparent to the electron-microscope designers and engineers, who from force of habit criticize all electron micrographs from the point of view of image quality regardless of their scientific significance, that the variations in the quality of the micrographs have been too great. This is emphasized when it is realized that most of the published micrographs in this country have been obtained with very similar, if not identical, instruments. An inquiry into the reasons for these variations and methods for eliminating them may be said to constitute an important phase of the continuing development of the electron microscope as a research tool.

II. FIGURE OF MERIT

In studying the performance of the electron microscope it is obvious that some standard of comparison or figure of merit should be set up. It is unfortunate that the figure of merit ordinarily used by the electron microscope designers —that is, the *limiting* resolving power, is also commonly used to indicate the performance of an electron microscope under every-day working conditions. Usually the limiting resolving power has been obtained from a measurement of the least separation observable in a single micrograph of a specially prepared specimen containing extremely minute dense particles. The micrograph used for the measurements is, of course, the best of a large number taken under carefully controlled conditions. This is, at present, the best known technique for determining the optimum resolving power of an electron microscope and may be used as a fairly accurate measure of the electron optical quality of a particular design. That such measurements bear little, if any, relationship to the *every-day* performance of a particular instrument is obvious when it is realized that the resolving power is dependent on the physical properties of the individual specimen points and varies *in a single electron micrograph* by as much as two orders of magnitude. Furthermore, they do not take into account spoilage of micrographs caused by defects of specimen technique, by inaccuracies in the adjustment, and by contamination of the instrument.

The most obvious criterion for the *average* performance of an electron microscope is the mean of the *maximum* useful magnifications achieved in each and all the electron micrographs obtained in a specified period. In practice, however, such a criterion becomes unwieldy because of the amount of work involved in obtaining the data. A modification of the method has been found more workable.

Each exposure made during a selected period of time and at an instrumental magnification between 5000 and 10,000 is examined separately on a transparency viewing box. Using the unaided eye as the means of judging the quality of the micrographs they were separated into three classes: (1) Spoiled and completely useless. (2) Partially useful, but with obvious image defects. (3) Apparently perfect. Finally those falling into group (3) were re-examined with a 10× eye lens and subdivided into two groups according to whether at the higher magnification they showed any sign of image defects or not.

If it is assumed that the resolving power of the unaided eye is 0.2 mm and that each of the

TABLE I.

Group no.	Class	Useful magnification
1	Spoiled—useless	0–1000
2	Spoiled—useful	1000–5000
3	Slight defects	5000–40,000
4	No defects	40,000–100,000

micrographs had particles which would provide a means of determining the limiting resolving power attained, the four groups can be designated roughly by the ranges of useful magnification given in Table I. Figure 1 is a frequency plot obtained by this system of judging image quality. About two hundred successive exposures of biological and chemical specimens made by an operator with about two years of experience were used.

A careful analysis of the above distribution shows that a large percentage of the very poor results are caused by defects in the specimens themselves. On the other hand, slight defects are almost always electron optical defects caused by inaccuracies in the adjustment of the illuminating system, inaccuracies in the alignment of the lenses, and contamination of the lens openings. In the following the theory of the illuminating system and of the alignment technique will be discussed in order that the defects which are the result of inaccuracies in these adjustments may be understood and avoided. Some improvements and their effect on the above frequency distribution will also be described.

III. FIRST-ORDER THEORY OF ELECTRON MICROSCOPE ILLUMINATION

In light microscopy the lens systems are of such high quality that the most important aberration is that which is inherent in the nature of the light itself, namely, diffraction. In order to minimize the diffraction defect, the apertures of the lenses are made as large as possible. In electron microscopes, however, the opposite is true at present. The lens aberrations are all quite large requiring the use of extremely small apertures (effective, if not actual) if high resolving power is to be obtained. For instance, the first-order formulae for the two most important aberrations of the objective are

$$d_{\text{sph}}=0.4Cf_o(\alpha_c+\alpha_s)^3 \tag{1}$$

and

$$d_{\text{chr}}=K(\Delta V/V)f_o(\alpha_c+\alpha_s), \tag{2}$$

where d_{sph} and d_{chr} are the resolving powers of the objective as limited by spherical and chromatic aberration respectively. C is a dimensionless constant characteristic of the objective and f_o its focal length. V is the accelerating potential of the electron beam, and K is a constant which is substantially unity. α_c is the angular aperture of the illumination on the specimen, and α_s is half the angular half-width of the scattering introduced by a particular specimen point. The expression

$$\alpha_c+\alpha_s<\alpha_o, \tag{3}$$

where α_o is the angular aperture of the objective as defined by a physical aperture must be satisfied in all cases. To these aberrations must be added the diffraction defect which is given by the expression

$$d_{\text{diff}}=0.61\lambda/(\alpha_c+\alpha_s). \tag{4}$$

It is obvious since d_{sph} increases while d_{diff} decreases with increasing $(\alpha_c+\alpha_s)$ that there is an optimum value of $(\alpha_c+\alpha_s)$ for which the best resolving power will be achieved. To ensure that an objective is working at this optimum aperture it is necessary to place a perfectly clean aperture of exactly the right dimensions at the exact *electron optical center* (not mechanical) of the objective; a practical problem which has not yet been solved satisfactorily. Actually, tests in this laboratory have shown that if α_s is

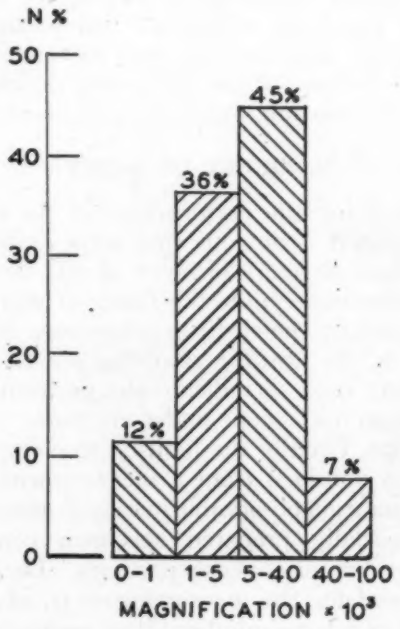

FIG. 1. A frequency plot showing the performance of an RCA type B electron microscope working under average conditions.

small and α_e is properly controlled it is not necessary to provide a physical aperture of optimum size except in a few special cases (see Fig. 2). In fact, the physical apertures used for most work are one or two orders of magnitude larger than the optimum.

Another factor which determines the average quality of electron microscope images is the depth of field. This may be expressed by

$$T_d = 2\Delta u_o = 2d/(\alpha_e + \alpha_s), \qquad (5)$$

where T_d is the depth of field, Δu_o is the maximum permissible displacement of the plane imaged by the objective from the object plane, and d is the desired resolving power. Thus, image quality as influenced by inaccuracies of focusing also depends on the value of α_e and α_s.

It is obvious from the above discussion that the control of the angular aperture of the illumination is the most important single factor in the operation of the present-day electron microscope.

Figure 3 is a diagrammatic cross section of a conventional electron microscope illuminating system. It is seen to include a thermionic cathode at a high negative potential, a cathode shield at either the same or at some small variable negative potential relative to the cathode, an anode at ground potential and a condenser lens of variable power.

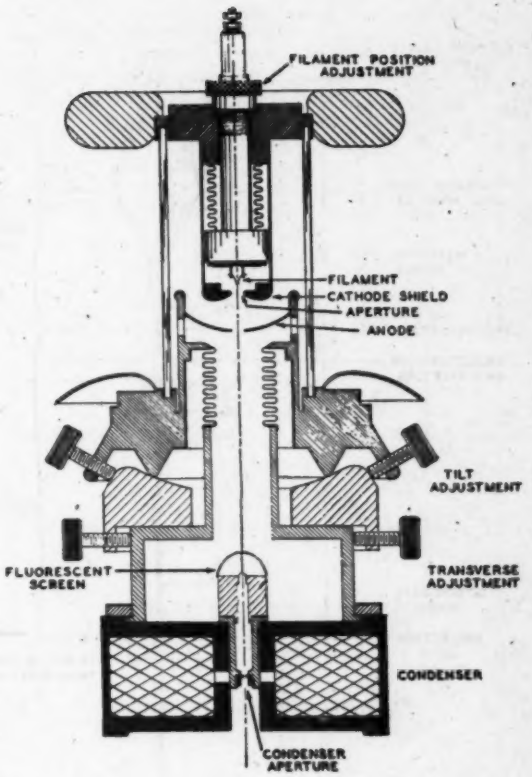

FIG. 3. A schematic cross section of the illumination system of the RCA type B electron microscope.

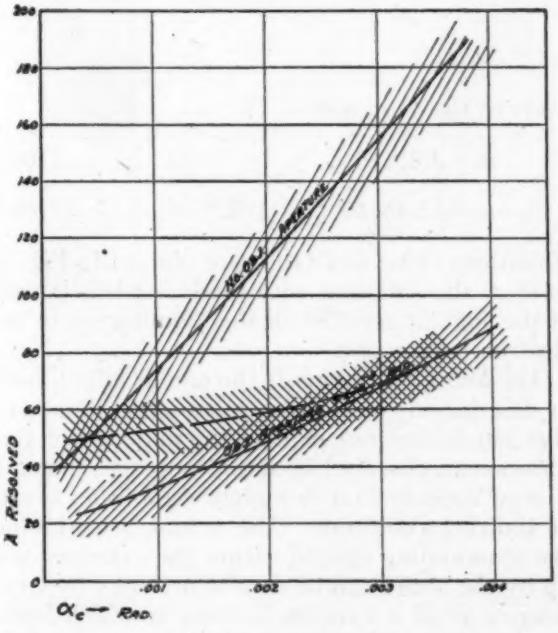

FIG. 2. A curve showing the dependence of the resolving power of the electron microscope on the angular aperture of the illumination.
——— For particles of evaporated gold.
– – – – For biological specimens and organic molecules.

In early discussions[1] the cathode system was considered as producing a narrow cross-over a short distance below the cathode assembly. The image of this cross-over, as produced somewhere on the axis of the system by the condenser lens, was considered as being responsible for the illumination of the specimen.

Figure 4, which is a ray diagram of the complete electron microscope, gives the symbols used in the following discussion. Here d_k is the diameter of the image of the cross-over as produced by the condenser lens. Then the angular aperture of illumination α_e is defined as half the angle subtended at a specimen point by this image of the cross-over and amounts to

$$\alpha_e = d_k'/2(v_c - v_c'). \qquad (6)$$

Using the simple lens formula for the condenser

$$1/u_c - 1/v_c = 1/f_c, \qquad (7)$$

[1] B. von Borries and E. Ruska, Zeits. f. tech. Physik 20, 225–235 (1939).

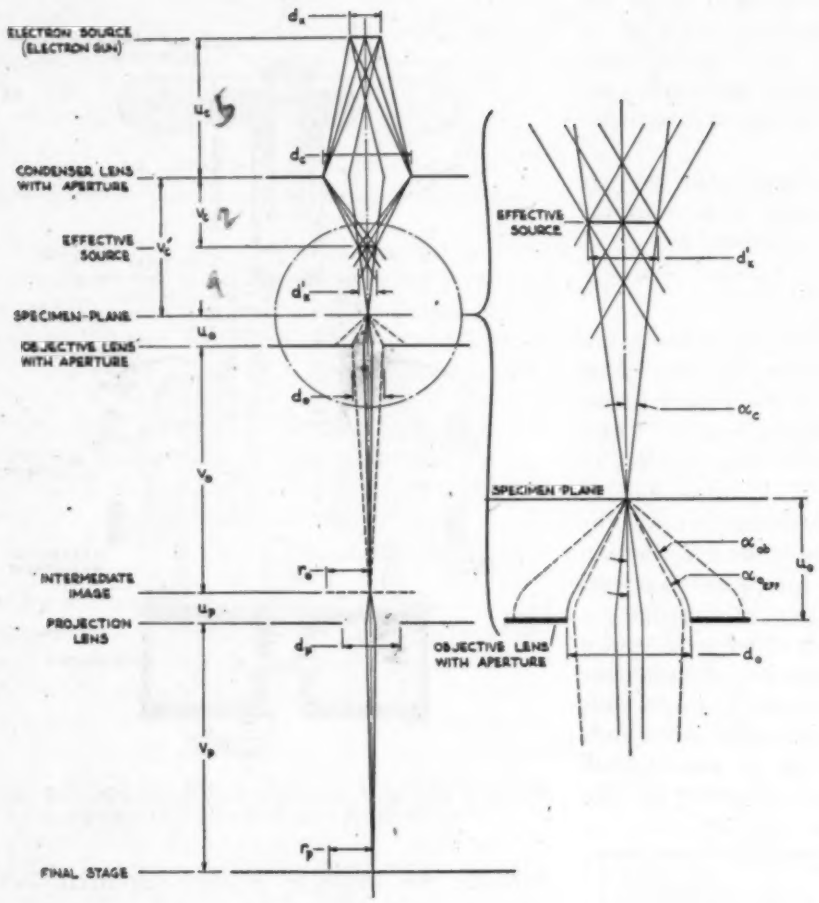

FIG. 4. A ray diagram of the electron microscope in which the cross-over produced by the electron gun is used as a fixed source.

Eq. (6) can be written in the form

$$\alpha_c = v_c d_k / 2u_c(v_c - v_c') = -d_k/2\left(\frac{u_c v_c'}{f_c} + v_c' - u_c\right), \quad (8)$$

where u_c and d_k are considered constant for the present. If the electron source is above the condenser as indicated in Fig. 4, that is, if u_c is negative, the angular aperture as expressed in Eq. (8) becomes infinite for one value of $1/f_c$.* In practice, however, the aperture of the condenser lens sets a maximum value for α_c which is given by the expression

$$\alpha_c(\max) = d_c/2v_c'. \quad (9)$$

Substituting a set of practical values: $d_c = 1.0$ mm, $d_k = 0.030$ mm, $u_c = -160$ mm, $v_c' = 160$ mm, leads to the expressions

$$\alpha_c = 3.2 \times 10^{-3}, \quad (10a)$$

$$\alpha_c = [5.4 \times 10^{-2}]/[(1/80) - (1/f_c)]. \quad (10b)$$

Equations (10a) and (10b) are plotted in Fig. 5 to show the variation with condenser lens power of the angular aperture of the illumination in an electron microscope.

The above discussion is the one usually found in descriptions of electron microscope illumination but it does not explain the majority of the phenomena observed in actual practice. Instead it now appears that it merely establishes a set of limiting conditions. The actual behavior of the illuminating system within the extremes set up by the above can be determined only by considering it as a two-lens system in which both lenses are variable. These two lenses are the cathode lens (an electrostatic lens formed by the filament, cathode shield, and anode) and the condenser lens. The application of a negative

* The expression for α_c given in Eq. (8) is valid only for small angles. Obviously the maximum possible value for α_c is $\pi/2$ radians.

potential to the cathode shield or the use of a mechanical adjustment of the position of the filament has always provided a means of adjusting the electron beam, but the idea that this adjustment involves the control of the strength of a lens does not seem to have been brought out clearly.

It will be assumed that a lens of variable strength $1/f_k$, of aperture d_k'' and of object distance u_k exists at the cathode aperture. Figure 6 is a diagram showing the arrangement of the lenses in this case and the symbols used. For simplicity, the position (designated by v_k) of the image formed by the cathode lens will be taken as the independent parameter in the following discussion. In this way the only discrepancy introduced by any lack of knowledge of the behavior of the cathode lens will be a constant magnification factor determining the value of d_k.

When the illumination of the specimen is provided by a two-lens system its angular aperture is controlled by the smallest of three angles as specified in the following:

(1) One-half the angle subtended at the specimen point by the condenser aperture. This quantity is independent of the power of the

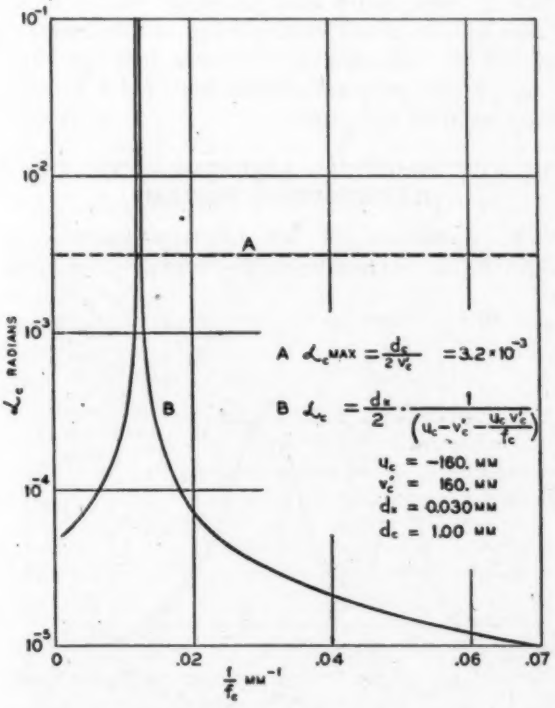

FIG. 5. Showing the dependence of the angular aperture of illumination on the power of the condenser lens for the conditions illustrated in Fig. 4.

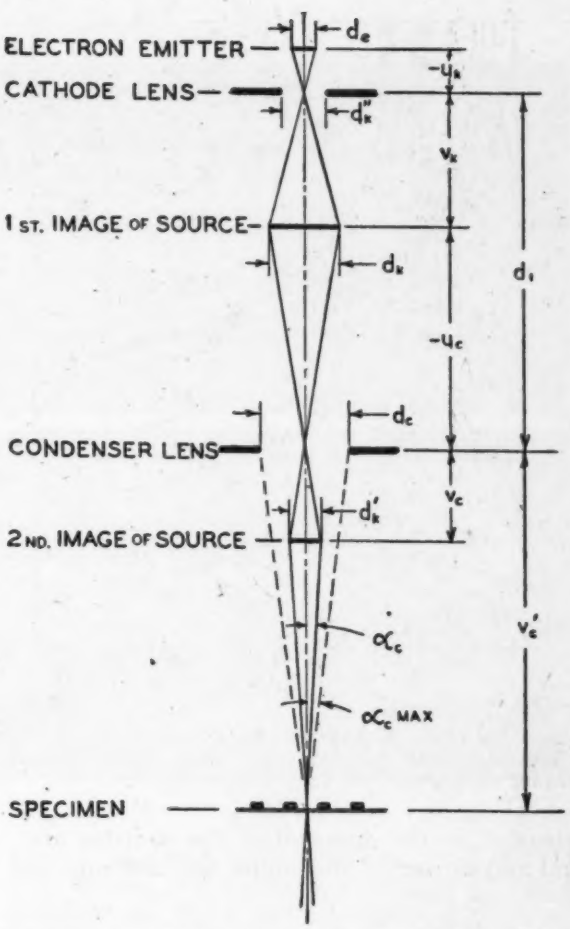

FIG. 6. Ray diagram in which the illuminating system of an electron microscope is considered as a two-lens system.

lenses in the system and represents the maximum possible value of α_c,

$$\alpha_c \leq \alpha_c(\max) = d_c/2v_c'. \tag{11}$$

(2) One-half the angle subtended at the specimen point by the image as produced by the condenser of the cathode aperture of diameter d_k''. In this case

$$\alpha_c \leq \frac{-d_k''}{2\{(u_c v_c'/f_c) + v_c' - u_c\}}. \tag{12}$$

(3) One-half the angle subtended at the specimen point by the image of the electron emitter as produced by the combined action of the condenser and cathode lenses. In this case

$$\alpha_c \leq \frac{d_e}{2} \cdot \frac{v_k}{u_k} \cdot \frac{v_c}{u_c} \cdot \frac{1}{v_c - v_c'}, \tag{13}$$

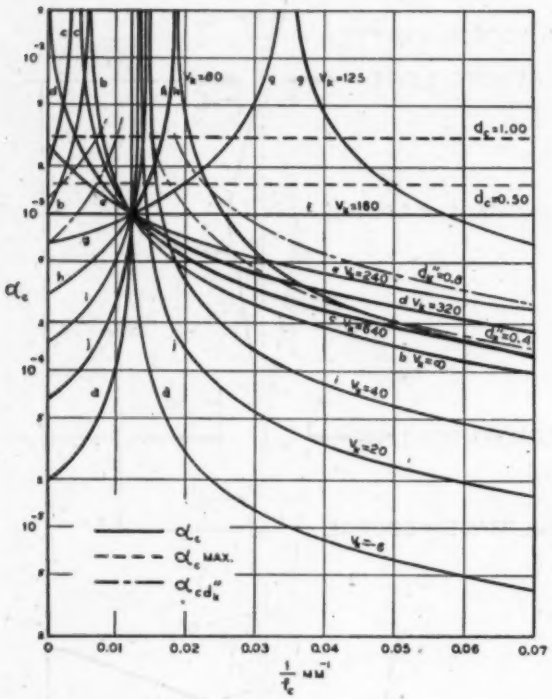

FIG. 7. Curves showing the dependence of the angular aperture of the illumination on the power of the condenser lens for various adjustments of the cathode lens.

where d_e is the diameter of the emitting area, and making use of the simple lens formula and $u_c=v_k-d_1$ gives

$$\alpha_c=\frac{d_e}{2}\cdot\frac{v_k}{u_k}\cdot\frac{1}{v_c'}\cdot\frac{1}{(v_k-d_1)\{(1/f_c)-(1/v_c')\}+1}. \quad (14)$$

Assuming that $d_e=0.008$ mm, $d_k''=0.8$ and 0.4, and $u_k=4$ mm, and that the other quantities have the values given above, these curves have been plotted in Fig. 7* where it can be seen that changes in the electron gun adjustment can produce radical changes in the way in which α_c depends on $1/f_c$. In fact, for values of v_k lying between d_1 and d_1+v_c', the image of the source cannot be made to coincide with the specimen plane for any condenser power. In this case α_c as given by Eq. (14) is a steadily decreasing function of $1/f_c$.

When $v_k=d_1$, that is, when the image of the source as produced by the cathode lens coincides with the plane of the condenser, α_c becomes constant, and the condenser has no effect whatever on the position of the image of the source. In these special cases the dependence of α_c on Eqs. (11) and (12) is not changed.

The intensity of the illumination is related to its angular aperture by the well-known law of Helmholtz-Lagrange;

$$I_s=I_k\alpha_c^2/\alpha_k^2, \quad (15)$$

where I_s is the intensity of illumination, at the specimen plane, I_k is the specific electronic emission from the filament, and α_k is the effective acceptance angular aperture of the cathode lens. Applying this formula to the present case shows that to a first approximation

$$I_s=-I_k(u_k/d_k'')^2\alpha_c^2. \quad (16)$$

Equation (16) provides a fairly accurate means of comparing, for (u_k/d_k)=constant, values of α_c given by Eqs. (11)–(13) with those obtained in practice.

Figure 8, on the other hand, is an experimental curve relating the maximum intensity of illumination (for variation in $1/f_c$) with filament position (u_k) for the type of electron gun in which a mechanical adjustment provides the means of varying the cathode-lens strength. There is a good qualitative agreement between the dependence of I_s on u_k and α_c and the behavior of the maxima on the curves in Fig. 7. However, while I_s approaches zero for small values of u_k, it also falls to small values when u_k is increasing indefinitely. This discrepancy is undoubtedly due to space charge conditions which exist for this adjustment of the gun.

IV. THE PRACTICAL ADJUSTMENT OF THE ILLUMINATING SYSTEM

The operation of an electron microscope would be a relatively simple matter if it were

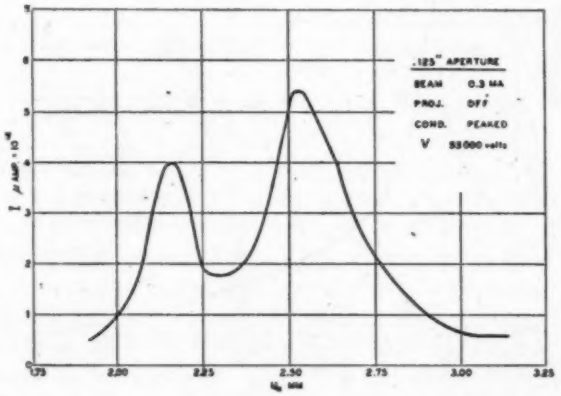

FIG. 8. An experimental curve showing the dependence of the maximum intensity of illumination on the adjustment of the cathode lens.

* The values given here are effective values estimated from experimental measurements. They do not necessarily represent the physical dimensions of the parts involved.

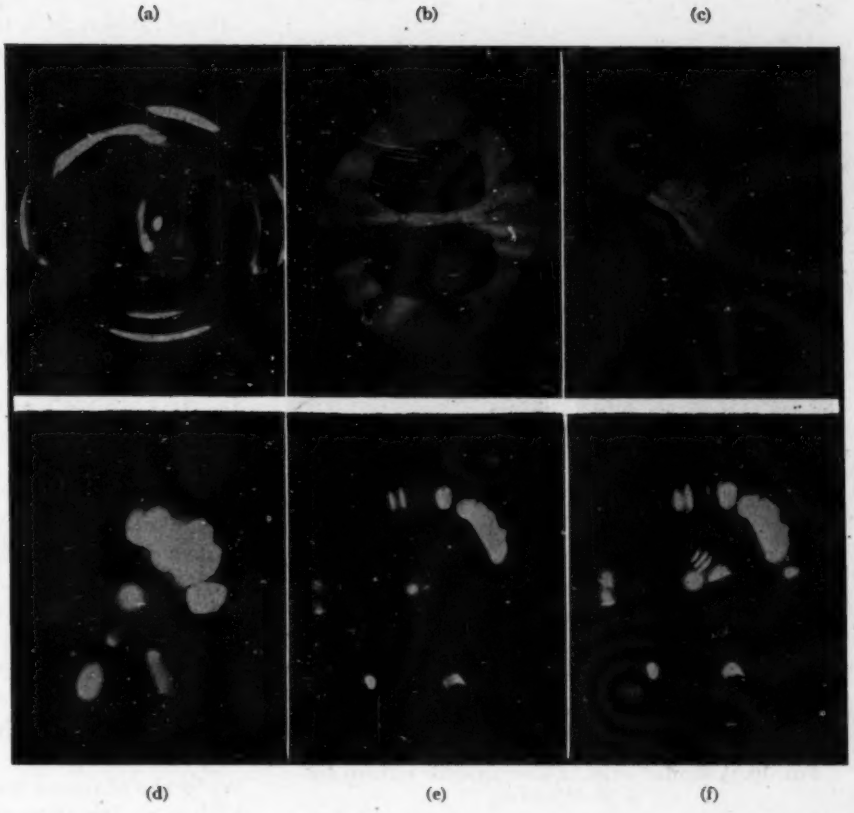

FIG. 9. Photographic records of the intermediate image for different adjustments of the cathode lens. The condenser is adjusted so that the image of the filament is focused on the plane of the specimen. The specimen is removed and the power of the objective is reduced below its normal focal value.

possible, as in light microscopy, to observe, focus, and record the images at the upper limit of useful magnification. Unfortunately, the limited field of view obtainable ($A=A_p/M^2$, where A is the area of the field of view, A_p the plate area, and M the instrumental magnification), the extremely low intensity of the image ($I_i=I_s/M^2$ if $\alpha_c<\alpha_o$) and the increased stability required of the power supplies make this technique quite impractical at the present time. Instead, it is customary to utilize the high resolving power of fine grain photographic emulsions, thus permitting the micrographs to be made at relatively low instrumental magnifications.

If we introduce the resolving power of the unaided eye, d_{eye}, and of the photographic emulsion, d_{phot}, in Eq. (5) we obtain the expressions:

$$T_{\text{vis}}=2d_{\text{eye}}/M(\alpha_c+\alpha_s),$$

and

$$T_{\text{phot}}=2d_{\text{phot}}/M(\alpha_c+\alpha_s), \tag{17}$$

where the value of M is determined from the auxiliary equation

$$M\geq d_{\text{phot}}/d. \tag{18}$$

For any value of $(\alpha_c+\alpha_s)$ which is maintained constant between the visual focusing and photographic recording, the visual depth of field is greater than the photographic depth of field in the ratio $d_{\text{eye}}/d_{\text{phot}}$ and an instrument focused visually under these conditions will provide the desired resolving power in only a fraction of the exposures made. This fundamental difficulty in the operation of the electron microscope at instrumental magnifications considerably below its useful limit is overcome, in practice, either by reducing α_c between the operations of visual focusing and photographic recording by an amount sufficient to make T_{vis} and T_{phot} equal or by the use of auxiliary light optical magnification. The reduction in α_c required by the former technique may be determined from the equation

$$d_{\text{eye}}/d_{\text{phot}}=(\alpha_c(\max)+\alpha_s)/(\alpha_c+\alpha_s), \tag{19}$$

where it is assumed that $\alpha_c(\max)$ and hence maximum intensity, is used for visual observation and focusing. The reduction of the value of α_c between the visual adjustment of focus and the final recording of the image may be accomplished either by an actual reduction of the size of the condenser aperture or by the proper control of the value of the condenser power $1/f_c$ in accordance with the curves of Fig. 7. It should be pointed out that it is not possible to make

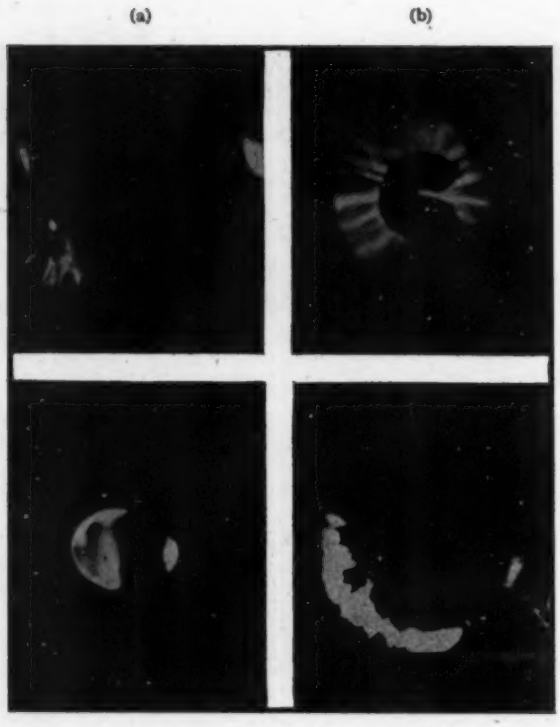

FIG. 10. A similar series of photographic records for a tilted source.

T_{vis} and T_{phot} equal by this method if

$$\alpha_s > \alpha_c(\max)/(d_{eye}/d_{phot}) - 1, \qquad (20)$$

a condition which commonly occurs in normal electron-microscope specimens.

This last fact provides a strong argument in favor of the use of the latter technique in which light optical magnification, sufficient to attain the useful limit of the instrument, makes $T_{vis} = T_{phot}$ for all conditions of illumination. In this case

$$M_o = d_{eye}/d_{phot}, \qquad (21)$$

where M_o is the required magnification of the light optical stage.

The above discussion and the experimental work which has been done to verify the theory presented provide a number of criteria by means of which the illuminating system of an electron microscope may be adjusted easily to its optimum.

If the specimen is removed and the objective power reduced to about one-third its normal operating value the intensity distribution in the specimen plane and the effects on that distribution of changes in the power of the cathode or condenser lens can be observed on the intermediate image screen at a magnification of about 30–50 diameters. The photographic records used in the present discussion were obtained by replacing the projection lens with a dummy tube thus permitting the intermediate image to fall on the final screen or photographic plate.

Figure 9 is a sequence of such records made with a standard RCA type B electron microscope. These show the appearance of the illumination when the condenser power is adjusted to provide a focused image of the filament and the filament is set in a series of successively higher positions. In Fig. 9a the image produced by the cathode lens of the emitting area is either above the filament tip or below the specimen ($u_k > v_k > -\infty$ or $\infty > v_k > d_1 + v_c'$). In Fig. 9b the filament has been raised slightly causing the image of the source to fall between the condenser lens and the object ($d_1 + v_c' > v_k > d_1$). Because of the extremely high spherical aberration of the cathode lens those parts of the image which are formed by its outer zones fall above the condenser. This condition combined with the limiting effect of the condenser aperture and the fact that the source possesses length is responsible for the pattern observed. In Figs. 9c–9f the filament has been raised to successively higher positions so that the image of the source falls at correspondingly higher positions above the condenser lens. As a result, the image of the source formed in the plane of the object becomes progressively smaller. (In Fig. 9f the image of the source appears larger because of over exposure of the negative.)

The most obvious discrepancy between these results and the predictions of the theory is the fact that the intensity distribution does not consist only of an image of the tip of the filament but usually of a rather complicated pattern, particularly for the low and high positions shown in Figs. 9a, 9d–9f. The low* position (9a) is characterized by the fairly symmetrical appearance of the "side spots" which appear to be independent of the conditions of either the filament or of the cathode aperture. The high position is characterized by the appearance of a rather irregular ring of spots which increase in intensity (relative to that of the central spot)

* The above discussion applies specifically to that type of electron-microscope source in which the position of the filament can be adjusted mechanically relative to the cathode shield. However, it applies equally well to the type in which a variable negative potential is applied to the cathode shield and the filament remains in one position. In this case the low negative potentials on the cathode shield correspond to low positions of the filament and *vice versa*.

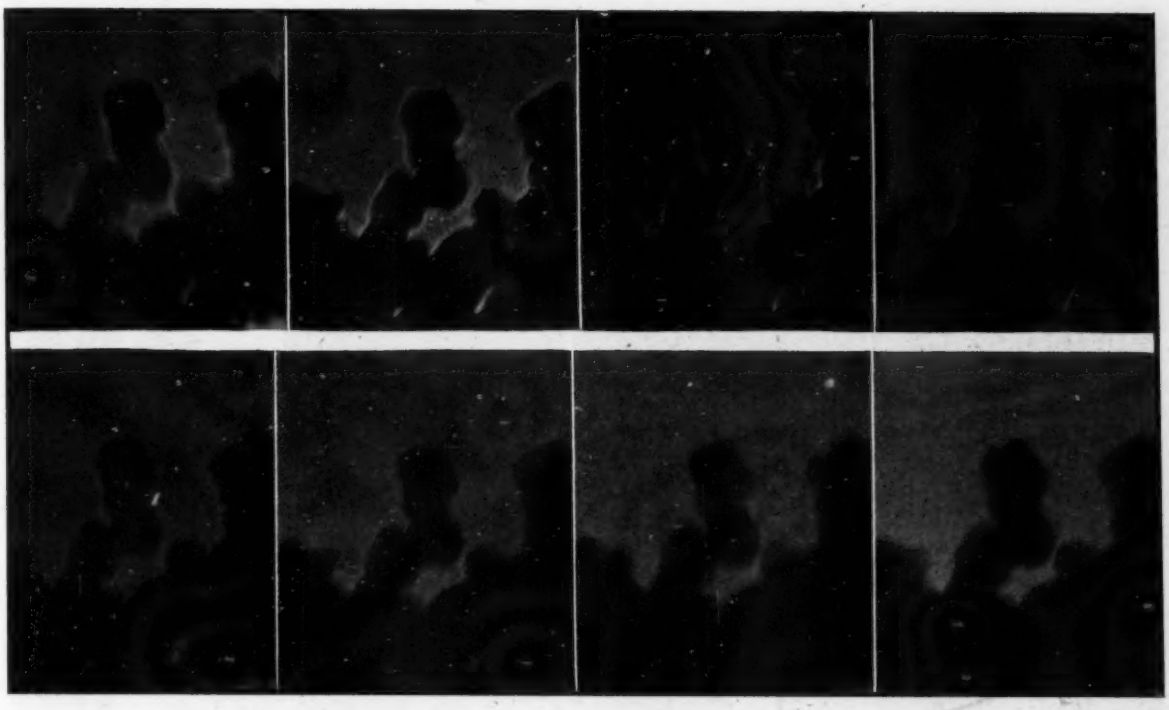

FIG. 11. A focal series of electron micrographs of carbon black taken with the cathode lens adjusted as in Fig. 9a. In this case the condenser lens power has been increased so that the angular aperture of the illumination is around 10^{-3} radian. (50,000×.)

as the filament is raised. These spots are not explained by the above theory nor by consideration of the normal spherical aberration of the cathode lens. Instead they appear to be caused by a total reflection phenomenon which results from the shape of the equipotential surfaces near the edge of the aperture in the cathode shield. The positions of the spots have been shown to correspond to highly emitting areas on the filament. The relative intensities in the spots depend to a certain extent on the accuracy of centering of the filament relative to the cathode aperture and also on the angle between the axis of the gun and the axis of the condenser lens.

The optimum adjustment of the electron source (that is, of u_k or $1/f_k$) can be seen from the above discussion to be one for which it is possible to vary α_c over a wide range of values from α_c(max) to 0 by means of a reasonable change in the value of $1/f_c$. The values of u_k or $1/f_k$ producing curve (a) or curve (j) in Fig. 7 and corresponding to the adjustments shown in Fig. 9a and Figs. 9d, 9e, and 9f respectively are equally suitable for the attainment of this condition.

Since the length of exposure is an important factor in determining the percentage of successful micrographs obtained with a given instrument it is also necessary to consider the intensity in determining the optimum adjustment of the source. It can be seen immediately from the curves in Figs. 7 and 8, considered in conjunction with Eq. (16), that the maximum intensity for all values of α_c is obtainable when the filament is set at the adjustment corresponding to the second maximum in Fig. 8. The intensity distribution on the specimen obtained at this adjustment is that illustrated in Fig. 9d.

In addition to adjusting the focus of the cathode lens, the complete adjustment of an electron microscope source requires that the axis of symmetry of the source be brought into coincidence with the axis of symmetry of the entire instrument. This may also be accomplished by observation of the reduced intermediate image. In order to make possible the complete alignment of the electron source, two sets of adjustments are usually provided. The first of these is a translation in any direction in a plane normal to the axis of the system, enabling the filament to be placed accurately on the axis. The second is a tilting in any direction enabling the axis of the symmetry of the source to be made parallel to the axis of the remainder of the system.

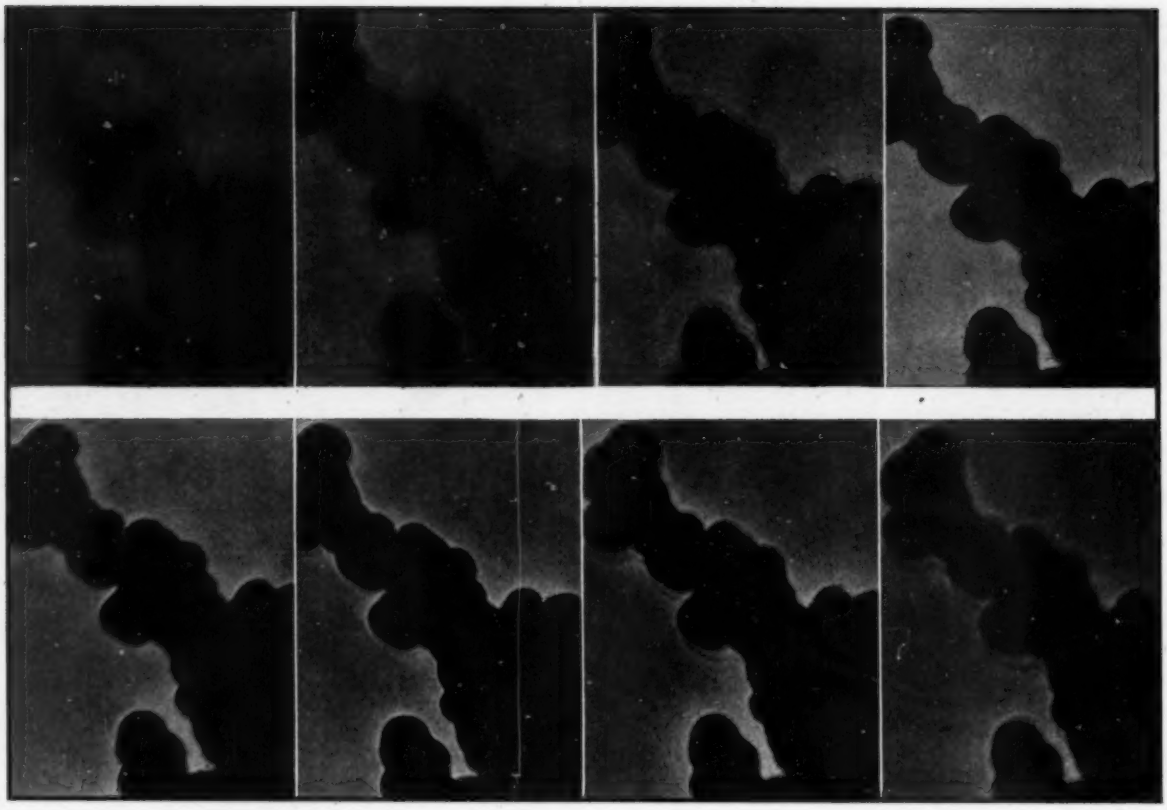

FIG. 12. A similar series taken with the adjustment indicated in Fig. 9b. In this case the condenser power was increased by the same amount as for Fig. 11, but there is no reduction in the angular aperture of the illumination. (50,000×.)

If it is assumed that the axes of the condenser and objective lenses are collinear, the filament is effectively on the axis of the system when the center of the field of view of the objective appears illuminated symmetrically for all values of $1/f_c$; a condition that is easily attained in practice.

The correct adjustment of the tilt of the source is obtained by observing the intensity distribution as described above and changing the tilt until the distribution appears quite symmetrical as in Fig. 9. Using the values of u_k corresponding to Figs. 9a–9c and 9e, records were made of the intensity distribution obtained when the source was tilted. The resulting exposures are given in Fig. 10. As in Fig. 9, the condenser was adjusted so that the image of the source was focused on the specimen plane, except in Fig. 10c where the cathode aperture is imaged on the specimen plane. The images in Fig. 10 provide a sensitive criterion for adjusting the tilt of the electron microscope source. This is particularly true in the case of Fig. 10c which can be used when there are no side-spots present in the distribution.

In order to investigate further the effect of the filament adjustment on the final image, a number of series of electron micrographs were made of a standard specimen at various filament settings. To obtain these series the objective current was varied through the focal value by constant steps read on an accurate meter. The value of α_c was reduced as much as possible from $\alpha_c(\max)$ by increasing $1/f_c$ without introducing the multiple illumination described below. These micrographs give further evidence of the validity of the criteria set up in the above. In addition they indicate that a more precise discussion should include the effects of Fresnel diffraction in the case of specimens with sharp discontinuities.

Three of the more significant series are reproduced in Figs. 11–13. The filament settings used for these correspond to Figs. 9a, 9b, and 9d, respectively.

V. MULTIPLE IMAGES

In electron microscopy one of the most frequently encountered electron optical defects is commonly described as "image doubling." Electron images having this defect appear to consist of two or more well-focused but slightly displaced images. When this condition occurs a closer examination will always show that each specimen point is illuminated by two or more discrete pencils of electrons.

If $\alpha_s \ll \alpha_c(\max)$ the individual pencils of illumination will produce individual well-focused images. Furthermore, these images will be slightly displaced if the deviation of the objective power from the exact focal value lies between half the depth of field of an individual pencil and half the depth of field of the entire group. This condition is illustrated in Fig. 14 and may be expressed analytically as follows:

$$d/(\alpha_c+\alpha_s) > \Delta u_0 > d/(\alpha_c(\max)+\alpha_s), \quad (22)$$

where d is the resolving power of the instrument and $\alpha_s \ll \alpha_c(\max)$.

In practice multiple pencils can arise in a large number of ways. Two of these are most commonly encountered and will be described.

In the adjustment of the electron-microscope source as described in the above, the desirable condition has been found to be that illustrated in Fig. 9d. This, however, is the intensity distribution on the specimen plane for the maximum value of the angular aperture. To obtain satisfactory micrographs, it is necessary to increase or decrease $1/f_c$ so that α_c is reduced according to curve (j) in Fig. 7. This reduction of α_c could be carried on without limit if the illumination consisted of the single spot considered in the above theory. Actually, however, the illumination consists of the rather elaborate pattern shown in Fig. 9d so that when the value of $1/f_c$ is changed from the focal value each point of the distribution expands into a circle of illumination which, when the change in $1/f_c$ is sufficiently great, will extend to the central point of the specimen. Figure 15 is a photographic record of this condition. Figures 16 (a) and (b) are ray diagrams illustrating the optics of the conditions shown in Figs. 9d and 15. It can be seen that while α_c for the central pencil is reduced with an increase in $1/f_c$ according to curve (j) in Fig. 7 a critical value of $1/f_c$ is reached where the illumination from the side spots reaches the specimen with an angular separation approximately equal to $\alpha_c(\max)$.

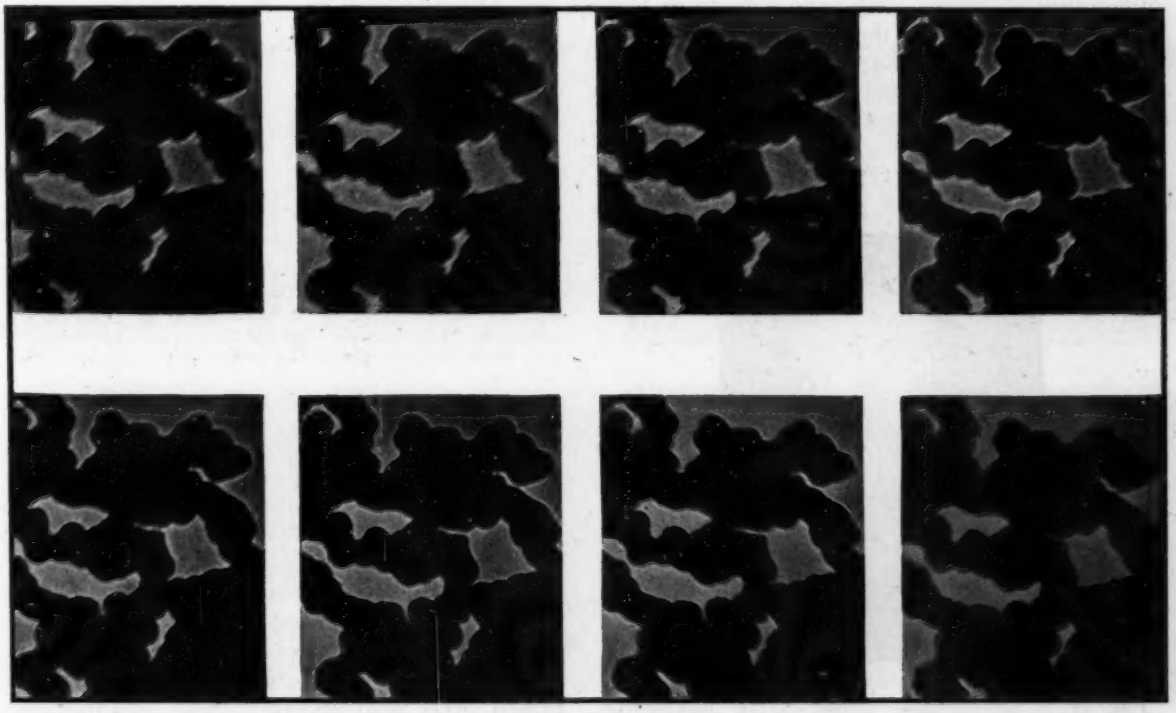

FIG. 13. A similar series corresponding to cathode lens adjustments showing Fig. 9d. The angular aperture of illumination is also about 10^{-3} radian. (50,000×.)

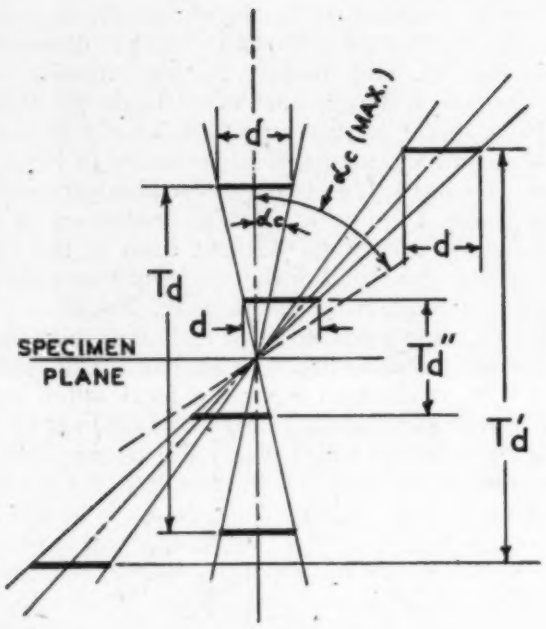

FIG. 14.

It is obvious from Fig. 10 that the permissible increase in $1/f_c$ is greatly restricted if the tilt adjustment of the gun is not exactly correct. Figure 17 is a series of high magnification electron micrographs taken with the electron-source adjustment illustrated in Fig. 10d and with $1/f_c$ increased by about the same amount as in Fig. 13.

If the filament is adjusted to give the illuminations illustrated in Figs. 9b and 9c, multiple images are obtained for all values of $1/f_c$ as shown in Fig. 12. This is caused by the fact that the illumination of the specimen is coming from an enlarged image of the specific areas of emission on the filament and that the value of $1/f_c$ has very little effect on the angular aperture of the distribution.

It is obvious from the above that proper adjustment of the filament and proper control of the value of $1/f_c$ will eliminate multiple images arising from this source. In practice the presence of multiple pencils of illumination can always be checked by observing the image of the specimen as it is considerably defocused. In a properly adjusted instrument defocused image points should show absolutely no tendency to split up into multiple shadows. This test must be carried out with $1/f_c$ set at the value at which the photographic exposure is to be made.

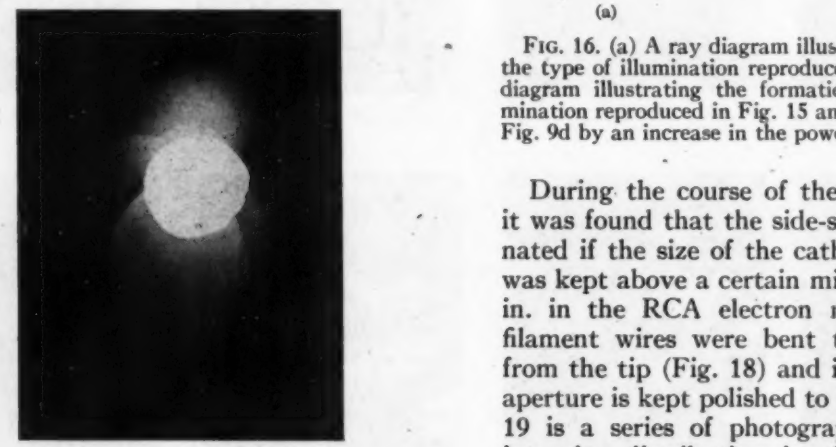

FIG. 15. A photographic record of the intermediate image when the condenser power has been increased or decreased and is producing multiple illumination of the field of view of the specimen.

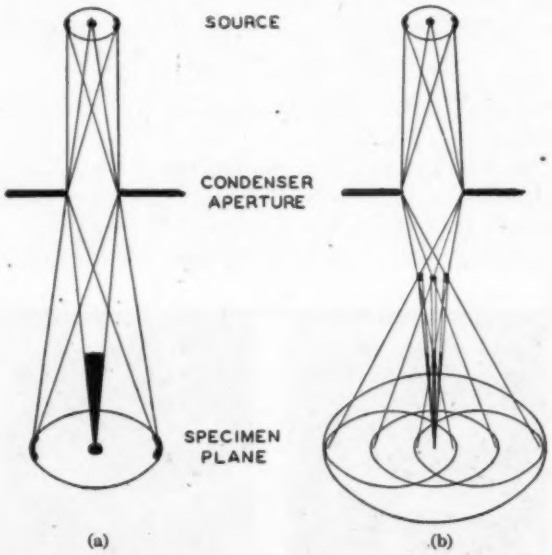

FIG. 16. (a) A ray diagram illustrating the formation of the type of illumination reproduced in Fig. 9d. (b) A ray diagram illustrating the formation of the type of illumination reproduced in Fig. 15 and obtained from that of Fig. 9d by an increase in the power of the condenser lens.

During the course of the above experiments it was found that the side-spots could be eliminated if the size of the cathode shield aperture was kept above a certain minimum value (0.150 in. in the RCA electron microscopes), if the filament wires were bent to go directly back from the tip (Fig. 18) and if the cathode shield aperture is kept polished to bright metal. Figure 19 is a series of photographic records of the intensity distribution in the illumination obtained after incorporating these modifications. The adjustments used in the individual exposures are the same as those of Fig. 9. If u_k

or $1/f_k$ are properly adjusted it is virtually impossible to produce multiple images with this arrangement.

In conclusion it is of interest to consider how far the last described arrangement departs from an ideal source of illumination for the electron microscope focused visually at magnifications considerably below the useful limit of the instrument. Associated with the necessary change in α_c accomplished by means of adjustment of $1/f_c$ are a number of phenomena which disturb the conditions and adjustment of the remainder of the instrument. Since there is no possibility of a visual check on these phenomena, they very often account for spoiled micrographs.

The first and most important effect is the redistribution of charge on the specimen plane. When α_c is reduced by varying $1/f_c$, the irradiation is spread over a much larger area of the specimen and at the same time the intensity is reduced so that an entirely new equilibrium condition must be established. This causes a slow drifting of the image which may continue through the exposure period. The second disturbance arises from the changed thermal conditions which causes motion of the specimen from thermal expansion, until a new equilibrium is established. The third of these is a result of the space charge in the image of the source produced by the condenser. When adjusted for visual observation $\alpha_c = \alpha_c(\max)$, this space charge exists at the specimen and is responsible for a diverging effect on the pencils of electrons leaving the specimen. This, in turn, requires a slightly high objective power for exact focus. When the position of the image source is moved

FIG. 18. An enlarged photograph of the tip of an electron-microscope filament.

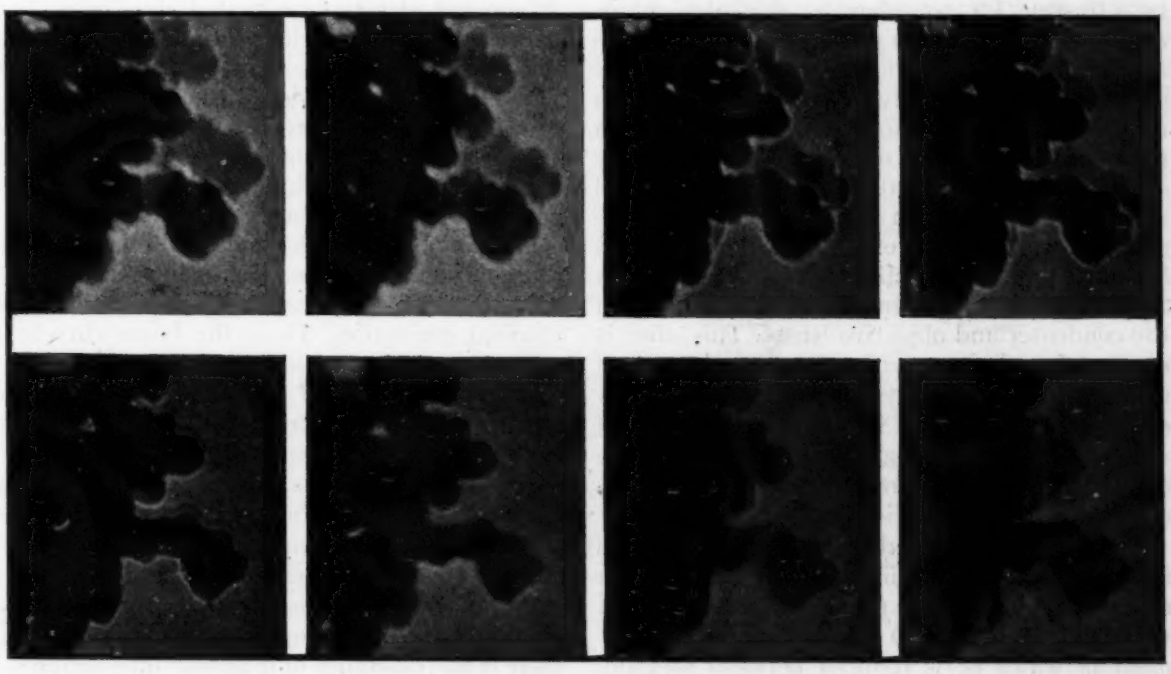

FIG. 17. Electron micrographs of carbon black taken with the electron-source adjustment illustrated in Fig. 9d, and with the condenser power increased by about the same amount as in Fig. 13.

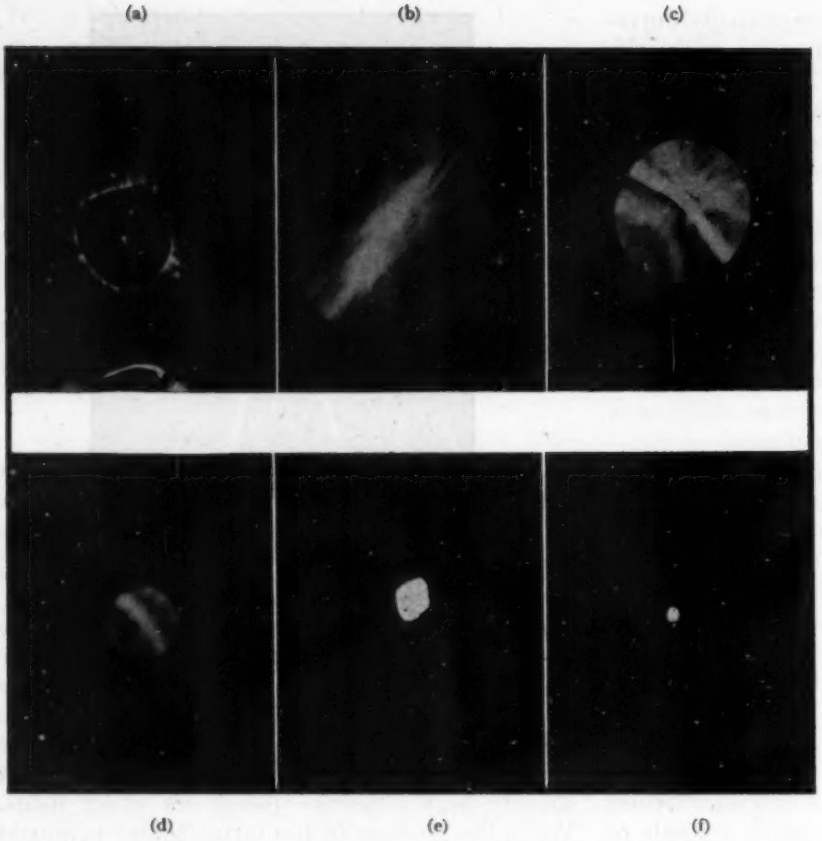

FIG. 19. A series of photographic records of the intermediate image with cathode-lens adjustments corresponding to those in Fig. 9 and showing the complete elimination of the side spots.

by adjusting $1/f_c$ to reduce α_c, the space charge condition is moved to a position above the specimen but reappears in the cross-over immediately below the objective. The objective is then no longer accurately focused for the specimen plane. In practice this difficulty is overcome by determining experimentally (by making focal series) the reduction in objective current necessary to correct for the effect. The fourth effect is a change in the objective lens strength which arises as a result of magnetic interaction between the condenser and objective lenses. This effect is smaller than that caused by the space charge and may be of either polarity according to the current directions to the two lenses. It is eliminated automatically in making the correction for space charge if the connections are not changed subsequent to the determination.

All these effects (and those due to multiple illumination) can be eliminated by the use of a means for obtaining a reduction in α_c without varying $1/f_c$. Figure 20 shows such an arrangement in which α_c is reduced between focusing and exposure by replacing the condenser aperture with a smaller one; $1/f_c$ being left constant. It consists of a lever operated slide fitted with a thin plate drilled with two apertures—a large one corresponding to $\alpha_c(\max) = 3.12 \times 10^{-3}$ rad. and a smaller one giving $\alpha_c(\max) = 0.312 \times 10^{-3}$. (See Eq. (9).) This system is operated always with the image of the source focused on the specimen plane so that the centering of the apertures in the condenser lens is not critical.

In the use of this device the intensity of illumination at the specimen is kept at the same value for both apertures by proper control of the filament excitation. Thus, the beam current is reduced, and the large aperture is put in a place for visual focusing of the image. Then as the smaller aperture is introduced the beam current is increased by the square of the ratio of the aperture sizes (that is, by one-hundred-fold in the above example). In this way the charge distribution on the specimen, the thermal condition, and the space-charge effect, are maintained constant for both the visual observation and the making of the photographic record. Finally, while there is no possibility of magnetic interaction between the objective and condenser lenses, there is a dependence of the high voltage supplies on

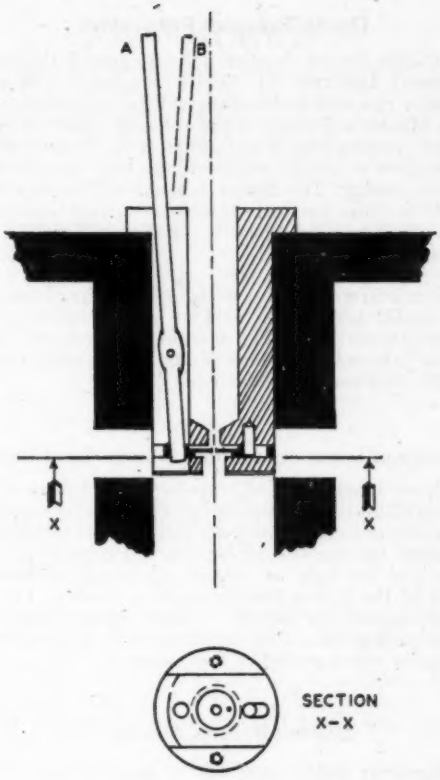

FIG. 20. A schematic cross section of a device permitting the exchange of condenser apertures during operation.

the beam current load which must be considered. For electronically regulated systems this dependence can be made negligible.

In order to test the validity of the above reasoning the device shown in Fig. 20 was

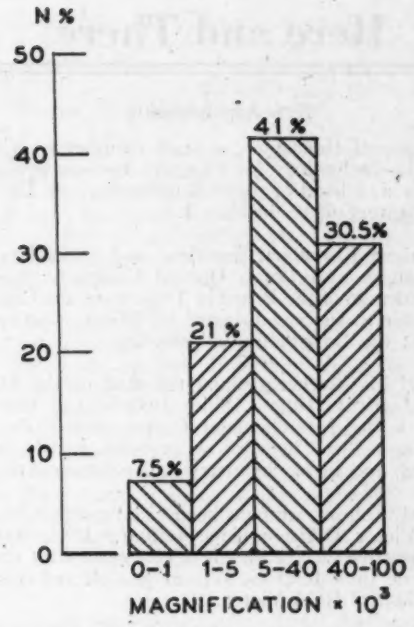

FIG. 21. A frequency plot showing the performance of the electron microscope when the device illustrated in Fig. 20 is used.

installed in an RCA type B electron microscope and a number of exposures were made. A distribution curve was made according to the method described above for the first 200 exposures and is reproduced in Fig. 21. The obvious improvement becomes even more striking when it is pointed out that the tests were made on a few difficult specimens and under conditions generally less favorable than those which existed in the case of Fig. 1.

Here and There

New Appointments

Dr. Maxwell Gensamer, a staff member at Carnegie Institute of Technology for 16 years, became professor of metallurgy and head of mineral technology at The Pennsylvania State College on May 1.

M. Herbert Eisenhart, president and general manager of the Bausch and Lomb Optical Company, has been elected chairman of the Board of Trustees of the University of Rochester to succeed Edward G. Miner, who resigned May 12 at the Board's annual meeting.

Dr. Carl M. Marberg joined the staff of the Midwest Research Institute June 1. Since 1939 he had been associated with the Interchemical Corporation, New York, where he specialized in work on proteins, textile printing inks, resins, and in biochemistry and pharmaceuticals.

Frank M. Folsom, who has been vice president in charge of RCA Victor Division since January 1944, has been elected executive vice president in charge of that division. At the same time John G. Wilson was elected operating vice president of RCA Victor.

Dr. Richard von Mises, lecturer in the Graduate School of Engineering of Harvard University, has been appointed Gordon McKay professor of aerodynamics and applied mathematics, effective July 1.

Science reports that Dr. Marcel Schein of the department of physics of the University of Chicago has been engaged as a consulting physicist by the Research Laboratory of the General Electric Company. He is working on problems connected with the radiations of the 100-million-volt induction electron accelerator. Alfred J. Hartzler, formerly of the department of physics of the University of Chicago, has become a member of the staff, for studies of the radiations produced by the 100-million-volt induction accelerator. Dr. Arthur M. Ross, Jr., until recently of Columbia University, has rejoined the chemical section. Dr. Ross was a member of the Research Laboratory in 1939–40 and later of the staff of the Works Laboratory in Bridgeport.

Instrument Society

A new national society to be known as "The Instrument Society of America" was organized in Pittsburgh on April 28 at a conference attended by delegates from fifteen measurement and control instrument societies that have been growing in various industrial centers throughout the country. The purpose of the Society will be to advance the arts and sciences that are connected with the theory, design, manufacture, and use of instruments. The Society is non-professional and offers membership to any person, firm, or institution interested in the objectives of the Society. Pro-tem officers were elected as follows: President, A. F. Sperry of Chicago; Vice President, C. F. Kayan of New York; Treasurer, C. E. Fry of Pittsburgh; Secretary, Richard Rimbach of Pittsburgh. The office of the Secretary is the temporary office of the Society and is located at 1117 Wolfendale Street, Pittsburgh 12, Pennsylvania.

New Westinghouse Name

The name of Westinghouse Electric and Manufacturing Company was changed to Westinghouse Electric Corporation, effective May 12.

Health Research Fellowships

The Public Health Service has announced the creation of National Institute of Health Research Fellowships. The Junior research fellowships will be available to those holding Master's degrees in the sciences (such as physics, chemistry, entomology, etc.) allied to public health, from an institution of recognized standing. The stipend will be $2400 per annum. The Senior research fellowships will be available to those holding a doctorate degree in one of the sciences allied to public health. The stipend will be $3000 per annum.

These fellowships will offer an opportunity for study and research in association with highly trained specialists in the candidates' chosen field at the Institute or some other institution of higher learning. Letters of inquiry should be addressed to The Director, National Institute of Health, Bethesda 14, Maryland.

American Locomotive-Union College Agreement

American Locomotive Company and Union College have entered into a contract under which the company will substantially enlarge the physics laboratories of the college in exchange for the use of certain laboratory and other facilities and for help on specific technical problems by members of the Union College science faculty. The company has agreed to provide Union ten or twelve new laboratories. Facilities and faculty are to be available to the company for a period of five years.

Science Reports Awards

Dr. Vannevar Bush, president of the Carnegie Institution and director of the Office of Scientific Research and Development, was presented on May 25 at a dinner meeting of the National Institute of Social Sciences in New York City with one of the gold medals awarded by the Institute. The medal was awarded for "distinguished services in the field of science, in engineering education, and in the application of research to the solving of problems of fundamental value to civilization." The presentation was made by Dr. Karl T. Compton, president of the Massachusetts Institute of Technology.

The prize in pure chemistry of $1000 of the American Chemical Society for 1945 has been awarded to Dr. Frederick T. Wall, associate professor of physical chemistry at the University of Illinois, in recognition of his work on the thermodynamics and statistical mechanics of polymers. The award is made annually to encourage fundamental studies by young chemists working in North America.

Dr. Katharine B. Blodgett, of the General Electric Research Laboratory, Schenectady, New York, has received the Achievement Award of $2500 given by the American Association of University Women for distinguished research in developing films of almost infinitesimal thickness.

Corning Glass Expansion

Corning Glass Works has purchased a new plant at Leaside, Ontario, Canada, for the manufacture of a complete line of glass baking ware, the first to be made in the Dominion. Operations will be broadened as rapidly as possible to cover the manufacture of other types of glassware. This Canadian development represents Corning's third move in the foreign field during the past two years; the company has acquired part interest in glass companies in Argentina and Brazil.

New Booklets

The News Bureau of Illinois Institute of Technology has released a 53-page mimeographed *Press Book No. 1* on the Armour Magnetic Wire Sound Recorder and Reproducer, developed by the Armour Research Foundation of the Institute. Twelve pages of illustrations are included. Address the Institute's News Bureau, 3329 Federal Street, Chicago 16, Illinois.

Bulletin 125 of the Ohmite Manufacturing Company, 4835 Flournoy Street, Chicago 44, Illinois, announces two new series of Riteohm Precision Resistors. A few common applications for these resistors are voltmeter multipliers, laboratory equipment, radio and electrical test sets, attenuation pads, and electronic equipment requiring extremely accurate resistance components.

The International Nickel Company has published the second quarterly edition of *Nickel Cast Iron News* for 1945. Recent developments in nickel and iron production are discussed in articles amply illustrated with photographs. 8 pages. Address the Company at 67 Wall Street, New York 5, New York.

Klem Chemical Works, manufacturer of industrial chemicals, has issued an 8-page folder covering cleaning, derusting, phosphotizing, soldering, and maintenance processes. Written for the purchasing agent, shop superintendent, factory manager, chemist, metallurgist, or process engineer. Address the company at 1500 East Woodbridge, Detroit 7, Michigan.

Wartime accomplishments of an American industrial organization are told in a 56-page booklet issued recently by Bausch and Lomb Optical Company of Rochester, New York. Profusely illustrated, the booklet, entitled *Seeing It Through* is a report to employees, servicemen, and friends on the production of optical instruments of war and their successful use on every front.

The Forest Industries Blaze New Trails, a brochure published by the Timber Engineering Company, recites the long story of wood's usefulness to man, describes the current technological developments of wood as an engineering medium and as the raw material of plastics and chemicals, and heralds the dawn of a new Age of Wood with limitless horizons for America's geatest renewable natural resource. Wood, according to the booklet, is capable of being made the most universally useful of all industrial materials. It predicts that the winner of the "battle of the giants" in the next quarter century will be determined largely by science and the laboratories in mastering the mysteries of cellulose and lignin. 36 pages, five colors, many illustrations. Available from Timber Engineering Company, 1319 Eighteenth Street, N.W., Washington 6, D. C.

A new bulletin on *The Ultra Violet Lamp in Education*, written by Jack De Ment, deals with the use of ultraviolet fluorescent rays in improved educational methods. 4 pages. Available free from Ultra-Violet Products, Inc., 5205 Santa Monica Boulevard, Los Angeles 27, California.

In April appeared the first issue of *Polymer Bulletin*, published by Interscience Publishers, Inc., with the cooperation of the Bureau of High Polymer Research, Polytechnic Institute of Brooklyn. Paul M. Doty is editor. It is intended that the Bulletin will provide a medium for the dissemination of information on trends, developments, and research in the rapidly growing field of high polymers. The editor will welcome news items concerning persons and events in this field, and extends an invitation to all workers in this field to contribute articles for the magazine. Issued bimonthly. Subscription $2.40 a year; foreign and Canada, $2.90 a year. Interscience Publishers, Inc., 215 Fourth Avenue, New York 3, New York.

Precision Scientific Company, 1750 North Springfield Avenue, Chicago 47, Illinois, has issued Catalog 325, containing 48 illustrated pages pertaining to "Precision"-Freas constant temperature control cabinets, including an extensive variety of standard models as well as many photographs of constant temperature cabinets and baths built to specifications. Catalog is accompanied by price list.

North American Philips Company, Inc., 100 East 42nd Street, New York 17, New York, has announced a new 8-page illustrated booklet describing the *Geiger-Counter Spectrometer for Industrial Research*. Written by H. Friedman of the Naval Research Laboratory for a trade magazine, the article has been reprinted in booklet form by permission of the Navy Department. The author discusses in detail the theory underlying x-ray powder diffraction, how the Norelco spectrometer works, its performance and applications. Photos, diagrams, and curves are used to illustrate the text matter. Geiger-counter tubes, circuits and losses are covered at some length, and an explanation is given of the "flip-flop" counting action.

Interchemical Review for Spring 1945, contains the following principal articles: "Specification of Color," "Active Chlorine Compounds," "Microanalysis—Development and Use." 32 pages. Interchemical Corporation, 432 West 45th Street, New York 19, New York.

Taber Instrument Corporation, 111 Goundry Street, North Tonawanda, New York, has published Bulletin No. 4506, in which is announced a new Taber V-5 power driven stiffness gauge for determining standard measurements of the stiffness and resilient qualities of flexible materials up to $\frac{1}{4}$" in thickness, such as laminated plastic, cardboard, light metallic sheet, and wire. The same company has also issued a new *Abraser Testing Handbook*, describing Taber equipment for testing the wearability of materials and surfaces. 16 pages, illustrated with photographs.

New Books

Bibliography of Solid Adsorbents

By Victor R. Deitz. Pp. 877+lxxxi. A contribution from the United States Cane Sugar Refiners and Bone Char Manufacturers Association and the National Bureau of Standards, Washington, D. C., 1944. Price $12.00

This book will be highly appreciated by all persons interested in the subject of activated carbons and other technical adsorbents. The book consists of a condensed and instructive introduction of approximately 60 pages relating to the history of commercial adsorbents. This is followed by approximately 10 pages devoted to a tabulation of commercial solid adsorbents available in the United States and elsewhere, after which is presented in well-classified sections abstracts of 6,002 articles, bulletins, books, etc., which have appeared between the years 1900 to 1942 inclusive.

While the primary object was to make a survey of scientific literature relating to solid materials suitable for use in the purification of sugar liquors, no generally recog-

nized type of solid adsorbent has been overlooked. Special attention has been given charcoals, bone char, silica gel, clays, the oxides, and other important adsorbents. The different chapters deal with (1) adsorption of gases and vapors, (2) adsorption from solution, (3) thermal effects in adsorption processes, (4) theories of adsorption, (5) refining of sugars and other applications of adsorbents, (6) general information on adsorbents and special methods of investigation, and (7) preparation of various carbon adsorbents.

Considering the scope of the subject embraced, the bibliography is surprisingly complete. In nearly every case the abstracts are sufficiently comprehensive to enable the reader to obtain the outstanding points of novelty of the original article. This bibliography will be prized by those working in the field of adsorbents. The author is to be congratulated on his meticulous work, and the sixteen industrial sponsors of the project, as also the Research Committee members of the National Bureau of Standards, are to be commended for their assistance in making this valuable work generally available.

F. E. BARTELL
University of Michigan

Medical Physics

EDITED BY OTTO GLASSER. Pp. 1744+xlviii. Figs. estimated at about 2,000, 18×26 cm. The Year Book Publishers, Inc., Chicago, Illinois, 1944.

This is indeed a monumental volume. It covers in an encyclopedic fashion a great many topics in biology and medicine that are related to advances in physics and many topics in physics that are now finding application in biology and medicine. The quality of the articles treating physical subjects will be readily apparent from the names of the contributors. We find, for instance, in the field of nuclear physics, contributions by Robley D. Evans, Paul C. Aebersold, M. Stanley Livingston, and Donald W. Kerst; in the discussion of the centrifuge, contribution by E. Newton Harvey; in color vision, by Deane B. Judd; in the discussion of the electron microscope, by V. K. Zworykin; in mathemathical biophysics, by N. Rashevsky; and in radiation therapy, by Edith H. Quimby.

These are only a sampling of the topics that are discussed. If one takes any one of these at random, he will find a very complete bibliography, a unified discussion of the entire field, and an account of the latest developments in the field.

The physicist will find this book useful not only in its relation to medical physics, but also as a good source book for a brief account of many of the most active fields of modern physics. The book is very well printed and has excellent illustrations.

Recent Applications of Physics

Prepared by CLARK GOODMAN, Associate Editor

Material to be included in this section should be submitted to Dr. Clark Goodman, Massachusetts Institute of Technology, Cambridge 39, Massachusetts.

Electronic Knockmeter It has been said that the Germans lost air superiority to the British because of a difference of 10 units in the knock ratings of the aviation gasolines used. While this sweeping generalization is certainly not accurate, it is undoubtedly true that the improved performance made possible by better fuel was an important factor. Recently developed engine-pressure indicators provide a means of checking the presence of detonation in each cylinder of multi-engine planes during flight. Two types of pressure pick-ups have been developed independently. A double quartz piezoelectric unit is available through Industrial Electronics, Inc. of Detroit,[1] and a magnetostrictive unit is used in the system developed by Lane-Wells Company of Los Angeles.[2] Each is about the size of an average spark plug and screws into a special opening in the cylinder head. After amplification the output of the pick-up is fed to a cathode-ray oscilloscope, which may be part of the standard equipment of the plane. The shape of the pressure pattern curve is a sensitive indicator of the performance characteristics of the cylinder. A selector switch allows each cylinder to be tested and individual adjustments can thus be made to maintain maximum output.

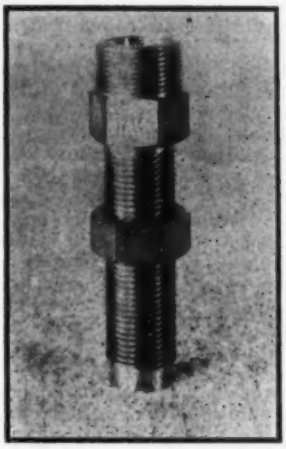

Piezoelectric pick-up.

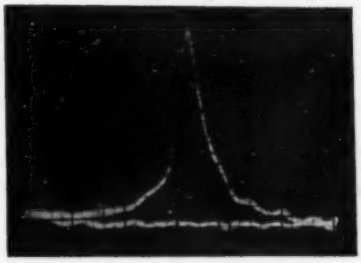

Pressure oscillograph.

These units will undoubtedly find application in post-war automobile engines, since considerable economy of fuel is made possible by proper tuning of the motor. It seems entirely feasible that in the future a combination spark plug and pressure indicator could be designed. In this way any properly equipped garage could insert a pick-up in place of a spark plug and adjust the individual cylinders of the automobile motor.

[1] J. W. Head, Electronics, 132–135 (Jan. 1945).
[2] R. M. Otis, Tomorrow's Tools—Today 10, 8–10 (1944).